Assessing the removal mechanisms of engineered nanoparticles in aerobic granular sludge systems

Pedro Miguel Teixeira da Silva

Thesis to obtain the Master of Science Degree in

Biotechnology

Supervisors: Profª. Nídia Dana Mariano Lourenço de Almeida

Profª. Maria Teresa Ferreira Marques Pinheiro

Examination Committee

Chairperson: Profª. Leonilde de Fátima Morais Moreira

Supervisor: Profª. Nídia Dana Mariano Lourenço de Almeida

Member of the Committee: Profª. Helena Maria Rodrigues Vasconcelos Pinheiro

December 2017

Acknowledgments

Um muito obrigado a todos aqueles que de alguma forma contribuíram para a realização deste projeto e que sempre me apoiaram a perseguir os meus objetivos, em especial:

Às professoras: Nídia Lourenço e Teresa Pinheiro, pela sua constante disponibilidade e por todo o apoio e carinho, foram realmente incansáveis;

Aos colegas Rita Franca e Miguel Coelho pela cedência dos dados de performance dos reatores por eles obtidos;

Ao Doutor Luís C. Alves pelo apoio na microscopia nuclear;

À Doutora Catarina Galinha do C2TN/IST pelo apoio na operação do ICP-MS;

Ao João Bento por todo o companheirismo e constante acompanhamento na realização deste projeto;

A todos os colegas de laboratório pelo excelente ambiente de trabalho que me proporcionaram;

A todos os colegas de curso pelos momentos de camaradagem partilhados;

À Verinha e aos Creeps por tudo o que vivemos durante esta aventura;

Aos meus Pais e ao meu irmão por sempre acreditarem em mim e me incentivarem a ir mais longe;

Aos restantes familiares e amigos que, como sabem, são parte muito importante de mim.

Este trabalho foi financiado pela Fundação para a Ciência e a Tecnologia (FCT, Portugal) através do projecto “Impact of engineered nanoparticles and microplastics on textile wastewater treatment with aerobic granular sludge technology – NanoMicroImpact”, PTDC/AAG-TEC/4501/2014.

Abstract

The textile industry stands as one of the most polluting industrial sectors, being one of the main causes of water pollution, especially in underdeveloped countries. Due to their antimicrobial properties, the application of silver nanoparticles (AgNPs) in this industry has been increasing and their occurrence in wastewater is expected to rise accordingly. Wastewater treatment plants can act as important barriers to prevent nanoparticles (NPs) from reaching the environment. In this study, two sequencing batch reactors (SBRs; one AgNP-fed and one AgNP-free control) operating with aerobic granular sludge (AGS) were monitored during a 16-week period with the main purpose of assessing the impact of AgNPs on the performance of the AGS SBR system and their possible removal mechanisms. Different EPS extraction techniques were tested and the corresponding polysaccharide and protein contents were characterized. The results obtained indicated that polysaccharides were the EPS major component. The presence of AgNPs did not significantly influence the EPS protein content, but polysaccharides content consistently decreased by report to control SBR. Nonetheless, AgNPs appeared to have no toxic effect on AGS as the Ag-fed SBR consistently presented a higher organic carbon removal as well as higher proportion of granular biomass and better settling capabilities. AgNPs were proven to be substantially retained in AGS with elemental distribution imaging in granule sections revealing a preferential deposition at the periphery of the granule with a sharp decrease towards inner regions. It was also demonstrated that structural and trace elemental distributions across granules exhibited significant differences when exposed to AgNPs.

Keywords: Textile wastewater; Aerobic granular sludge; Sequencing batch reactor; Silver nanoparticles; Extracellular polymeric substances; Elemental mapping.

Resumo

A indústria têxtil constitui um dos setores industriais mais poluentes, sendo uma das principais causas de poluição da água, especialmente em países subdesenvolvidos. Devido às suas propriedades antimicrobianas, a utilização de nanopartículas de prata (AgNPs) nesta indústria tem vindo a aumentar, sendo a sua ocorrência em águas residuais espectável. As estações de tratamento de águas residuais podem atuar como barreiras importantes evitando que nanopartículas (NPs) atinjam o meio ambiente. Neste estudo, dois reatores descontínuos sequenciais (SBRs, um suplementado com AgNPs e um controlo sem AgNPs) operaram com grânulos aeróbios (AGS) sendo monitorizados durante 16 semanas com o intuito de avaliar o impacto de AgNPs sobre o desempenho do sistema AGS SBR e seus possíveis mecanismos de remoção. Foram testadas diferentes técnicas de extração de EPS e o conteúdo em polissacáridos e proteínas foi caracterizado. Os resultados indicaram os polissacáridos como componente principal do EPS. A presença de AgNPs não influenciou significativamente o conteúdo de proteína no EPS, contudo o conteúdo de polissacáridos foi consistentemente menor relativamente ao SBR controlo. AgNPs pareceram não exercer efeitos tóxicos sobre AGS, pois o SBR suplementado com AgNPs apresentou maior proporção de biomassa granular, assim como melhor capacidade de sedimentação e remoção de carbono orgânico. AgNPs provaram ser substancialmente retidas na AGS. Técnicas de geração de imagem e quantificação elementar revelaram uma deposição preferencial de Ag na periferia do grânulo, diminuindo significativamente em regiões mais interiores. Provou-se que as distribuições de elementos estruturais e traço em grânulos variaram significativamente quando expostas a AgNPs.

Palavras-chave: Águas residuais têxteis; Grânulos aeróbios; Reatores descontínuos sequenciais; Nanopartículas de prata; Substâncias poliméricas extracelulares; Mapeamento elementar.

Figure Index

Table Index

Abbreviations

AgNPs Silver nanoparticles
AGS Aerobic granular sludge
AOB Ammonia-oxidizing bacteria
AR14 Acid red 14
BCA Bicinchoninic acid
BOD Biochemical oxygen demand
BSA Bovine serum albumin
CER Cation exchange resin
COD Chemical oxygen demand
CRM Certified reference material
CTN/IST Campus Tecnológico e Nuclear/ Instituto superior técnico
DO Dissolved oxygen
EDX Energy dispersive x-ray spectroscopy
EM Electron microscopy
EPS Extracellular polymeric substances
FAS Ferroin ammonium sulphate
Feed - C Carbon feed solution
Feed - N Nitrogen dye-containing feed solution
GAOs Glycogen accumulating organisms
HRT Hydraulic residence time
ICP-MS Inductively-coupled plasma mass spectrometry
LB-EPS Loosely bound EPS
NPs Nanoparticles
ORL Organic loading rate
PAOs Phosphate accumulating organisms
PIXE Particle induced X-ray emission
PN Proteins
PS Polysaccharides
RBS Rutherford backscattering spectroscopy
SBR Sequencing batch reactor
SEM Scanning electron microscopy
SS Suspended solids
STD Standard deviation
STIM Scanning transmission ion microscopy
SVI Sludge volume Index
SVI30 SVI after 30 min of settling
SVI5 SVI after 5 min of settling
TB-EPS Tightly bound EPS
TCA Trichloroacetic acid
TEM Transmission electron microscopy
TOC Total organic carbon
TSS Total suspended solids
VSS Volatile suspended solids
WWTP Wastewater treatment plant

Table of Contents

1. Introduction

1.1. Textile industry

1.1.1. Overview

Currently, the textile industry moves billions of dollars worldwide and assumes an important position in the world economy, playing a critical role in the industrial development of some countries such as China, India, Pakistan, Bangladesh and Malaysia (Bilińska, Gmurek, and Ledakowicz 2016). As of 2015, China, the European Union and India were the top three textile exporters, representing 66.4% of total textile exports around the globe (World Trade Organization 2016).

The textile industry from a reductionist point of view comprehends all the processes to assure the conversion of fibres into fabrics. A large variety of fibres are used, some being natural (e.g. cotton, wool, silk and linen) and others synthetic (e.g. polyester, nylon and polypropylene) (Ghaly et al. 2014). Nevertheless, all the fibres undergo several processing steps in order to reach the final product, ready for commercialization. Common operations in this industry include processes like scouring, dyeing, printing, finishing, and washing (Li et al. 2012; Sarayu and Sandhya 2012). These processing stages contribute largely to the total amount of the generated wastewater mainly due to the high quantities of water used in the dyeing processes (Saratale et al. 2011). The volume and composition of wastewater can exhibit wide heterogeneity, being closely related to several factors such as the final product characteristics, quality, origin of the raw material, physical and chemical characteristics of the applied dye (Dasgupta et al. 2015), as well as internal pollution prevention and process management strategies (Dasgupta et al. 2015; U.S. Environmental Protection Agency 1997).

The textile industry is characterized not only by its enormous water consumption (in some cases as high as 3,000 m^3 per day), but also by the variety and complexity of chemicals employed (Sarayu and Sandhya 2012). To this day, textile industry stands as one of the most polluting of all industrial sectors (Lourenço et al. 2015; Vajnhandl and Valh 2014).

1.1.2. Textile wastewater

With the escalating demand for textile products, wastewater generation has been increasing proportionally and, as previously mentioned, this can be considered as the main reason why this industry presents a serious environmental problem (Khan and Malik 2014). Despite the wide variability of untreated textile effluents, generally they present high values for colour, chemical oxygen demand (COD), biochemical oxygen demand (BOD), total organic carbon (TOC), suspended solids (SS), pH, temperature, turbidity and salinity (Verma, Dash, and Bhunia 2012). Most of the BOD:COD ratios are found to be around 1:4, indicating the presence of non-biodegradable substances (Ghaly et al. 2014; Pang and Abdullah 2012).

Among the various complex constituents present in textile wastewaters, the dyeing compounds can be inarguably considered one of the most peremptory sources of contamination. Azo dyes represent approximately 70% of all dyestuffs used worldwide by weight and are consequently the most widely present synthetic colorants in textile wastewaters (Saratale et al. 2011; Zollinger 2004).

1.1.3. The particular case of AgNPs in textile wastewater

Textile products are often treated with antimicrobial agents for a range of reasons, depending on the market sector and application area (Windler, Height, and Nowack 2013). These compounds play an important role in assuring hygiene in clinical and sensitive environments by minimizing the chances for microbial colonization of textiles (Heine et al. 2007). Silver-based compounds are among the main antimicrobials used in textiles, along with silane quaternary ammonium compounds, triclosan, and zinc pyrithione (Windler et al. 2013). The bactericidal efficacy of silver is caused by numerous mechanisms, including the strong binding of Ag^+ with disulfide (S–S) and sulfhydryl (−SH) groups found in the proteins of microbial cell walls (Silvestry-Rodriguez et al. 2007). Ag^+ ions disrupt normal metabolic processes by causing the displacement of essential metal ions, such as Ca^{2+} or Zn^{2+}, leading to cell death (Schierholz 1998). Due to their good antimicrobial properties, the use of silver nanoparticles (AgNPs) in the textile industry has been rapidly increasing and their significant occurrence in wastewater is now a worrying consequence (Mueller and Nowack 2008; Som et al. 2011; Windler et al. 2013)

Textile antimicrobials need to meet several requirements for their use to be advantageous, namely: efficacy against microorganisms, suitability for textile processing, durability, and a favourable safety and environmentally-friendly profile (Gao and Cranston 2008). The last one is of extreme importance, since the biological activity of these antimicrobials can affect the environment and the human health. The safety assessment of biocidal products is strictly regulated to ensure that the use of these products is safe. Consequently, the development of new and improved antimicrobials is an ongoing topic of research (Bshena et al. 2011; Dastjerdi and Montazer 2010).

Wastewater treatment plants (WWTPs) act as important barriers to prevent nanoparticles (NPs) from reaching the environment (Quan et al. 2015). Some previous studies have already elucidated the possible mechanisms through which AgNPs can be removed in WWTPs, namely via aggregation, settling, precipitation, biosorption, or other sludge mediated processes (Kiser et al. 2010; Liang, Das, and Hu 2010). Furthermore, some research groups have already focused on the release of AgNPs from textiles during washing to measure the environmental exposure through this process (Benn and Westerhoff 2008; Lorenz et al. 2012). However, few studies have been reported on the AgNPs discharge impacts in bacterial growth and/or the properties of sludge itself in WWTPs (Liang et al. 2010). This is even more evident regarding aerobic granular sludge (AGS) systems. In 2010 both Kiser et al. and Liang et al. have described some interactions of AgNPs with the more commonly used flocculent activated sludge. Kiser et al. (2010) found that the vast majority of AgNPs was removed by aggregation and sedimentation. Liang et al. (2010) investigated the bacterial response to a shock load of AgNPs (1 mg/L for 12 h, average particle size of 21 nm) in an activated sludge treatment system, and found a significant inhibition of nitrification (46.5%) after more than one-month operation. Moreover, nitrification in activated sludge was observed to be more strongly inhibited by AgNPs than by the equivalent amount of Ag (1 mg/L) as Ag^+ ion (Liang et al. 2010).

Published studies performed by Quan et al. (2015) and Gu et al. (2014) have provided some conclusions regarding the interaction of AgNPs (average particle size of 50 nm) with AGS systems. The study conducted by Quan in 2015, where an AGS SBR with AgNPs was compared to a AgNPs-free control, showed similar levels of extracellular polymeric substances (EPS) after 69 days of operation,

but the proportion of EPS components had changed significantly with an apparent increase of proteins (PN) and decrease of polysaccharides (PS) in the AgNPs-exposed AGS (Quan et al. 2015). Both studies confirmed that despite the high tolerance to the presence of AgNPs exhibited initially, the prolonged exposure induced chronic toxicity on AGS and led to cell death, resulting in the loss of microbial activity. On the other hand, these studies also showed that the microbial community of AGS remained stable, retaining a large granule size, a good settling ability and even contributed to the removal of the NPs. Overall, despite not causing acute toxicity to the AGS, the chronic toxic effects of AgNPs are still cause for great concern (Gu et al. 2014; Quan et al. 2015).

1.1.4. The particular case of azo dyes in textile wastewater

The already mentioned growth of the worldwide textile industry in the last two centuries had seen a proportional increase in the use of synthetic dyes, resulting in a rise of pollution due to wastewater contaminated with dyestuffs (Pandey, Singh, and Iyengar 2007). By 2007 it was estimated that 280,000 tons of textile dyes were discharged in industrial effluents every year worldwide (Jin et al. 2007).

The extensive use of azo dyes in the textile industry can be explained by several factors, among them: the ease and cost effectiveness of their synthesis, their stability and the variety of colours available when compared to natural dyes (Lourenço et al. 2015). The processing stages and types of synthetic dyes applied in the textile industry influence several wastewater characteristics, contributing to the wastewaters' coloured appearance (Banat et al. 1996).

Azo dye degradation by bacteria can be carried out in a two-step process: (1) The breaking or reduction of the azo bond by bacteria under anaerobic conditions (Figure 1) due to the electron-withdrawing nature of azo bonds and (2) the partial or complete mineralization of the reduction products (aromatic or aliphatic amines) generated in the first step, this time under aerobic conditions (González-Gutiérrez, González-Alatorre, and Escamilla-Silva 2009). Azo dye reduction products have been raising health concerns throughout the years, since some of these breakdown products have been considered toxic to the aquatic biota and carcinogenic to humans (Lourenço et al. 2015; Wijetunga, Li, and Jian 2010).

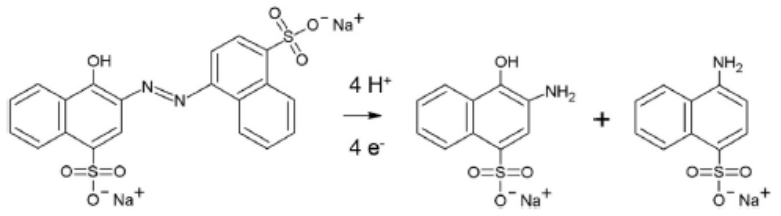

AR14 1N2A4S 4A1NS

Figure 1. Chemical structures of the azo dye Acid Red 14 (AR14) and of the two aromatic amines formed during azo bond reduction, 1-naphthol-2-amino-4-sulfonic acid (1N2A4S) and 4-amino-naphthalene-1-sulfonic acid (4A1NS). (Adapted from Franca et al. 2015)

1.1.5. Environmental impact of the textile industry

Associated with the increasing demand of textile products, the environmental impact of the textile sector has also increased, causing a major problem of pollution worldwide. The discharge of untreated coloured textile wastewater into the fresh water bodies adversely affects their aesthetic merit, water transparency and dissolved oxygen content (Duarte et al. 2013; Wang et al. 2009). Besides contributing to a clear environmental degradation, textile wastewater can also give origin to human health problems. As an example, up to 40 % of globally used colorants contain organically bound chlorine components, among which are known carcinogens (Khan and Malik, 2014).

The occurrence of heavy metals in textile wastewater has also been verified. The utilization of NPs, namely AgNPs, is fairly common to confer antimicrobial activity in different textile materials. Moreover, given the textile industry characteristics and the increasing tendency of widespread use of AgNPs, it is not unwise to assume that textile goods may become a large source of AgNPs emissions in the future (Arvidsson, Molander, and Sandén, 2011). Despite all this, not much is known about the fate of AgNPs during exploitation and maintenance of textile goods. Thus, information on the amount and form of AgNPs released into water is still to unveil, this knowledge would be critical to assess the potential environmental risks (Radetić 2013).

There is still no evidence that humans are adversely affected by AgNPs exposure while using the products with AgNPs. However, by becoming a commonly applied nanomaterial, its release to the environment is foreseeable and since these compounds are not biodegradable, they can accumulate in the organs of both aquatic and terrestrial life forms upon consumption, leading to various symptoms and causing long-term health effects and adversely affecting the ecosystems (Khan and Malik 2014; Verma et al. 2012). The bioaccumulation may become a problem, hence the growing concern for environmental and human health risks. (Fabrega et al. 2011; Radetić 2013)

1.2. Textile wastewater treatment in sequencing batch reactor (SBR) systems

1.2.1. SBR technology

Biological systems combining anaerobic and aerobic phases have been proposed for the treatment of textile effluents, with azo dye reduction occurring in the anaerobic phase, resulting in decolourization, and further organic load removal being obtained in the subsequent aerobic phase, with possible oxidation of dye reduction metabolites (Lourenço, Novais, and Pinheiro 2001; Van Der Zee and Villaverde 2005).

The use of SBR technology has been considered as a good option for the treatment of textile wastewater since it combines the anaerobic and aerobic phases in one system. The SBR configuration offers compact layout, operational flexibility and simplicity (Lourenço et al. 2001). SBR treatment systems are characterized by cyclic, fill-an-draw operations in a single tank, dispensing the use of dedicated settlers. An SBR cycle can be adapted to meet specific purposes, but a standard cycle comprises five steps: fill (influent feed, with or without agitation), react (with agitation and/or aeration), settle (sedimentation of the biomass/clarification of the treated liquor), drain (removal of part of the

treated liquor) and idle (Metcalf, Eddy, and Tchobanoglous, 2004). The different steps are illustrated in Figure 2.

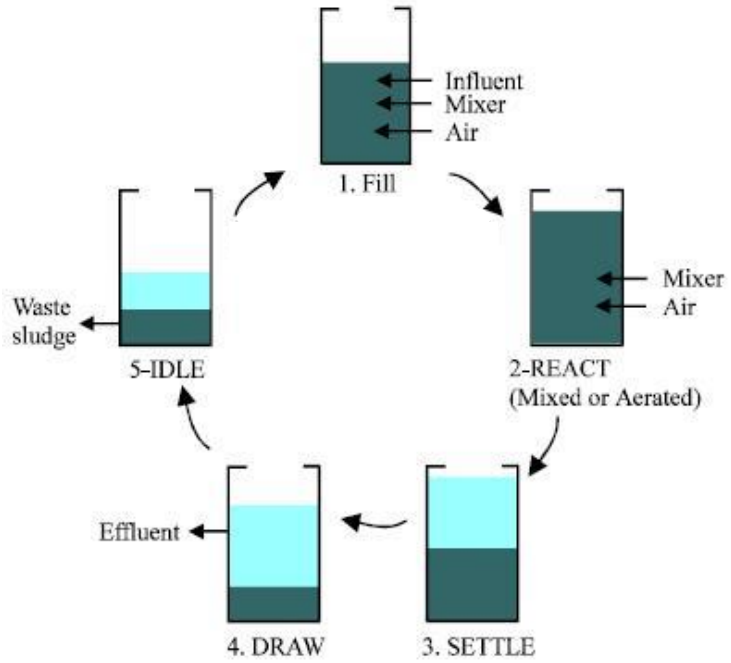

Figure 2. SBR cycle with five discrete time periods of Fill, React, Settle, Draw, and Idle (adapted from Irvine and Ketchum, 2004).

1.2.2. Flocculent sludge technology

In this approach, floc-forming biomass is used to achieve decolourization and further aromatic amine mineralization (Farabegoli et al. 2010; Van Der Zee and Villaverde 2005). For textile wastewater treatment, an SBR operated with flocculent activated sludge can achieve levels of 70% for COD removal and up to 80% of colour removal (Lourenço et al. 2015). Given the properties of the operational features provided by the SBR system, there are some problems inherent to the use of flocculent sludge technology, such as the low resistance to shear stress (Wu et al. 2009) and especially poor settling characteristics that require a large settler footprint and compromise the treatment efficiency (De Bruin et al. 2004).

1.2.3. Aerobic granular sludge (AGS) technology

The dominant wastewater treatment systems are based on flocculent activated sludge (AS). The biology of these systems has been optimised and the limits of the system have been reached. However, some aspects such as sludge settleability and washout remain a point of attention. Other major concerns of water authorities are: minimising costs of wastewater treatment; meeting effluent requirements; being prepared for future developments in effluent demands; area availability; environmental aspects such as smell and noise; energy consumption (De Kreuk, Kishida, and Van Loosdrecht 2007).

1.2.3.1. Definition

Aerobic granular sludge (AGS) technology was developed in the late 1990s (Beun et al. 1999) and was firstly successfully applied for treatment of high strength organic wastewater in 2002 (Moy et al. 2002). In SBR systems operated with AGS, the biomass granules are densely packed microbial aggregates with a diameter of at least 0.2mm (De Kreuk et al. 2007). The density of this aggregates is much higher than those of conventional activated sludge. These characteristics result in practical advantages of the AGS technology: (1) The excellent settling properties allow shorter settling times for good solid–liquid separation requiring a lower construction area; (2) The good biomass retention results in higher biomass concentrations in the SBR and consequently, lower reaction time and/or reactor volume. The ability to withstand toxicity and high organic loading rates makes the system attractive for industrial wastewater treatment applications and the existence of aerobic and anoxic/anaerobic zones within the granules allows organic matter, nitrogen and phosphorus removal in the same system, potentially contributing to the process of azo dye mineralization (Lourenço et al. 2015). These properties combined with the general advantages of the staged SBR technology, allow AGS systems to present a unique combination of attributes with a great potential for the treatment of the highly variable textile wastewaters (Adav et al. 2008), including the biodecolorization of textile dyes and degradation of phenols (Chou and Huang 2005) with significant reductions in footprint and energy consumption (Lourenço et al. 2015). For textile wastewater treatment, an SBR operated with AGS can achieve levels of 80% both for COD and colour removal (Franca et al. 2015; Lourenço et al. 2015).

1.2.3.2. Aerobic granulation

According to the explanation proposed by (Liu and Tay 2002), the granulation process can be divided in four steps, where different types of forces assume great importance: (1) Microbe-to-microbe contact to form aggregates by hydrodynamic, diffusion, gravity and/or thermodynamic forces; (2) Initial attraction to form aggregates by physical forces (van der Waals, opposite charge and thermodynamic), chemical forces (ionic pairing, triplet ionic pairing and inter-particulate bridging) or biochemical forces (cell membrane fusion, cell receptor attraction and cell surface dehydration); (3) Microbial forces to form aggregates by biological glue like cellular clustering and secretion of EPS; (4) Hydrodynamic shear force to stabilize the three-dimensional structure of the granule. Thus, many factors are held responsible for the formation and stability of AGS, among which is possible to highlight: the appearance of specific self-aggregating cultures; the selection by settling velocity; the applied shear stress; the growth rate of the organisms; the substrate gradients inside the granules and the formation of EPS (De Kreuk et al. 2007). Moreover, granulation can be affected by several operational parameters, such as seed sludge, substrate composition, organic loading rate, feeding strategy and reactor design (Adav et al. 2008).

In order to obtain AGS, several operational parameters are manipulated in a way that the generation of granular structures is facilitated, using flocculent sludge as a starting point. The manipulated parameters are typically: settling time, hydraulic residence time, hydrodynamic shear force and feeding strategy.

Some reactor start-up conditions lead to the wash-out of flocculent biomass and are selective for a fast-settling biomass like aerobic granules (Van Loosdrecht, Martins, and Ekama 2008). This effect is promoted when the settling time is kept short (3–5 min) as sludge granules have a high settling velocity compared to sludge flocs, due to the marked difference in density. Therefore, granules require less time to settle than flocs. A short settling period will eventually select for biomass particles with a high settling velocity.

Relatively high hydrodynamic shear forces are also required in the granulation process (Zima et al. 2007). High up-flow aeration not only can induce high shear and compaction forces at the surface of granules, but also appears to stimulate the production of EPS as well as hydrophobic adhesive interactions, ultimately contributing to the granulation process (Dulekgurgen et al. 2008; Liu and Tay 2002).

The adjustment of the hydraulic residence time (HRT) in the granulation stage is performed on the same basis of the settling time. A low HRT should suppress suspended biomass growth, due to wash-out of this suspended biomass (Tijhuis, Loosdrecht, and Heijnen 1994). The exact HRT should be estimated taking into account the operational system in use. Nevertheless, it is generally accepted that HRT values shorter than normal are beneficial for granulation (Morgenroth et al. 1997).

Regarding the feeding strategy, the feast-famine regimes are commonly used to attain successful granulation (Van Loosdrecht et al. 2008). The feast phase corresponds to a period where substrate is provided in excess, or non-limiting conditions, being therefore available for growth and storage. In the famine phase no substrate is provided, forcing the organisms to recur to their stored substrate reserves (Bento 2016; De Kreuk and Van Loosdrecht 2004). Typically, a feast-famine regime in this type of system involve a pulse of feeding (3–5 min) followed by prolonged aeration period (3–4 h) (Beun et al. 1999; Jin et al. 2007), or anaerobic feeding (1 h) followed by aerobic starvation (2 h) (De Kreuk, Heijnen, and Van Loosdrecht 2005; Weissbrodt et al. 2012).

1.2.3.3. Granular morphology, microbial structure and diversity

The granules in AGS are densely packed microbial aggregates, mainly composed of bacteria, and EPS. These structures can be described as spherical biofilms in suspension and their densities are much higher than those of conventional activated sludge (Weber et al. 2007). In addition, the aerobic granules are known to exhibit attributes such as regular, smooth and a nearly round shape, excellent settleability, dense and strong microbial structure, high biomass retention and ability to withstand high organic loads. These aggregates settle significantly faster than activated sludge flocs (Adav et al. 2008; De Bruin et al. 2004). Aerobic granules presenting the above-mentioned characteristics associated with tailored metabolic activities for the removal of carbon, nitrogen, and phosphorus are desired for the operation of robust AGS WWTP (De Kreuk et al. 2007).

Some crucial factors of granule development were already discussed and some key parameters have been studied and modified in order to optimize the granulation process. However, the selection of granules over flocs is not the only accountable factor to accomplish a good granulation process. The presence of slow-growing microorganisms, such as phosphate and glycogen accumulating organisms (PAOs and GAOs, respectively) plays a key role in order to get dense and stable aerobic granules (De

Kreuk and Van Loosdrecht 2004). Moreover, within one granule some communities are selected over others. This will assume an important role in the formation of the granules and their functionality. Likewise, the overgrowth of some communities must be avoided in order to prevent process disturbances. Nevertheless, the removal efficiency of nutrients in biological wastewater treatment systems has been proposed to be positively correlated to species richness (number of bacteria) and its distribution in a population (Winkler, Kleerebezem, and De Bruin 2012). Being the formation of mature granules a dynamic process, it is expected that premature granules present a natural morphology and microbial diversity in some degree dissimilar from mature granules.

The aerobic granule structure is characterized by the presence of an aerobic outer layer and anaerobic/anoxic core. Different layers comprise distinct bacterial species with various functional tasks (Aoi, Tsuneda, and Hirata 2004). Recurring to different techniques, (Weber et al. 2007) was able to partly unveil the microbial composition of mature granules. The peripheral zone contained ciliates and fungi growing on granule surfaces, while the core comprised a dense mixture of bacteria and EPS. Remnants of fungal filaments and ciliate stalks were included in the outer parts of the core zone (Weber et al. 2007). Depending on the size of the granules, the inner part of the core zone may contain only dead cell debris (Mcswain et al. 2005). As a consequence of the distinct microbial layers in aerobic granules, the microorganisms present in the granule present a non-arbitrary distribution, as they are dispersed according to their metabolic requirements. The oxygenation gradient in each granule enables the co-existence of aerobic nitrifying organisms in the outer layers and of PAOs, GAOs, denitrifying bacteria, as well as (facultative) anaerobic organisms towards the centre (Figure 3) (Winkler et al. 2012). This layer-based architecture in AGS allows the simultaneous removal of phosphorus, nitrogen and organic matter in the same system (Bento 2016; Beun, Heijnen, and Loosdrecht 2001; Mosquera-Corral et al. 2005).

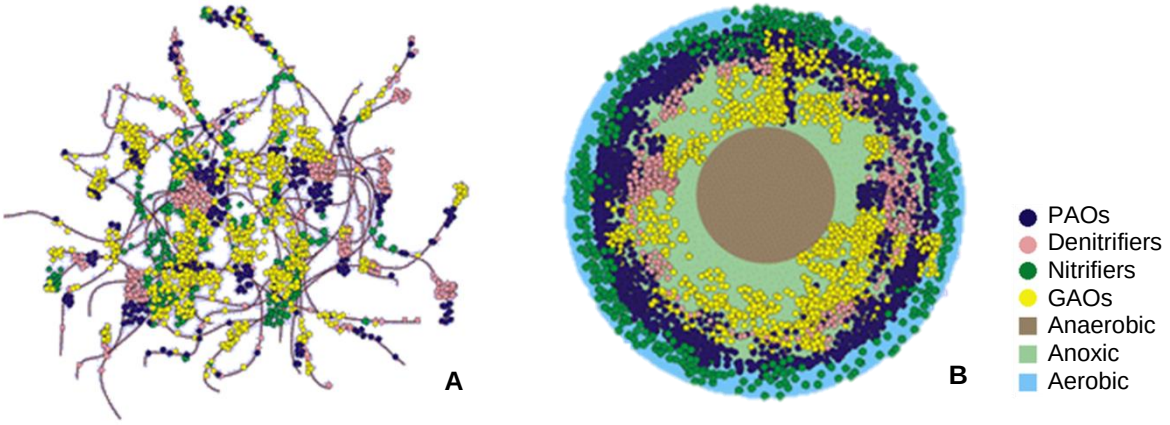

Figure 3. Distribution of different microbial communities (PAOs, GAOs, Nitrifiers and Denitrifiers) in conventional activated sludge (A) and aerobic granular sludge (B). (Adapted from Winkler et al. 2012)

Aside the difference in the spatial distribution of communities when comparing flocculant and granular sludge, there are some other slight differences regarding the communities in the two systems. A study conducted by (Winkler et al. 2012) concluded that the ammonium-oxidizing community of both sludge systems was more uneven than the general bacterial community. *Nitrosomonas* was clearly the dominant ammonia-oxidizing bacteria (AOB) in flocculent sludge, whereas in granular sludge, *Nitrosomonas* and *Nitrosospira* were present in equal amounts. It is proved that *Nitrosospira* is

negatively affected by high dissolved oxygen concentrations, prevailing mainly in environments low in dissolved oxygen (DO) (Park, Regan, and Noguera 2002). In the granular sludge, diffusion limitation is more severe, and finding organisms more adapted to low DO environments is therefore not surprising (Winkler et al. 2012).

1.2.3.4. Extracellular polymeric substances (EPS)

The abbreviation “EPS” is commonly used referring to extracellular polysaccharides or exopolysaccharides. However, EPS have been shown to be a rich matrix of polymers, including the two major components, polysaccharides (PS) and proteins (PN), but also humic substances, lipids, nucleic acids, uronic acids and some other inorganic components (Gao, Yuan, and Liang 2011; Mcswain et al. 2005; Sheng, Yu, and Li 2010). These diverse polymeric substances interact with each other through electrostatic forces, hydrogen bonds, attractive ionic forces and biochemical reactions, forming a dense and compact network structure. The polymers in EPS which are able to form hydrogels (Seviour et al. 2009) and contribute to the formation of the tertiary network structure are in this respect considered as structural EPS, a subset of the total EPS. EPS are accountable for the chemical structure and physical properties of aerobic granules (Flemming and Wingender 2010). It is therefore crucial to understand the function of each EPS component (Felz et al. 2016). The presence of EPS not only plays a key role in the formation of a gel-like network that keeps bacteria together in biofilms, but also protects bacteria against noxious environmental conditions and can even serve as carbon or energy sources in nutrient limitation conditions (Geyik and Çeçen 2015; De Kreuk et al. 2007; Mcswain et al. 2005).

The main structural difference between the particular case of AGS and a conventional biofilm is that AGS is formed spontaneously without involvement of any carrier material (Seviour et al. 2009). In AGS, like in biofilms, microorganisms produce a significant amount of highly hydrated EPS to form a hydrogel matrix in which they are self-immobilized (Felz et al. 2016). Some studies proposed that the EPS present in AGS was produced not only by bacteria, but also by other organisms present in the observed biofilm community, such as ciliates and fungi (Weber et al. 2007). The EPS that exist outside the cells can be subdivided into two distinct fractions: bound EPS (comprising sheaths, capsular polymers, condensed gels, loosely bound polymers, and attached organic materials) and soluble EPS (containing soluble macromolecules, colloids, and slimes) (Sheng et al. 2010). Bound EPS are closely bound to cells, while soluble EPS are weakly bound or dissolved into the solution. Similarly to the layered morphology of granules, the fraction of bound EPS closely englobing them is also heterogeneously distributed in a double layered manner. An inner layer of tightly bound EPS (TB-EPS) directly surrounds the cells while an outer one, composed by loosely bound EPS (LB-EPS), diffuses from the TB-EPS. Whilst the TB-EPS has been reported to be responsible for cell adhesion and attachment in the inner granule structure through strong interactions, LB-EPS is a loose and dispersible slime layer without an obvious edge, establishing weak interactions with surround substances, such as NPs (Liu et al. 2010; Sheng et al. 2010).

Despite being widely accepted as contributor to sludge aggregation, the precise role of EPS in this process is not clear yet. Some studies have demonstrated that the proportion of LB-EPS and TB-EPS, rather than their quantities, is more important in sludge aggregation (Liao et al. 2001). The

excessive LB-EPS in the outer region might deteriorate sludge aggregation, while it was not true for the case of the TB-EPS (Li and Yang 2007). The complex composition of EPS makes it difficult to explore the specific role of each constituent in sludge aggregation, and thus, the contribution of EPS has not been quantified (Liu et al. 2010). However, most of the parameters exposed in section 1.2.3.2., such as hydrodynamic shear force, have also been reported to influence the EPS development, namely the PS production that aids in the formation and stability of aerobic granules (Chen, Zhou, and Li 2010; Yang et al. 2016), thus confirming the apparent role of EPS in the granulation process. Still, several arguments exist against high shear force being a necessary factor for granule formation. Most notably, granules were not stable in airlift reactors operated with longer settling times and high aeration rates. Therefore, the relationship between shear force, EPS formation, and granule stability is still unclear (Mcswain et al. 2005).

1.3. Interaction of AgNPs with AGS

As aforementioned, AGS has been reported to present good tolerance levels to the presence of AgNPs in an initial phase, but the prolonged exposure induced chronic toxicity on AGS and led to cell death, resulting in the loss of microbial activity (Gu et al. 2014; Quan et al. 2015). Synthetizing, despite not causing acute toxicity to the AGS, the chronic toxic effects of AgNPs are still alarming. Thus, the analysis of AgNPs in biological samples is critical.

1.3.1. AgNPs analysis in biological samples

1.3.1.1. Overview

Due to the small size of nanoparticles, their localization and quantification in biological media and within cells constitute extremely challenging issues. Therefore, various cutting-edge techniques are required to detect and to quantify the metal content in biological materials, which comprise the NPs fraction, such as AgNPs.

Techniques, such as those based on characteristic X-ray analysis (e.g. particle induced X-ray emission - PIXE) (Johansson, Campbell, and Malmqvist 1995), and inductively-coupled plasma mass spectrometry (ICP-MS) (Fabricius et al. 2014) are multielemental techniques, which can accurately quantify the metal content in NPs, as in AgNPs. In general terms techniques based on mass spectrometry are the best ones available for elemental analysis. The sensitivity of these methods is variable. Despite providing bulk sample elemental concentrations these techniques are unable to offer a picture of NPs distribution in the sample matrix.

As aforementioned ICP-MS can assist in the determination of the bulk metal content associated with NPs in the biological material. Moreover ICP-MS presents high-sensitivity and high-accuracy for metal quantification, therefore both whole NPs and particle dissolution can be estimated following meticulous fractionation of the media (Kaegi et al. 2011; Shafer, Overdier, and Armstong 1998). Recent developments of ICP-MS operated in so-called single particle mode enable the characterization of inorganic NPs, simultaneously providing information regarding the elemental composition, number of particles, size, and size distribution. This requires a different approach than measuring dissolved elements. The mass-to-charge ratios (m/z) and intensity parameters are the most important for dissolved

ions, whereas for single particle a fast quadrupole speed is essential in order to separate transient signals for a single m/z ratio (Stephan and Neubauer 2014; Yang et al. 2016). Other ICP-MS modalities, which rely on hyphenation of chromatography systems (Mitrano et al. 2014) (HPLC), (Tiede et al. 2010) (hydrodynamic), (Franze and Engelhard 2014) (electrokinetic), have been applied to investigate the fate of AgNPs in wastewaters. These methods invariably require complex sample treatment to separate biomass fractions from supernatant without perturbing bound/adsorbed NPs. Thus quantifying NPs dispersed in the wastewater media is not a straightforward task. To tackle this problem there is a need of undemanding micro-analytical techniques capable of resolving NPs localization and their relative amounts in AGS fractions, especially within their biological structures.

The use of different methodologies is required in order to study the localization of NPs inside cells and in their specific compartments. Electron microscopy (EM) techniques are currently the gold standard, namely transmission electron microscopy (TEM) and scanning electron microscopy (SEM). The exceptional spatial resolution achieved, in the order of a few nanometers, provides the means to resolve single NPs from agglomerates, and determine the size and shape of the particles (Plascencia-Villa et al. 2012). Both techniques are based on the transmission of an electron beam (80–300 keV) as in TEM or on scattering of electrons (1– 30 keV). SEM focuses on the sample surface allowing large number of samples to be analysed but can only provide sample morphology on a three-dimensional (3D) representation. On the other hand TEM delivers two-dimensional (2D) images of the thin sample providing internal composition and structure but is restricted to ultra-thin sections, rising representativeness issues especially when NPs have to be assessed (Dudkiewicz et al. 2011).

The main drawback associated with TEM resides in sample preparation: chemical fixation, straining and dehydration are often required. In SEM the sample preparation problem occurs as well, the electron irradiation promotes the accumulation of static electric fields at the specimen. To overcome this problem samples are coated with a conducting material, occasionally resulting in loss of information. (Tiede et al. 2008) To characterize NPs in the biological environment a method with elemental analysis capabilities is required. This is possible with TEM and SEM by using Energy Dispersive X-ray Spectroscopy (EDX), although the method is not fully quantitative and sensitivity is poor due to high radiation background. In principle, sample image acquisition can be performed simultaneously to EDX allowing the localization of the electron dense NPs and detect the elements present in those entities. (Ostrowski et al. 2015; Tulve et al. 2015)

Other approaches recurring, for example, to optical microscopy modalities based on fluorescently tagged NP, such as confocal laser scanning microscopy and fluorescent correlation spectroscopy are relatively more simple alternatives to study NP interactions in either live or fixed cells (Fleischer and Payne 2014; Ostrowski et al. 2015; Vanhecke, Blank, and Petri-fink 2014).The drawback of these approaches, besides the limited axial resolution in specimens thicker than the focal point and fluorophore bleaching, is NP surface manipulation that inevitably will modify NP and eventually their mode of action (Tenzer et al. 2013).

1.3.1.2. Nuclear microscopy

Nuclear microscopy, also known as Nuclear Microprobe, is a powerful way to get information about the NP interactions with biological samples in general and cells in particular through the use of focused MeV ion beams, usually hydrogen and helium ions. As ions are charged they can be deflected and focused by electromagnetic and electrostatic fields. Due to their high momentum such ions penetrate the surface of materials and are able to probe the material into a depth that is determined by the ion energy. It was not until early 1980s when John Cookson at Harwell and Geoff Grime and Frank Watt at the University of Oxford designed and engineered a lens system capable of focusing a 2.0MeV ion beam to 1 μm diameter in vacuum, that a great breakthrough in ion beam analysis was realized (Mulware 2014). Currently, micron and even sub-micron spatial resolutions can be achieved to provide elemental imaging and quantitative elemental analysis of biological tissue down to μg/g level of analytical sensitivity (Mulware 2014).

The rationale behind an analysis of nuclear microscopy is image construction from the scattered particles impinging on the sample and elemental concentration calculation from spectral data acquired. The focused beam is scanned over the sample surface, and the strength of the relevant analytical signal is measured at each position of the beam in the scanned area to generate an image of the sample. Nuclear microscopy, combines several ion beam analytical techniques in order to obtain nano-micro-sized 2 dimensional (2D) images of the sample morphology and elemental distribution with depth information extracted from the calculated beam energy loss (Breese, Jamieson, and King 1996; Jeynes and Colaux 2016; Nastasi, Mayer, and Wang 2014; Watt et al. 2013).

The three most commonly used nuclear microscopy techniques are STIM (scanning transmission ion microscopy), PIXE (proton induced X-ray emission) and RBS (Rutherford backscattering spectrometry). By simultaneously using these techniques it is possible to extract spectral information to produce images of sample features and quantify elemental contents in the sample. Through the use of STIM, a map of the density variations in relatively thick or thin tissues/samples can be obtained, which enable sample structure visualization. Also, a trace map of elemental distributions at the cellular level can be obtained with PIXE, whereas RBS has the ability to examine the sub-surface layers of a sample and providing matrix composition and sample thickness for each beam position enabling fully quantitative analysis of elements detected with PIXE (Breese et al. 1996; Jeynes and Colaux 2016).

The physical basis of RBS relies on the detection and analysis of the projectile ions that are backscattered after interacting with the nucleus of the elements that compose the sample matrix. This allows the identification of the elements in the sample matrix, and the depth profile of those elements, as a consequence of the elastic collision between the incident ion and an atomic nucleus of the sample matrix, and the energy loss of the ion while traversing the sample during its path in and out of the sample, respectively (Oura et al. 2013). Elemental identification is possible since the energy of the backscattered particle depends on the mass of the atom that has been hit by the incident ion and on both charges. Also, the scattering is dependent on the depth of the atom in the sample, as protons lose energy in the trajectory in and out of the sample. The technique is well described and the most important parameters to consider are the kinematic factor *k* that relates the energy of the incident particle (E_0) with the energy of the scattered particle (E_1), (equation 1).

$$E_1 = k\, E_0 \qquad \text{(Equation 1)}$$

When the MeV ion beam is sufficiently energetic to pass through the sample, the energy lost by the transmitted particles, that did not suffer nuclear backscattering collisions at each position in the scanned area, depends exclusively on the sample elemental composition and on the density variations of the sample (thickness). The STIM technique measures the transmitted ion energies and the number of ions at each pixel within the scanned area (Mulware 2015). The map of the density variations can be obtained, routinely delivering high-resolution images (<0.5µm) of the sample morphology (Pinheiro, Ynsa, and Alves 2007). This technique is very useful as density variations are sensitive enough to depict cell structures, such as nuclei and various other structures depending on the specimen characteristics (Pinheiro et al. 2014, 2007; Watt et al. 2013).

In the case where the beam energy is sufficient to cause inner-shell ionization of atoms in the sample, the vacancy created will be promptly filled (in approximately 10^{-17}s) by neighbour electrons from an outer shell bringing the atom to its fundamental state. This transition results in a release of energy (photon), an X-ray, corresponding to the energy difference between the two states (Ortega, Devès, and Carmona 2009). Each element has a unique collection of energy levels that produce a unique set of X-rays, which are characteristic of the atomic species. This is the physical principle of the PIXE technique.

PIXE offers several advantages, being a multielemental technique, it provides analytical information from a wide-ranging number of elements simultaneously (virtually from Na to U). Compared to electron based X-ray spectrometric techniques, PIXE offers much better peak to noise ratios resulting in high trace element sensitivity, averaging in the µg/g range. For low atomic number matrices such as the ones found in biological samples the sensitivity increases to values below the ppm (Pinheiro et al. 2007). Moreover, PIXE enables trace elemental analysis from extremely small sample quantities, such as sample volumes under a micrometre dimension beam, without sensitivity loss. However, the matrix may vary strongly over a scale comparable with the beam diameter so that the bulk composition may not be appropriate for calculating matrix corrections. Also the beam charge may vary across the sample hampering an accurate beam charge calculation. This can be solved by using simultaneously RBS and PIXE. The analysis of the RBS spectra at each beam position gives local matrix composition and charge calculation, allowing the normalization of PIXE data.

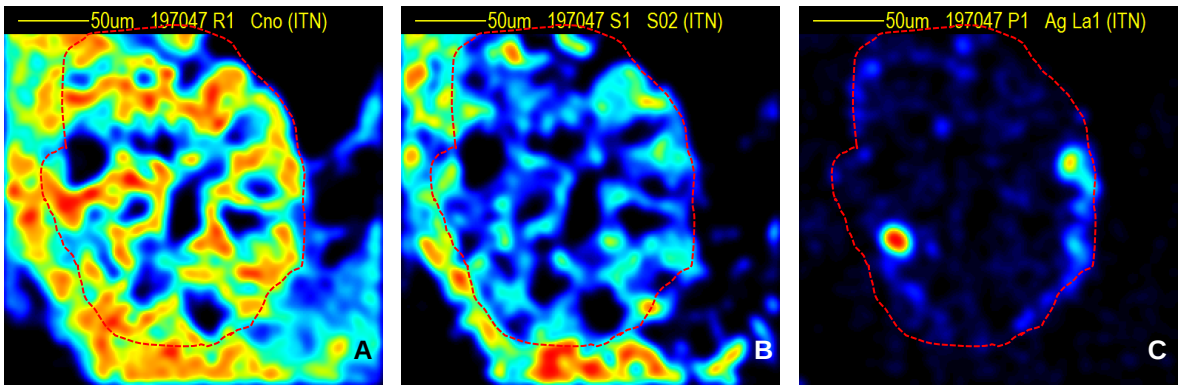

Figure 4. Nuclear microscopy images of a single section of an AGS granule. Sample thickness map provided by RBS (A), density variation map provided by STIM (B) where a radial like structure can be depicted and Ag elemental distribution map provided by PIXE (C), showing preferential Ag deposition at the periphery of the granule.

Besides quantitative analysis, the nuclear microscopy techniques also offers the advantage of performing correlative imaging (Figure 4). For instance, the images of the sample structure based on density variations extracted from the STIM spectral data can be correlated with elemental distributions obtained by PIXE enabling a direct association of one specific element to sample features.

Therefore, nuclear microscopy presents unique advantages in the study of NP interaction with individualized cells and biological systems. In addition, due to the minimal sample preparation required (Pinheiro et al. 2007) nuclear microscopy can be a useful tool to assess the acquisition of intracellular NP quantities (Vasco et al. 2017), their localization in specific compartments (Godinho et al. 2014), and ultimately contribute to unravel key cellular mechanisms of NP binding, uptake and transport.

1.4. Interaction between AgNPs and aerobic granule EPS

As aforementioned in section 1.2.3.4. the presence of EPS in sludge system proves to have a protective effect in bacteria against noxious environmental conditions (Mcswain et al. 2005). Considering the particular case of heavy metal exposure, a protective effect is verified as a permeability barrier blocks intracellular penetration of metals. The naturally amphiphilic composition of some EPS constituents and the presence of multiple active functional groups and/or charged moieties (e.g., carboxyl, phosphoric, sulfhydryl, phenolic and hydroxyl groups), as well as hydrophobic moieties that can complex with heavy metals, thus attenuate toxicity (Kang, Alvarez, and Zhu 2013; Sheng et al. 2010; Wang et al. 2016). It was recently demonstrated that EPS can biosorb both Ag^{+} and AgNPs, mitigating the well documented antibacterial activity of Ag+ (Bento 2016; Geyik and Çeçen 2015). The reduction of Ag^{+} to AgNPs by EPS was also previously shown, the originated AgNPs would be then entrapped within the EPS matrix (Kang et al. 2013). Other researchers have suggested that these extracellular biomolecules can effectively adsorb on NPs, forming a protein corona which imparts them with biological identity, thereby altering the cell membrane affinity, uptake, and retention of NPs and reducing their bactericidal activity (Fleischer and Payne 2014).

Another unclear issue regarding EPS concerns the extraction methodologies, despite some studies proving that the EPS distribution depends on: the microbial aggregate types; structures and origins; culture growth phase; process parameters; and bioreactor type (Nielsen and Jahn 1999). The major components of EPS fractions, and total EPS quantity (Adav et al. 2008; Comte, Guibaud, and Baudu 2006), also depend strongly on the extraction methods (Sheng et al. 2010).Various approaches are applied to extract EPS (Adav et al. 2008; Comte et al. 2006; Fang and Jia 1996; Liu and Fang 2002; Pan et al. 2010). However, due to their extreme complexity, it is almost impossible to extract all the EPS components by one single method. The ideal method to extract and quantify the totality of EPS components is yet to be developed. Depending on the type of sludge and the EPS of interest, different methods proved to be useful (Felz et al. 2016). Nonetheless a typical EPS extraction procedure includes the following steps: (1) *pre-treatment*, including sampling, washing, and physical disruption. This allows the microbial cells to be dispersed. For EPS extraction from microbial granules, physical disruption is usually needed; (2) *EPS extraction*; (3) *Purification*; (4) *Analysis*. Given the multiple difficulties in quantification of known EPS constituents, only the quantification of PN and PS fractions were considered in this study.

1.5. Scope and objectives

The major aim of this thesis was to characterize the interaction of AgNPs with an AGS system. One of the focal points was the assessment of the AgNPs long-term exposure effects and spatial distribution within an AGS system. Two SBR systems were set up in the same operational conditions, one supplemented with AgNPs and the other used as AgNPs-free control, and their performance was consistently evaluated. Recurring to nuclear microscopy technics, efforts were made to quantify the AgNPs concentration in granular sludge structures, in the adopted SBR systems. This work also aimed to achieve an optimized procedure to extract and quantify the major EPS components, i.e., protein and polysaccharides, in order to later assess their content variations in both reactors. Thus, the effects of the AgNPs exposure on the EPS content of the biomass were also subject of investigation.

2. Methods

2.1. SBR operation and performance assessment

2.1.1. Experimental layout and SBR cycle operation

The experimental system included two bubble-column SBRs, SBR1 and SBR2. Both reactors had a working volume of 1.5 L (height/diameter ratio of 2.5) and were set-up in identical conditions. The following operational parameters were adopted: 6-h cycles (12-h HRT) with 5 sequential phases, namely, fill (30 min), react (anaerobic and aerobic, 1.5h and 3.5h respectively), settle (5 min), drain (1 min) and idle (30 min).

The SBRs were fed with a synthetic textile wastewater provided separately as carbon feed solution (Feed-C) and nitrogen dye-containing feed solution (Feed-N) to minimize the risk of contamination, with an exchange ratio of 50% and a volumetric organic loading rate (OLR) of 2.0 kg COD m^{-3} d^{-1}. The reactors, were fed through a peripheral site at the bottom of the reactor, with the feed rapidly channelling across the settled biomass with no relevant contact between biomass and feed solution during the fill phase.

The difference between the SBRs reside in the fact that at the end of the fill phase, SBR1 was supplied with AgNPs (<100 nm) at the top of the bioreactor whereas SBR2 was used as AgNPs-free control. Nonetheless, the provided synthetic wastewater components were in the same relative proportions in the two SBR.

Peristaltic pumps (Mini-S 660, Ismatec, Switzerland) were used to feed the synthetic wastewater to the reactors, and after AGS settling, the drain of the supernatant was achieved using gear pumps (Reglo-Z, Ismatec, Switzerland). Mechanical mixing during the non-aerated reaction was provided by magnetic stirring using an anchor-like impeller at 70 rpm. During the aerobic reaction, aeration (2 v.v.m) was supplied through air compressors (SPP-20 GJ-L, Hiblow, Japan) via a porous membrane diffuser at the bottom of each bioreactor. The pumping, aeration and agitation functions were automatically controlled, via an interface, by a dedicated software.

2.1.2. Simulated textile wastewater

2.1.2.1. Feed-C preparation

The Feed-C solution was prepared by diluting the carbon source stock solution (100 g/L) in distilled water to a COD content of 1000 mgO_2/L (1.15 g/L Emsize E1) and supplemented with the following nutrients: $CaCl_2$ (27.5 mg/L); $MgSO_4 \cdot 7H_2O$ (22.5 mg/L); $FeCl_3 \cdot 6H_2O$ (250 µg/L). Emsize E1 (Emsland-Starke GmbH, Germany) is a potato-starch-based sizing agent used in the textile industry. One litre of stock solution is obtained by dissolving 100 g of Emsize E1 and 40 g of sodium hydroxide in 500mL distilled water during 15 hours stirred at room temperature. At that point the hydrolysed solution is neutralized to pH 7 with 80 mL HCl (37%) and diluted with distilled water to make up a final volume of 1L.

2.1.2.2. Feed-N preparation

The feed N was prepared by diluting in distilled water phosphorus and nitrogen salts, an azo dye (AR14, Chromotrope FB, Sigma Aldrich, 50% dye content) and other micro-nutrients. The dissolved components were: $Na_2HPO_4 \cdot 12H_2O$ (2.31 g/L); KH_2PO_4 (762 mg/L); NH_4Cl (143 mg/L); AR14 Chromotrope FB, Sigma Aldrich, 50% dye content (40 mg/L); $MnSO_4 \cdot 4H_2O$ (40 µg/L); H_3BO_3 (57 µg/L); $ZnSO_4 \cdot 7H_2O$ (43 µg/L) and $(NH_4)_6Mo_7O_{24} \cdot 4H_2O$ (35 µg/L). The dye stock solution was prepared by dissolving AR14 in distilled water to a final concentration of 5.0 g/L. The AR14 concentration at the onset of the reaction phase (after the fill phase) was 20 mg/L.

2.1.3. AgNPs feed suspension preparation

The AgNPs suspension was prepared by diffusing 100mg AgNP nanopowder (<100 nm particle size, Sigma Aldrich) in 1L milli-Q water using sonication (60 minutes at 80W) (VWR, international bvba/sprl, Belgium) to promote the NPs dispersion. After sonication, this suspension was once again diluted with 1L milli-Q water to a final concentration of 50 mg/L. The AgNPs concentration in SBR1 at the onset of the reaction phase (after the fill phase) was 10 mg/L.

2.1.4. SBR inoculation and aerobic granulation

The SBRs were inoculated with the same biomass composed by activated sludge flocs (1.4 g TSS/L) harvested from a full scale, conventional municipal WWTP (Chelas, Lisboa, Portugal). Aerobic granulation was induced by progressively reducing the settling time while providing sufficient high shear stress and a feast/famine regime. The settling times were progressively reduced from 1 hour to 5 minutes along the first 28 days of operation and maintained at 5 minutes during the rest of the experimental run. The shear stress was provided by mechanical mixing during the anaerobic phase and by aeration in the aerobic phase.

2.1.5. SBR cycle monitoring

The two SBRs were monitored once a week during the total operational period (268-days). The performed analyses are listed below, being the applied procedures the same for both bioreactors. The SBR cycle operation was interrupted between days 193 and 212. During this 18-day period the biomass was stored in the dark at 4ºC in closed glass containers. After this hiatus the biomass was added to the respective SBR and the operation resumed under the same, previously used, conditions.

2.1.5.1. Total and volatile suspended solids

Total suspended solids (TSS) and volatile suspended solids (VSS) were measured in samples collected from the effluent and the mixed liquor of the reactors according to standard procedures (APHA , 1995). Briefly, different volumes were retrieved from effluent and the mixed liquor, 20 mL and 10 mL, respectively, due to their different solids content. Glass microfiber filter discs (Whatman, GF/C, ø 47 mm) were firstly washed with distilled water in a vacuum filtration system and later dried in a drying

balance (HB-43-S, Mettler-Toledo). The filter discs were then heated in a muffle furnace (Nabertherm, L3/S27, Germany) for 1 hour at 550°C to eliminate any possible contamination. Lastly, the filter disks were weighted in an analytical balance (Mettler AE160) to determine the mass of each empty filter.

Each sample was collected with agitation either from the reactors (mixed liquor) or effluent containers (effluent), being filtered in the same vacuum filtration system, using the previously prepared filters. Afterwards, the discs used to filter the samples were dried and weighted in the drying balance. TSS content was calculated by equation 2.

In order to calculate VSS content the same filters were submitted to a 550ºC heating in the muffle furnace and weighted in the analytical balance. VSS content was calculated by equation 3.

$$\text{TSS content} = \frac{\text{mass dry filter (with sample)} - \text{mass filter (empty)}}{\text{Volume of sample}} \quad \text{(Equation 2)}$$

$$\text{VSS content} = \frac{\text{mass dry filter (with sample)} - \text{mass dry filter (with sample after 550ºC heating)}}{\text{Volume of sample}} \quad \text{(Equation 3)}$$

2.1.5.2. Quantification of mass fractions

This assay was based on the above-described VSS procedure since this was the adopted method to quantify the biomass in the different considered fractions. A 20 mL sample was retrieved from each bioreactor and successively sieved through diverse sieves in a decreasing order of pore diameter. The use of sieves with different pore diameters allows the separation of biomass in three different fractions: d>0.65mm (large granules), 0.20mm<d<0.65mm (granules) and d<0.20mm (flocs). This categorization considered the granules as the aggregates with a diameter of at least 0.2mm, as firstly proposed by De Kreuk et al. 2007. The obtained biomass fractions were then independently estimated by VSS, ultimately revealing the relative presence of granular and flocculent biomass in each reactor.

2.1.5.3. Sludge volume index (SVI)

SVI assays were conducted in Imhoff cones. SVI_5 and SVI_{30} were determined by measuring the volume occupied by the sludge settled from 1L of mixed liquor after 5-min and 30-min settling, respectively, and dividing it by the mixed liquor TSS value.

2.1.5.4. Chemical Oxygen Demand (COD)

For COD analysis, six samples were collected from each reactor along the reaction step of each monitored treatment cycle, three samples in the anaerobic phase and other three in the aerobic phase. Using a micropipette, 10mL samples were collected simultaneously from the centre of each reactor. The samples were then centrifuged (10 min at 4000 rpm), the pellet was discarded and further analysis were done recurring to the obtained supernatant. The procedure was adapted from APHA (1995). Firstly, 1.5mL of sample was put in a glass tube followed by the addition of 1 mL of potassium dichromate ($Cr_2O_7^{2-}$) solution, and 2 mL of solution of sulphuric acid (H_2SO_4) containing silver sulphate (Ag_2SO_4), in a highly exothermic reaction. At this time, after carefully closing and mixing the tubes, these were placed

in a digester at 148ºC for 2 hours (thermoreactor TR420, Spectroquant, Merck). After cooling to room temperature, the content of each tube was transferred to a 50mL Erlenmeyer and a drop of ferroin was added. Ferroin solution acted as the oxidation-reduction indicator. The dichromate in excess was determined by titration with a 0.025M ferrous ammonium sulphate solution (FAS). The solution containing the sample progressed from green to light blue and transparent before turning orange, indicating the end of the titration. The volumes of the consumed FAS required were measured twice since the assay was performed for two identical duplicates, distilled water was used as blank.

2.1.5.5. Colour assessment

For colour analysis, part of the supernatant obtained after centrifugation of the 10mL samples was used. The concentration of Acid Red 14 (AR14) present in these samples was determined recurring to a spectrophotometer (Specord 200; Analytik Jena, Germany). By reading the absorbance of samples at 515 nm and applying a previously established calibration curve (Annex 1), it was possible to obtain the concentration of dye along the reactors reaction step. Distilled water was used as blank.

2.1.5.6. pH analysis

Once again, the same supernatants were used to perform pH measurements using a Metrohm 6.0202.100 glass electrode connected to a Metrohm 691 potentiometer (Metrohm, Switzerland).

2.2. EPS analysis optimization

Being this thesis a direct prolongation of the work already carried out in Bento (2016), the starting point for methodology optimization was somewhat defined. Additional tests were carried out to further optimize the methods for EPS analysis assessing the influence of external factors. Some of these performed tests justified the execution of the following ones. Thus, to better comprehend the reasons supporting the execution of these tests in higher detail please consult section 3.2.

The optimized procedure used to analyse EPS content in section 3.4. was a direct result of the conducted experiments in this thesis. The comprehensive description of the applied protocol can be found in the result section 3.3.

2.2.1. Influence of ionic silver (Ag+) on PN and PS quantification methods

The first preliminary test aimed to determine if the presence of Ag^+ interfered with the proposed PN and PS quantification methods. EPS were heat extracted from AgNPs-free control SBR2 and supplemented with different $AgNO_3$ concentrations (0, 1 and 5 mg/L).

2.2.2. Effects of different pre-extraction methods on EPS extraction efficiency

To evaluate the impacts of pre-extraction methods on PN extraction efficiency, three different approaches were tested. In Method 1, sludge samples collected from SBR 2, were only pre-treated by mixing vigorously with a pipette until a homogeneous sludge suspension was obtained. In Method 2, in

addition to method 1, the sludge suspensions were further sonicated during 60 minutes at 80W (VWR, international bvba/sprl, Belgium). Finally, in Method 3, after methods 1 and 2 were performed, the sludge samples were mixed for 30 seconds using a vortex mixer.

2.2.3. Effects of different extraction methods

EPS were extracted from different mixed liquor samples from SBR2 with two alternative procedures, one recurring to heat treatment and the other via Cation Exchange Resin (CER). Both PN and PS content were later quantified.

2.2.3.1. Cation exchange resin (CER) extraction

The bound EPS were extracted from sludge samples through incubation with a cation exchange resin (CER) (Dowex® MARATHON®, 20- 50 mesh, Sigma Aldrich, St Louis, USA) according to (Frølund et al. 1996)) with minor modifications. In brief, 75 mg of the Na^+ form of CER per g of volatile suspended solids (VSS) were added to the biomass pellet re-suspended in 5 mL EPS extraction buffer (2 mM $Na_3PO_4 \cdot H_2O$, 4 mM $NaH_2PO_4 \cdot 12H_2O$, 9 mM NaCl, 1 mM KCl, pH 7) and stirred at 600 rpm for 2h. Next, the sample was centrifuged at 4000 rpm for 20 min, the bound EPS fraction being uncovered in the supernatant.

2.2.3.2 Heat extraction

The extraction of the bound EPS from sludge samples was carried out by heating the mixture suspensions to 80°C for 30 min in a water bath. Then, the suspensions were cooled down to room temperature and centrifuged at 4000 rpm for 20 min. Prior to EPS component analysis, the supernatant was further filtered through glass microfiber filter discs (Whatman, GF/C, ø 25 mm).

2.2.4. Influence of different EPS sample dilutions on PN and PS quantification methods

EPS were extracted by heat treatment from different mixed liquor samples of both SBRs and were diluted in EPS extraction buffer prior to PN and PS quantification. The dilution factors were selected so that the final absorbance values of the EPS component determination remained within the assay working range (Annex 2 and 3). Dilution factors of 1, 2, 4 and 10 were tested

2.2.5. Protein precipitation using trichloroacetic acid (TCA)

Different concentration of trichloroacetic acid (TCA) were tested (13, 20 and 30%). Additionally, the influence of 1mg/L of $AgNO_3$ on protein precipitation efficiency was also assessed.

2.2.6. Influence of sample storage on EPS PN and PS content

Mixed liquor samples (5ml) were collected from SBR2 in different reaction time points and dewatered by centrifugation at 4000 rpm for 10 min. Next, these samples were either used directly for EPS extraction and analysis, or stored at -80ºC. After six days of storage, EPS were heat extracted and PN and PS content was analysed.

2.2.7. Influence of extracted EPS storage on PN and PS content

Mixed liquor samples (5ml) samples were collected from SBR2 in different reaction time points and dewatered by centrifugation at 4000 rpm for 10 min. Next, EPS was heat extracted and was either used directly for PN and PS analysis, or stored at -20ºC. After six days of storage, the PN and PS content was analysed.

2.3. Elemental distribution and quantification

2.3.1. Quantification of Ag in AGS granular fraction

2.3.1.1. Sample preparation (for nuclear microscopy)

In order to access the AgNPs distribution within the granule, samples of mixed liquor (2 mL) were collected from SBR1 and SBR2 at the beginning of the reaction phase (t=0h) along different days in the same operational period. With the help of a magnifier glass individualized granules were manually isolated and enclosed in a resin-like material (OCT™ compound) to allow the generation of thin slices. At this point the enclosed granules were quench-frozen in liquid nitrogen. The sectioning of the encapsulated granule was performed in a cryotome (-22ºC working temperature) (Cryotome 620E, Termo Shandon, Cheshire, UK). The attained granule-containing sections with 20 µm thickness were allowed to dry overnight in the cryostat (-22ºC). The obtained sections were kept in petrislides™ and stored at -80ºC until analysis. For nuclear microscopy analysis, the preserved sections were mounted in appropriate frames in a self-supporting mode hold by the edges in carbon conductive adhesive tape (Agar Scientific, UK).

2.3.1.2. The Nuclear Microscopy layout and data acquisition

Sections of AGS were analysed by nuclear microscopy using the set-up installed at the Van de Graaff accelerator of the Campus Tecnológico e Nuclear (CTN) of the Instituto Superior Técnico (Figure 5).

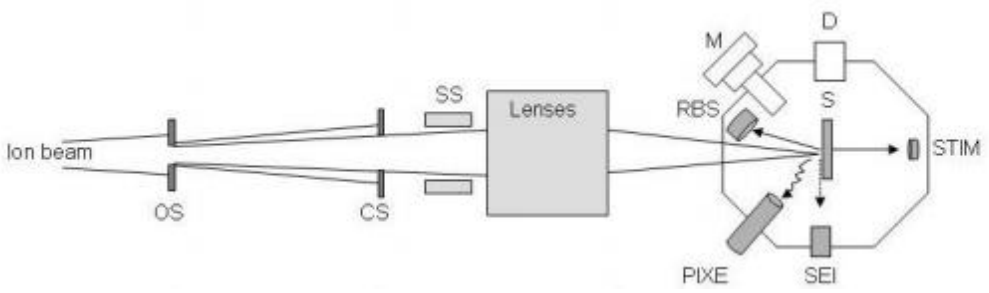

Figure 5. Diagram of the lay-out of the nuclear microprobe installed at Centro Tecnológico Nuclear (CTN). (Adapted from Pinheiro *et al.*, 2007). OS and CS – object and divergence limiting slits; Lenses – quadrupole lenses system for beam focusing; SS – scanning system for beam deflection. The chamber configuration (Oxford Microbeams Ltd. enables a microscope (M) and several detectors for X-rays (PIXE), for backscattered particles (Si surface barrier detector for RBS) for transmitted particles (collimated windowless photodiode for STIM), for secondary electrons (scintillator and photomultiplier system or a channeltron for SEI) and an additional position – D, for other detector.

The analyses were carried out with a 2.0 MeV proton beam focused with a quadrupole lenses system to micrometre dimensions, typically below 3x3 μm^2 and with a beam current of 100-200 pA. The focused beam was used to scan across AGS sections and selected areas of interest of those sections. Beam deflection is carried out with a dipolar magnetic system, that enables scanning the beam over the sample surface in 256 ×256 steps, encompassing a maximum area of 2.6 ×2.6 μm^2 for 2 MeV protons. The proton microprobe delivers 2 dimensional (2D) images of the sample morphology (STIM scanning transmission ion microscopy) and elemental distribution (PIXE – proton induced X-ray emission) with depth information extracted from the calculated beam energy loss with Rutherford backscattering spectrometry (RBS) (Breese et al. 1996; Jeynes and Colaux 2016; Nastasi et al. 2014; Watt et al. 2013). The use of PIXE allowed the production of distribution maps for the elements of interest such as P, S Cl, K, Ca, Fe, Zn and Ag.

The dedicated software OMDAQ (Grime and Dawson 1995) was used for data acquisition and map construction, whereas DAN32 (Grime 1996) computer code was used for spectra analysis and quantitative determination of elemental contents as discussed below.

2.3.1.3. Nuclear microscopy techniques and elemental quantitative analysis

Data from the STIM, RBS and PIXE are simultaneously obtained. Transmitted protons, which were collected to form the STIM image, were detected using a PIN-diode detector placed off beam axis at 20º to the beam (Figure 5). Images of the sample density obtained by STIM were used to identify the morphology of the AGS granular structure and external EPS organization. A silicon particle detector at a backward angle of 40^0 to the beam was used to detect backscattered particles and form the RBS image. The emitted X-rays (PIXE) were detected using a Si(Li) detector with an active 80 mm^2 area, positioned at 45º to the beam. The concentration of Ag has been determined by PIXE with high quantitative accuracy using the RBS data obtained for the sample matrix composition and thickness to mass normalization.

There are some uncertainties associated in an absolute PIXE analysis, as the results not only depend from the total deposited beam charge but also the local matrix composition, which may vary strongly over a scale comparable with the beam diameter. When PIXE and RBS analysis are performed simultaneously, the normalization procedure of PIXE data can be achieved recurring to the Q-factor method developed by Geoffrey Grime in 1996, thus enabling the calculation of absolute concentration values. This method consists in a ratio between the measured charge (provided by the area of the RBS spectrum) and the true charge (measured by the acquisition system) to correct the PIXE spectrum provided a well-defined, fixed geometry of RBS and PIXE detectors, and an appropriate calibration of the PIXE detector efficiency (Grime 1996). Given the concentration depth profile $C_{(Z)}$ of an element with atomic number Z in the sample is constant, the X-ray intensity $I_{(Z)}$ for the characteristic X-ray of this element in the sample is given by equation 4:

$$I_{(z)} = Q\, C_{(Z)}\, K_{(Z)} \qquad \text{(Equation 4)}$$

Where Q is the total beam charge and $K_{(Z)}$ is a calibration constant independent of the sample, in the case that both experimental geometry and sample matrix composition are constant (Grime and Dawson

1995).

This was the adopted approach, being the sensitivity of the method for Ag determination in the AGS biological material about 10-20 µg/g on a dry weight basis. Concentration profiles were obtained by analysing a sequential number of points (corresponding roughly to the focused beam area) along transepts of the scanned section. The AGS cryo-sections were analysed in vacuum and Ag concentrations are expressed in µg/g on a dry weight basis.

2.3.2. Quantification of Ag in reactor mixed liquor and effluent fractions

2.3.2.1. Sample preparation (for PIXE and ICP-MS)

Duplicate 5mL samples were retrieved from bioreactor 1 and 2, as well as from the respective effluents and AgNPs feed solution. Total AGS samples, biomass and supernatant fractions and effluent were analysed using two techniques according to sample characteristics. Solid fractions or residue obtained by drying, filtration, or centrifugation were analysed by PIXE, whereas liquid fractions (supernatants and filtrates) were analysed by ICP-MS.

To obtain biomass and effluent fractions, samples collected from the reactor and samples of the effluent, except the AgNPs feed, were filtered using polycarbonate filters of 0.2 μm pore (Whatman® Nuclepore™ Track-Etched Membranes) in order to separate the solid and liquid fraction. Biomass fraction was retained in the filters, which were stored in Petri slides and dried in a freeze dryer (Edwards, USA) and stored at -80ºC until further study. Depending on the amount of biomass fractions retained in the filters sample preparation for Ag concentration determination by PIXE may differ. If the biomass amount was large and it detaches from the filter, it has to be homogenized by shaking vigorously the material. The homogenized sample is then pelletized using 10 Ton pressure. If the biomass amount was adherent to the filter it can be analysed directly. Filters were weighed before use and after filtration to obtain the mass filtered (wet and dry mass). Volume filtered was also controlled therefore Ag concentrations can be expressed in both dry mass and volume fractions.

The liquid fractions of the filtered samples (from the reactor and effluent) were acidified with 10% v/v HNO_3 suprapure and homogenized in ultrasound bath at 40ºC for 3 cycles of 1h each. Samples were stored at -80ºC until further analysis. The sample preparation for Ag determination by ICP-MS required filtration before analysis (Whatman Swinnex filter of 0.2 μm pore), dilution and addition of an internal standard. For ICP-MS analysis, the filtered samples were diluted at least 2-fold with ultrapure water to obtain solutions of 5% HNO_3 (v/v) which are adequate for analysis. Subsequent dilutions whenever needed were done using acidified 5% (v/v) HNO_3 ultrapure water. Samples were doped with Y (Yttrium) as an internal standard at a concentration of 10µg/L.

Total AGS aliquots and AGS pellets obtained by centrifugation (4000 rpm, 10 min) were also analysed by PIXE. These samples were first freeze-dried and subjected to acid digestion with a mixture of H_2O_2 and HNO_3 (Merck suprapure reagents) in a proportion of 100 mg of sample to 200 µL of H_2O_2 and 2400 µL of HNO3. The digestion was carried out in Teflon Bombs (Parr, Inc, USA) using a commercial microwave (Miele™) at 300 W during 4 min. From the resulting solution 10 µL were deposited onto a polycarbonate film and analysed, as described elsewhere (Pinheiro et al. 1997; Pinheiro, Duflou, and Maenhaut 1990).

Stock solution of 1000 ± 10 µg/L of Y (AAS Specpure Y solution; Alpha Aesar,Ward Hill, MA,USA) was used for internal standardization and preparation of spiked samples. Ultrapure water of 18 MW·cm (Milli-Q Element; Millipore, Billerica, MA, USA) was used for dilution of samples, stock solutions and to prepare blank solutions. Concentrated Suprapur nitric acid (HNO_3) high-purity grade was obtained from Merck (Darmstadt, Germany)

2.3.2.2. PIXE measurements: Ag concentration in filters, dry residues and pellets

The PIXE technique is implemented at the Van de Graff accelerator of the CTN/IST. A 5mm diameter proton beam of 2.0 MeV with a typical current of 80-100 nA was used. The analyses were performed in vacuum. An instrumental calibration of the PIXE set-up was performed (Reis and Alves 1992), which is based on the analysis of monoelemental samples to generate an efficiency curve that can convert X-ray yields into concentrations. Briefly the relationship between the observed X ray intensity (I_i) emitted by sample bombardment with the incoming particle beam (number of particles or charge Q) and element concentration C_i is given by equation 5:

$$I_i = Q\ C_i\ K_i \qquad \text{(Equation 5)}$$

Where the calibration constant Ki is independent of the sample if both geometry of the experiment and sample matrix composition is homogeneous (Johansson et al. 1995). PIXE spectra were analysed through AXIL adjustment program using a non-linear least square method (Van Espen, Janssens, and Swenters 1986), and the concentration calculations performed with the computer code DATTPIXE as described elsewhere (Reis and Alves 1992).

2.3.2.3. ICP-MS measurements: Ag concentration in liquid fractions

All the analytical process was carried out according to the instructions of the equipment manufacturers regarding the chemical elements of interest (Stephan and Neubauer 2014).

The ICP-MS equipment, ELAN DRCe (PerkinElmer, SCIEX, Waltham, MA, USA) available at CTN/IST was operated at 1100 W, with argon gas flow of 15 L/min and 0.85 aerosol L/min gas carrier using a Peltier-cooled cyclonic spray chamber. Data acquisition was done at peak-hopping mode with 50 ms dwell time, 20 sweeps/reading, 1 reading/replicate, and 3 replicates. Quantitative analysis was carried out based on an external calibration using Y as an internal standard. Data were collected, processed, and analysed with ELAN 3.4 software.

Multielement standard ICP-MS STD3 solution (Perkin Elmer, USA) was used for calibration (Annex 4). Calibration standards were made in 5% HNO_3 at the levels of 5, 10, 20, 30, 40, 50 mg of Ag/L. Each standard concentration was doped with Y as an internal standard at a concentration of 10µg/L. The calibration blank was a 5% HNO_3 solution and blank subtraction was used. The ^{107}Ag isotope was monitored.

A certified reference material (CRM) Trace Elements in Water (1643e from the National Institute of Standards and Technology), with an aqueous matrix and containing Ag (1.062 $\pm$0.075 µg/L) was used

to validate the methodology and analytical procedure. The precision obtained in the CRM analysis was better than 5%.

3. Results and Discussion

3.1. SBR cycle monitoring

The operational data presented in the current section (3.1) was obtained by Rita Franca and Miguel Coelho, who gently conceded it to figure in this thesis, as it was considered of great relevance for the discussion. Only a slight portion of the data is displayed, concerning the results from operational days 162 to 268, translating in a total of 16 weeks. Thus, the granulation period is not contemplated and consequently, in the beginning of the reported period the two reactors presented a stable operation.

3.1.1. Total and volatile suspended solids

The biomass content in a biological wastewater treatment reactor is assessed through the analysis of VSS. However, as the method for TSS determination is faster than that for VSS, TSS values are commonly used as an indication of biomass content. Nonetheless, given the possible contribution of AgNPs to the inorganic solids fraction and consequent impact on TSS measurements, TSS and VSS were measured for the two bioreactors, for both mixed liquor and effluent fractions and the correspondent VSS/TSS ratios were calculated. These results are presented in Figure 6.

Overall, the VSS and TSS profiles obtained for the mixed liquor samples (Figure 6A and Figure 6C, respectively) indicated that the AgNPs-fed SBR1 had higher suspended solids (averaging 4.4 and 5.0 g/L for VSS and TSS, respectively) than the AgNPs-free SBR2 (averaging 3.3 and 3.7 g/L for VSS and TSS, respectively) during the reported experimental period. On the other hand, SBR2 presented higher VSS and TSS values in the effluent (Figure 6B and Figure 6D, respectively) for the majority of the cycles monitored during the reported period.

The patterns of both TSS and VSS values for the effluent fraction were more erratic, since the biomass discharged from the bioreactors at each cycle was variable. The TSS and VSS measurements concerning the effluent indicated that SBR2 discharged a larger amount of biomass than SBR1 after the 18-day storage period between days 193 and 212, possibly indicating that the settling capabilities were more affected in SBR2. This fact was also corroborated by the differences of morphology exposed in section 3.1.6. SBR2 consistently presented a smaller granular percentage than SBR1, which implicates a poorer settleability that ultimately leads to biomass washout.

The graphical representations of VSS/TSS ratio display the contribution of VSS for each TSS measurement, i.e. the percentage of organic matter in the total suspended solids for both mixed liquor and effluent (Figure 6E and Figure 6F, respectively), hence constituting an alternative way to present the VSS and TSS data. With these calculations the effect of AgNPs in the TSS measurements of the AgNPs-feed bioreactor is clear. Through Figure 6E it was possible to perceive that the AgNPs-free SBR2 presented slightly higher ratio values (averaging 89.6%) than SBR1 (87.4%). This result suggested that despite SBR2 being the reactor with the lower VSS amount, VSS assumed a larger contribution for the TSS values due to the reduced inorganic fraction partly caused by the absence of AgNPs. Figure 6F showed that all discharged effluents, before the storage period, presented similar VSS/TSS ratios, suggesting that the fed AgNPs were retained within SBR1, being negligible the content of AgNPs in the discharged biomass of SBR1. So, most likely, the majority of the biomass discharged was part of the

flocculent fraction, which might have a lower adsorption capacity for AgNPs due to the lower amount of EPS typically present in biomass flocs. The VSS/TSS ratio in the mixed liquor presented low variability across the monitored period. The storage period the biomass underwent did not affect these parameters. However, the TSS and VSS concerning the reactors effluents suffered an increase after this storage period.

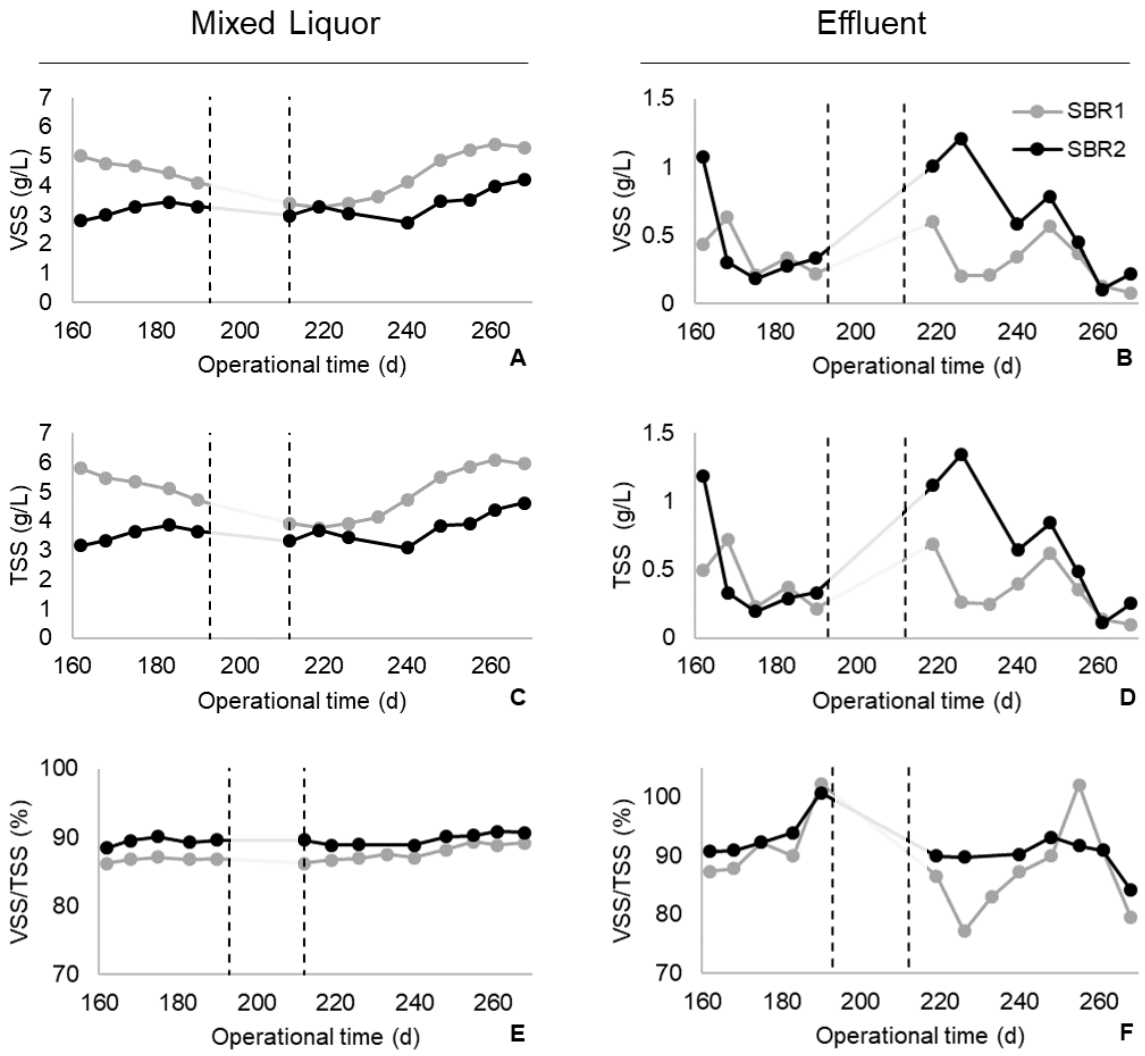

Figure 6. VSS content (g/L) of mixed liquor (A) and effluents (B). TSS content (g/L) of mixed liquor (C) and effluents (D). VSS/TSS ratios in mixed liquor (E) and effluents (F). The vertical lines comprise the storage period.

3.1.2. Sludge volume index (SVI)

The combination of SVI_5 and SVI_{30} can be very useful to deduce the settling capabilities of AGS. Typically, AGS presents low SVI values indicating good settleability capabilities. The SVI_5 and SVI_{30} are also expected to present similar values, indicating that the majority of biomass settles in the first five minutes.

In this case the settleability of AGS in the two reactors was compared. Through the analysis of the global SVI results (Figure 7) it is possible to see that the settleability in SBR1 and SBR2 deteriorated

immediately after the storage period (between days 193 and 212). It is also possible to perceive that, overall, AGS in SBR1 presented better settleability than in SBR2, suggesting that the presence of AgNPs has a positive effect in biomass settling properties. These results corroborate the ones presented in section 3.1.1. showing that, after the storage period, SBR2 presented considerable biomass washout immediately after the operation resumed.

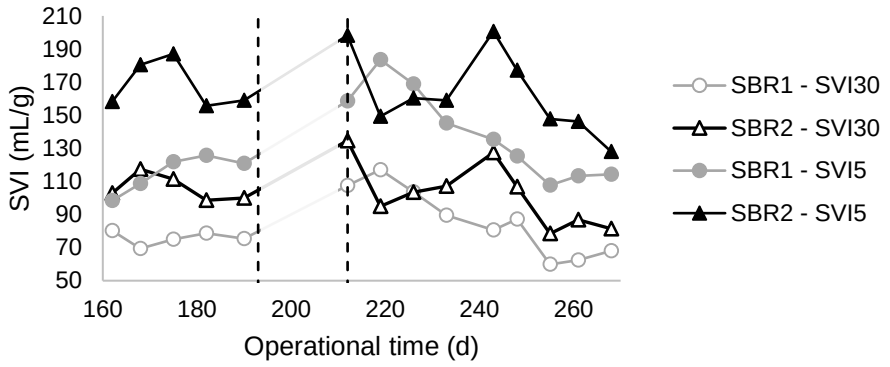

Figure 7. SVI 5 and SVI 30 evolution in SBR1 and SBR2 in the monitored period. The vertical lines comprise the storage period.

3.1.3. Chemical Oxygen Demand (COD)

The carbon load removal performance of the SBRs was evaluated through measurements of residual soluble COD. The obtained profiles are presented in Figure 8.

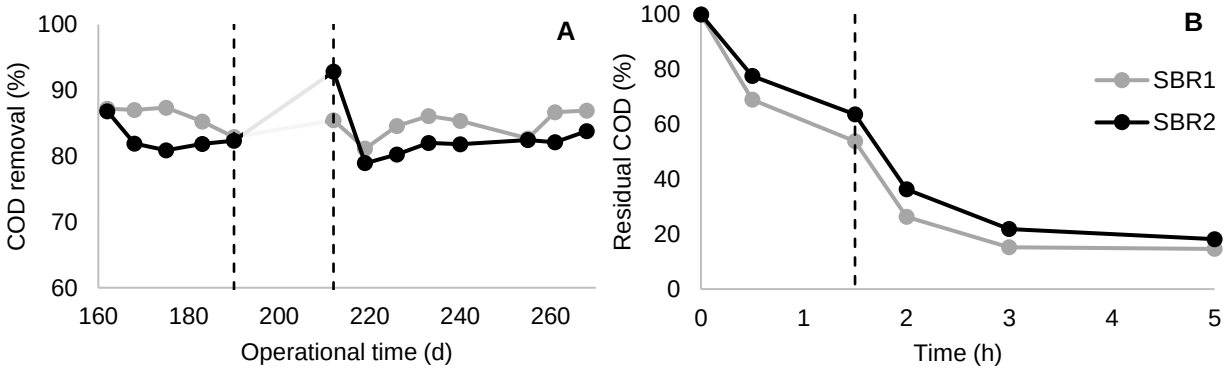

Figure 8. COD removal profile across the full monitored period (A) and a representative SBR cycle (data relative to operational day 240) (B). The vertical lines either delimit the storage period (A) or indicate the onset of aeration (B).

Overall, the SBRs exhibited a similar COD removal in the monitored period (Figure 8A). COD removal capabilities appeared to be improved by the existence of the storage period, since both reactors improved the COD removal from operational day 190 to 212. This effect is probably an attempt to compensate the starving conditions the biomass was subjected.

A representative 6-hour cycle profile obtained in each SBR is presented in Figure 8B, showing a similar COD removal performance irrespective of the presence of AgNPs. COD removal occurred at a higher rate in the first two hours of the reaction phase, corresponding to the entire anaerobic phase and the first 30 minutes of the aerobic phase. This profile suggested that the majority of the easily

biodegradable COD was consumed anaerobically during the feast phase. The consumption of easily biodegradable substrates in aerobic conditions has been linked to the formation of filamentous outgrowth with consequent unstable granulation and poor granule settling characteristics (De Kreuk et al. 2007). Thus, a high removal yield of easily biodegradable COD during the anaerobic phase is determinant to enhance granule formation and stability.

3.1.4. Colour assessment

Bacterial decolourization of azo dyes is generally accomplished through anaerobic azo bond reduction with colourless aromatic amine formation (Franca et al. 2015). In the specific case of the dye used in the fed synthetic wastewater (AR14), the degradation of the azo bond originates two colourless compounds: 1-naphthol-2-amino-4-sulfonic acid (1N2A4S) and 4-amino-naphthalene-1-sulfonic acid (4A1NS) (Figure 1).

Analysing the colour removal profile across the seven monitored weeks (Figure 9A), it is possible to observe that, in the period prior to the storage, high colour removal levels were attained in both bioreactors (generally above 80%). It is evident that the colour removal capacity was strongly affected by the storage period in the two bioreactors, however they both recovered within a few days. This rapid recovery might indicate that the communities responsible for colour removal resisted the storage period, being the reactivation an expedite process. Residual colour profiles along the 5-h reaction phase of a typical SBR cycle are presented in Figure 9B.

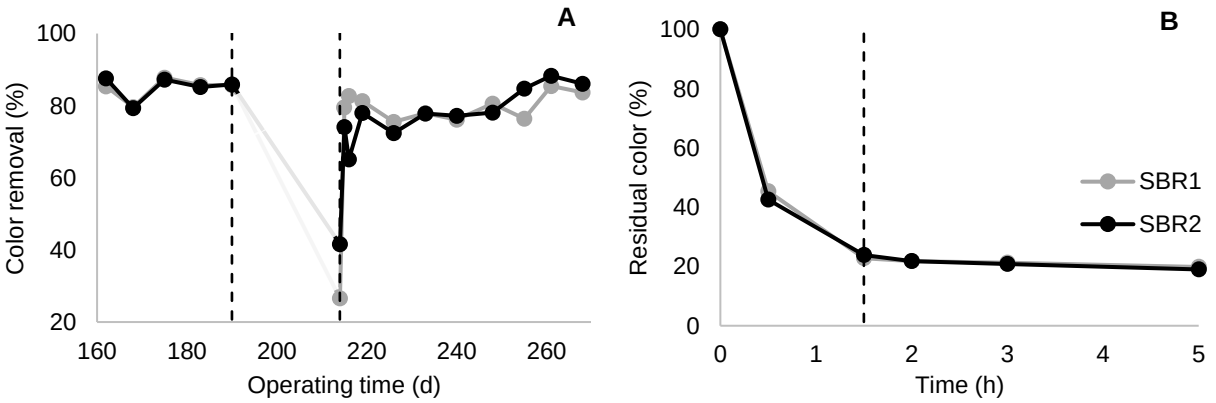

Figure 9. Color removal profile across the monitored period (A) and a representative SBR cycle (data relative to operational day 240) (B). The vertical lines either delimit the storage period (A) or indicate the onset of aeration (B).

3.1.5. pH analysis

By plotting the measured pH values along the 5-h reaction phase for each bioreactor (Figure 10), it was possible to detect a slight acidification during the anaerobic reaction phase. This behaviour has been previously observed and was suggested to be caused by the production of volatile fatty acids during the anaerobic fermentation of the carbon source (Bento 2016) hence, after the start of aeration, this trend was reversed. The similar pH profiles of the two bioreactors suggested that the presence of AgNPs did not affect the pH profile. Additionally, the storage period had no effect in the pH profiles obtained.

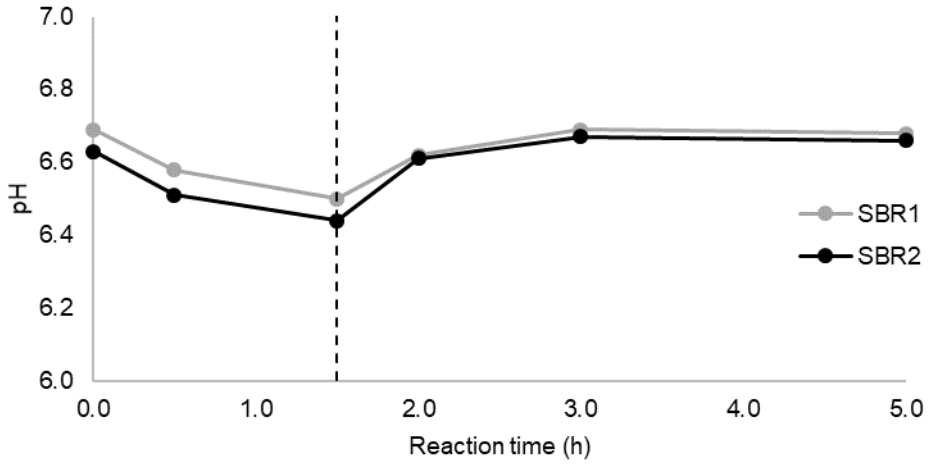

Figure 10. pH profiles along the 5-h reaction phase of a typical SBR cycle in the AgNPs-fed SBR1 and the AgNPs-free control SBR2. (data relative to operational day 190). The vertical line indicates the onset of aeration.

3.1.6. Quantification of mass fractions

As previously explained, the use of sieves with different diameters allowed the separation of biomass in three different fractions: d> 0.65mm (large granules), 0.20mm<d<0.65mm (granules) and d<0.20mm (flocs). The obtained biomass fractions were then independently estimated by VSS, ultimately revealing the relative presence of granules in each reactor. Figure 11 contains the results concerning this biomass characterization along the studied period.

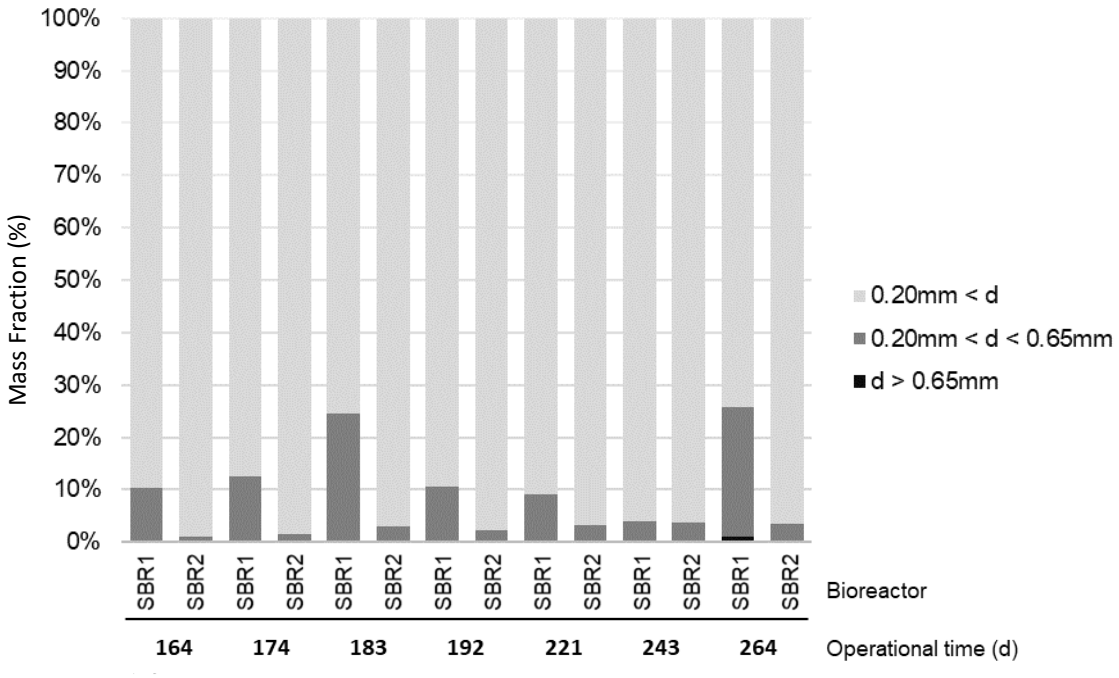

Figure 11. Relative proportion of the three different biomass fractions: d> 0.65mm (large granules), 0.20mm<d<0.65mm (granules) and d<0.20mm (flocs), in both bioreactors.

It is possible to perceive that SBR1 consistently presented higher relative granular biomass content, reaching up to 25%. Considering the results obtained in the operational days 192 and 221, the storage period appeared to have little or no effect in the estimated mass fraction of the reactors biomass. However, the obtained results for SBR1 regarding operational day 243 indicated a considerable decrease in the granular content, nonetheless a clear recovery can be observed (from day 243 to 264). SBR2 presented constant results throughout the monitored period reaching a maximum value of 4%.

The results herein obtained go in line with the mixed liquor VSS analysis, since SBR1 presented both higher granular and VSS content. This indicated an unsurprising direct correlation between estimated total biomass content and relative granular biomass content. Moreover, the SVI results obtained present a clear association with granular biomass content profiles as SBR1 presented better settling capabilities.

The proportions of granular biomass in the operational system stood lower than the ideal level in a AGS system. For both SBRs we are effectively in the presence of a mixed system were the majority of the biomass is in a flocculent state. The control SBR2 presented a lower overall performance in parameters such as SVI, VSS and TSS, when in comparison with the AgNPs-fed SBR1. Likewise, upon scrutinising these fractioning results, SBR2 presented the lower proportion of granular biomass. Since the SBR with the highest granular biomass content presented better overall performance, the role of the relative granular biomass content, although lower than desired, appeared to be significant. Most importantly, it seemed that the continuous biomass exposure to the presence of AgNPs has enhanced the granulation process.

To conclude, considering the combination of factors herein presented, it is incorrect to categorize SBR2 as an AGS system. Thus, some potential SBR2 outcomes, namely concerning the EPS analysis, can be more linked to the overall physical state of the biomass than to the fact that it was operated in the absence of AgNPs.

3.1.7. AgNPs concentration estimate: VSS/TSS-based method

By comparing the VSS and TSS values of SBR1 and SBR2, the concentration of AgNPs present within the first reactor can be estimated. For this, data relative to an early stage of the operation was used.

Firstly, using the existing data, an average VSS/TSS value was obtained for SBR2. This average ratio, and the SBR1 real VSS values were used to estimate SBR1 TSS values. This was possible assuming that the only difference between the reactors is the presence of AgNPs and that if they were not present in SBR1, this reactor would present the exact same values VSS/TSS of SBR2. The ratios between the two reactors were very stable and the use of an average value seemed to be adequate. Thus, the estimated TSS values would represent the TSS in SBR1 if it was operated without AgNPs, and therefore the difference obtained between the real TSS obtained through a standard analysis and the TSS estimated based on SBR2 VSS/TSS ratio reflected an estimation of the AgNPs concentration present in the SBR1 mixed liquor (equation 6).

$$[\mathrm{AgNPs}] = \mathrm{TSS}_{\mathrm{SBR1}} - \mathrm{VSS}_{\mathrm{SBR1}} \times \left(\frac{\mathrm{TSS}}{\mathrm{VSS}}\right)_{\mathrm{SBR2}} \quad \text{(Equation 6)}$$

The obtained results regarding estimated AgNPs concentration are presented in Figure 12, as well as the VSS for the AgNPs-fed SBR1.

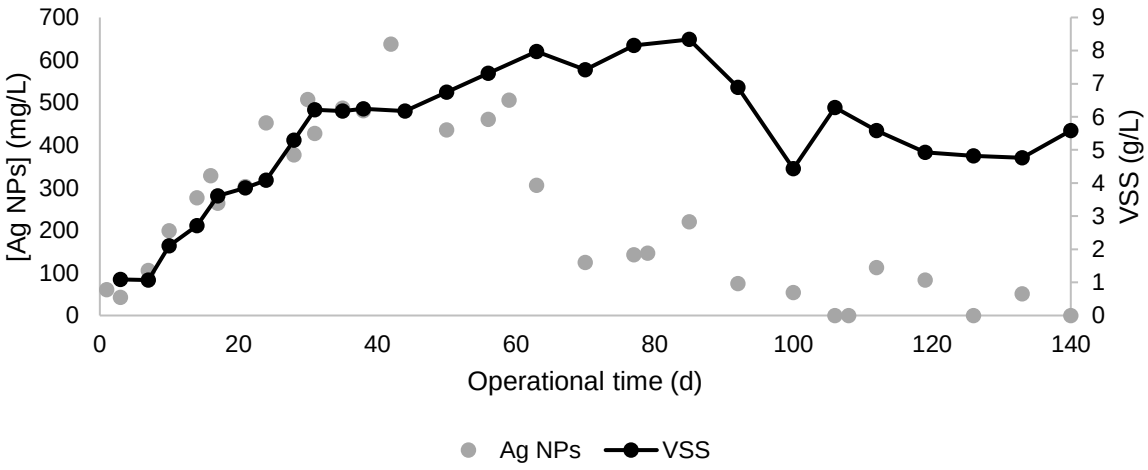

Figure 12. Estimation of AgNPs concentration (mg/L) and SBR1 VSS (g/L) calculations in the period between operational day 1 and 140.

It is possible to observe that the estimated AgNPs concentration is widely variable, ranging from 42 to 637 mg/L. This fact enforces the idea that the operational process can vary daily, affecting several monitored parameters. The sampling day highly affected the final results obtained.

In some cases, namely in some of the last monitored cycles, the estimated TSS value was even higher than the real one, originating negative AgNPs concentration values and thus being considered as zero. This of course proves that the applied estimation method had flaws. Moreover, there are several other contributors to the TSS fraction besides the used NPs, such as phosphorus that PAOs can store as polyphosphate (Poly-P) under specific conditions (Tarayre et al. 2016). Nonetheless, there is a fairly evident correlation between the AgNPs concentration estimations and SBR1 VSS values in the beginning of the operational period (day 1 to 40), which might suggest that the AgNPs retention in the bioreactor depend on the biomass content in the mixed liquor.

3.2. EPS analysis process optimization

3.2.1. Influence of ionic silver (Ag+) on PN and PS quantification methods

This preliminary test aimed to determine if the presence of Ag^+ interfered with the proposed PN and PS quantification methods. It is possible that after EPS extraction from samples concerning the AgNPs-fed SBR1 some ionic silver (Ag^+) resulting from AgNPs dissolution is present in the EPS samples. Thus, to confirm this potential inference effect, EPS were extracted from AgNPs-free control SBR2 and supplemented with different $AgNO_3$ concentrations. This inorganic salt is highly soluble, so the release of Ag+ ions is expected. The results obtained are presented in table 1 (due to a methodology

error the results concerning the influence of 5 mg/L of $AgNO_3$ in PS content determination were discarded).

Table 1. Influence of different ionic silver ($AgNO_3$) concentration on PN and PS quantification. STD represents standard deviation and N the number of replicates. (All data is relative to SBR2 samples, retrieved during non-aerated phase, t=1h reaction time). Fractions that were not analysed (NA).

$AgNO_3$ (mg/L)	PN (µg/mL)	STD	N	PS (µg/mL)	STD	N
0	276.26	3.03	6	396.80	8.13	13
1	277.30	6.81	9	383.33	7.20	4
5	282.77	5.31	8	NA	-	-

The tested concentrations appeared to have not significantly influenced the PN and PS quantification methods.

3.2.2. Effects of different pre-extraction methods on EPS extraction efficiency

The strategies of EPS extraction from aerobic granules are often inspired by protocols applied to activated sludge flocs. However, extracting EPS from aerobic granules is more difficult than from sludge flocs due to their low surface-to-volume ratio (Adav and Lee 2008; Liu and Fang 2002; Mcswain et al. 2005). Mcswain et al. (2005) extracted EPS from aerobic granules and reported that effective EPS extraction required pre-homogenization (980rpm) of the aggregates due to the large size of the granules. Adav & Lee (2008) also reported that using pre-ultrasound treatment (120W) largely improved the EPS extraction from compact aerobic granules. In contrast, the use of ultrasounds did not enhance EPS extraction from sludge flocs, probably due to the correspondingly loose attachment between EPS and flocculent cells.

Table 2 shows the PN concentration values obtained after applying each of the three pre-extraction methods followed by heat extraction (section 2.2.3.2.). The PN content of the EPS pre-treated by methods 1 and 3 did not differ significantly, demonstrating that a milder method, such as method 1, is sufficient to re-suspend and homogenize the sludge before the extraction method. This result was expected, since the mixed liquor of both SBRs was a hybrid system of both flocculent and granular sludge. In turn, the PN content of the EPS extracted from samples pre-treated by method 2 was slightly smaller than when methods 1 and 3 were used, possibly due to sludge sedimentation and compaction during the ultrasound step.

Table 2. Influence of three different pre-extraction methods on protein (PN) extraction efficiency. In Method 1, the sludge samples were only pre-treated by mixing vigorously with a pipette until a homogeneous sludge suspension was obtained. In Method 2, in addition to method 1, the sludge suspensions were further sonicated during 60 minutes at 80W. Finally, in Method 3, after methods 1 and 2 were performed, the sludge samples were mixed for 30 seconds using a vortex mixer. STD represents standard deviation and N the number of replicates. (All data is relative to SBR2 samples, retrieved during aerated phase, t=2h reaction time).

Pre-extraction method	PN (µg/mL)	STD	N
1	308.89	7.99	6
2	285.44	5.69	9
3	313.15	4.67	9

3.2.3. Cation Exchange Resin (CER) and heat EPS extraction

As aforementioned, there are no unquestionably accepted methodologies for EPS extraction from AGS, reinforcing the necessity of selecting the best possible approach to perform this kind of analysis in the particular case of the biomass generated in this study. To select the most appropriate and efficient method for EPS extraction, EPS were extracted from different mixed liquor samples from SBR2 with two alternative procedures, one recurring to heat treatment and the other via Cation Exchange Resin (CER). Both PN and PS content were later quantified.

Table 3 summarizes the PN and PS concentration yielded after EPS extraction with CER and with heat treatment. In some cases, the determined PN and PS concentration values presented high standard deviation (STD). Furthermore, the same EPS sample with different volumes measured to accomplish the same 1:2 dilution presented variations on PN concentration values. Both variations suggested the presence of interfering substances in the EPS composition that compromised the PN quantification method.

Table 3. Comparison between Cation Exchange Resin (CER) and heat treatment methods for extraction of proteins (PN) and polysaccharides (PS). STD represents standard deviation and N the number of replicates. (All data is relative to SBR2 samples, collected during aerated phase, t=2h reaction time). Fractions that were not analysed (NA). * These dilutions were performed inside the microplate.

Extraction method	Sample	EPS sample (µL): EPS extraction buffer (µL)	PN (µg/mL)	STD	N	PS (µg/mL)	STD	N
CER	A	12.5:12.5*	546.49	10.32	7	NA	-	-
		500:500	703.94	5.82	6			
	B	500:500	479.43	53.04	6	60.06	1.88	6
Heat	A	12.5:12.5*	264.39	10.14	9	NA	-	-
		500:500	356.67	5.62	6			
	B	500:500	217.59	17.81	5	259.10	40.15	6

However, it was possible to note that PN and PS extraction efficiencies varied significantly according to the method used for EPS extraction, as can be confirmed by Table 3. PN concentration was considerably higher when EPS were extracted by CER compared to that with heat treatment. On the contrary, CER method led to a lower PS concentration compared to heat treatment. This suggested that the use of CER to extract EPS possibly facilitated PN extraction compared to PS. However, the heat extraction method proved to be more reproducible as well as easier and faster to perform and, consequently, it was decided to use this method for the following optimization steps.

3.2.4. Influence of different EPS sample dilutions on PN and PS quantification methods

The variations observed in the previous assay suggested that possibly there were interfering substances in the EPS composition that influenced the PN quantification method. Several strategies exist for overcoming or eliminating sample incompatibilities with the quantification methods (Thermo Scientific, 2010). The simplest approach is to assay the sample after diluting it several-fold in a compatible buffer. Thus, EPS were extracted by heat treatment from different mixed liquor samples of both SBRs and were diluted in EPS extraction buffer prior to PN quantification. PN and PS concentration values attained for the different dilution factors tested are shown in Table 4 and 5 respectively.

Table 4. Influence of different EPS sample dilution factors on PN quantification methods. STD represents standard deviation and N the number of replicates. (Data relative to SBR1 and SBR2, samples A and B respectively, retrieved during aerated phase, t=2 reaction time). Dilutions were performed inside the microplate.

Sample	Dilution factor	EPS sample: EPS extraction buffer	[PN] µg/mL	STD	N
A (SBR1)	2	500:500	305.87	9.11	9
	4	250:750	342.21	9.04	9
	10	100:900	410.29	3.74	9
B (SBR2)	1	1000:0	276.45	8.68	9
	2	500:500	313.29	8.90	9
	4	250:750	352.04	6.93	9

Table 5. Influence of different EPS sample dilution factors on PS quantification methods. STD represents standard deviation and N the number of replicates. (All data is relative to SBR2, retrieved during the non-aerated phase, t=0h reaction time). Dilutions were performed inside the microplate.

Sample	Dilution factor	EPS sample: EPS extraction buffer	[PS] µg/mL	STD	N
A	2	500:500	393.45	4.56	9
	4	250:750	401.11	8.54	7
B	2	500:500	312.30	1.14	2
	4	250:750	321.45	3.26	2
	10	100:900	304.90	2.92	2

As can be seen in Table 4, the higher the dilution factor applied, the higher the PN concentration obtained. This suggested that the interfering substances artificially suppressed the response of the PN quantification method. In the case of PS content (Table 5), this trend was not observed.

3.2.5. Protein precipitation using trichloroacetic acid (TCA)

Protein precipitation using trichloroacetic acid (TCA) was used in an effort to eliminate possible EPS interfering substances that might have compromised the PN quantification method in the previous assays. To optimize this step, different concentration of TCA were tested. Additionally, the influence of 1mg/L of $AgNO_3$ on protein precipitation efficiency was also assessed. Results figure in table 6.

Table 6. Protein (PN) concentration obtained after PN precipitation with different percentages of trichloroacetic acid (TCA) and influence of 1mg/L of $AgNO_3$ on TCA-PN precipitation. STD represents standard deviation and N the number of replicates. (All data is relative to SBR2, retrieved during the aerated phase, t=2h reaction time).

Sample	TCA (%)	$AgNO_3$ (mg/L)	PN (µg/mL)	STD	N
A	20	0	52.14	2.01	7
	13	0	44.02	2.44	8
B	20	0	54.36	2.35	9
	30	0	45.61	2.32	9
	30	1	43.04	1.89	9

As can be confirmed by Table 6, the precipitation with 20% of TCA resulted in higher PN recovery and 1mg/L of $AgNO_3$ did not influence the precipitation efficiency. Therefore, it was decided to use this concentration of TCA in the following assays.

3.2.6. Influence of sample storage on EPS PN and PS content

To investigate the influence of sample storage on major EPS components, i.e. PN and PS, samples collected from SBR2 were either used directly for EPS extraction and analysis, or stored at -80ºC. After six days of storage, EPS were extracted and PN and PS content was analysed. Table 7 summarizes the PS and PN content yielded.

The PN content of the EPS extracted from stored biomass samples was higher relatively to that obtained from biomass samples without storage. This trend was probably related to the release of intracellular proteins, as consequence of cell lysis after thawing the samples for analysis. After thawed from -80ºC, the damaged cells, under the EPS extraction treatment, can suffer lysis and release intracellular proteins (Wingender, Neu, and Flemming 2012). The adoption of a phased thawing procedure might be useful to bypass this problem, since it does not include sharp temperature variations. The PS content of the EPS extracted from stored samples was lower than that from samples without storage. However, this trend requires further investigation.

Table 7. Influence of biomass storage on EPS protein (PN) and polysaccharide (PS) content. STD represents standard deviation and N the number of replicates. (All data is relative to SBR2, samples were collected at different reaction time points: t=0h (A); t=2h (B,C); t=5,5h (D). Note the onset of aeration is at t=1.5h).

	Biomass Sample	PN (µg/mL)	STD	N	PS (µg/mL)	STD	N
A	Without storage	44.96	1.39	9	312.88	7.69	3
	After 6-day storage at -80ºC	48.06	1.95	9	244.95	3.83	6
B	Without storage	41.76	1.73	9	285.93	9.84	3
	After 6-day storage at -80ºC	66.77	0.53	6	280.18	2.17	6
C	Without storage	29.81	1.24	8	283.90	1.72	3
	After 6-day storage -80ºC	56.56	1.28	6	260.61	11.41	3
D	Without storage	31.20	1.81	8	257.22	2.57	3
	After 6-day storage at -80ºC	58.80	1.93	7	235.27	2.64	3

3.2.7. Influence of extracted EPS storage on PN and PS content

To study the influence of extracted EPS storage on EPS-PN and –PS content, mixed liquor samples were collected and the EPS was heat extracted being either used directly for PN and PS analysis, or stored at -20ºC with the PN and PS content being analysed after six days of storage. Table 8 presents the PS and PN content obtained.

Table 8. Influence of extracted EPS storage on protein (PN) and polysaccharide (PS) content. STD represents standard deviation and N the number of replicates. (All data is relative to SBR2, samples were collected at different reaction time points: t=2h (A); t=5h (B,). Note the onset of aeration is at t=1.5h).

	EPS Sample	PN (µg/mL)	STD	N	PS (µg/mL)	STD	N
A	Without storage	29.81	1.24	8	283.90	1.72	3
	After 6-day storage at -20ºC	31.14	0.73	3	235.31	3.31	3
B	Without storage	31.20	1.81	8	257.22	2.57	3
	After 6-day storage at -20ºC	31.51	0.52	3	230.59	2.40	3

Although the EPS storage did not impact the PN content, apparently it seems to have influenced the PS content. However, similarly to the previous assay, this trend requires further investigation.

3.3. Optimized protocol for Extracellular polymeric substances (EPS) analysis

Despite being a very laborious and time-consuming task to perform uninterruptedly, the EPS analysis (comprising: pre-treatment, extraction and quantification) was always performed in a single day. The storage tests results for both whole samples and extracted EPS revealed that the components quantification was compromised by the applied storage periods.

3.3.1. Pre-treatment and extraction

For both PN and PS fractions, the sampling was performed by weekly retrieving 5 mL sample duplicates along the reaction phase of one treatment cycle. These samples were dewatered by centrifugation at 4000 rpm for 10 min (discarding the soluble EPS fraction). The obtained pellets were immediately covered in EPS extraction buffer solution (2 mM $Na_3PO_4 \cdot H_2O$, 4 mM $NaH_2PO_4 \cdot 12H_2O$, 9 mM NaCl, 1 mM KCl, pH 7) to the original volume. The samples were kept at 4ºC until further analysis. The pellet resuspension was performed by mixing vigorously with a pipette until a homogeneous sludge suspension was obtained immediately before the extraction procedure (method 1, see section 2.2.2). The heat extraction was the selected methodology being performed as described in section 2.2.3.2).

3.3.3. Quantification

3.3.3.1 Protein (PN) content

Since the optimization results suggested that some interfering substances artificially suppressed the response of the PN quantification method the PN content was determined after a purification step by precipitation. A modified method of trichloroacetic acid (TCA) was applied as described elsewhere

(Zhang et al. 2015). Briefly, the TCA solution (100% w/v) was added to the EPS sample solution making a 20% final concentration established and the mixture was incubated overnight at 4°C after being well mixed. Then, the mixture was centrifuged at 14000 rpm for 20min at 4°C and the supernatant was removed. The residual TCA in the precipitates was washed using acetone (1mL) and centrifuged at 14000 rpm for 5 min. This step was performed 3 times at 4°C. At last, the pellet was resuspended in buffer solution (300µL) and the protein (PN) content was determined with Pierce® BCA protein assay kit (Thermo Scientific, USA). Bovine serum albumin (BSA) was used as standard for method calibration, in a concentration range between 0 and 500 mg/L. (Annex 2.)

3.3.3.2. Polysaccharide (PS) content

The polysaccharide (PS) content was analysed in accordance to the method described in (Dubois et al. 1956) with some minor modifications. Briefly, 1 mL of 5% phenol (w/w) in water was added to 1 mL of sample. Then, 5 mL of concentrated sulphuric acid was added rapidly, on the liquid surface. The mixtures were allowed to react for 10 min, then were mixed and allowed to react for another 30 min at room temperature. 200µL of each tube content was pipetted to a microplate and the absorbance was measured at 490 nm using buffer solution as blank. Glucose was used as standard for method calibration, in a concentration range between 25 and 300 mg/L. (Annex 3.)

3.4. Protein and polysaccharide content quantification

After attaining optimized EPS extraction and quantification protocols (3.3), we proceeded to the sampling of the mixed liquor from the AgNPs-fed SBR1 as well as from the AgNPs-free control SBR2, along six-hour cycles in a seven-week period were the AGS was analysed for PN and PS total content (per unit of biomass) in extracted EPS, from now on referred only as PN and PS content, respectively. The first monitored cycle (operational day 191) was before an 18-day interruption, where the biomass was stored at 4ºC in closed glass containers, with all typical procedures involving the regular bioreactor functioning being interrupted during this period. The remaining cycles occurred after the mentioned interruption. The results concerning PN content obtained for the two bioreactors are presented in figure 13.

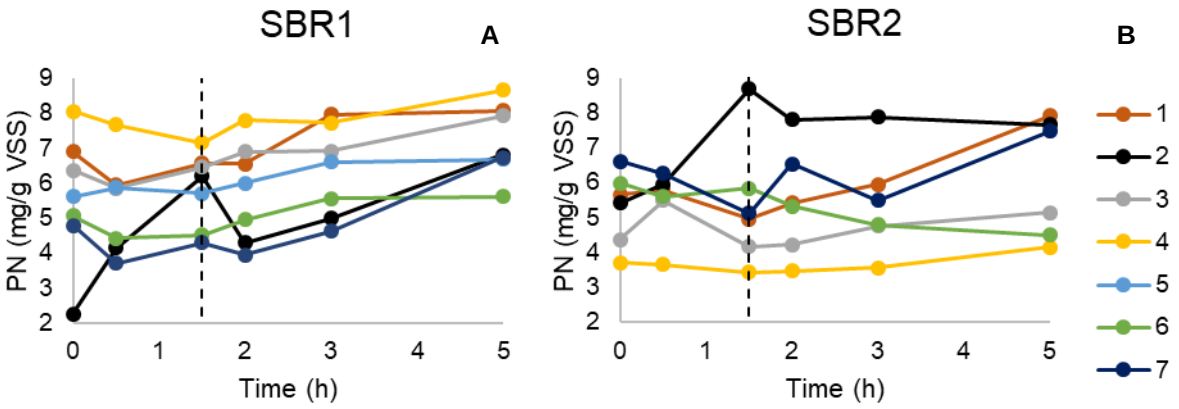

Figure 13. Evolution of the protein content in SBR1 (A) and SBR2 (B) across the reaction period of different cycles (1-7, numbered chronologically). Due to an experimental error cycle 5-SBR2 is not presented. Major STD = 1.59 mg/g VSS. The vertical line indicates the onset of aeration.

The SBRs presented a PN content somewhat erratic, values ranging from 2.3 to 8.7 (mg/g VSS) for SBR1 and from 3.4 to 8.7 (mg/g VSS) for SBR2. The first cycle after reactivation (cycle 2) was the one with the most variable profile in both SBRs, increasing significantly during the cycle anaerobic phase, then decreasing on the onset of aeration and resuming the increasing tendency in the remaining period of the aerobic reaction phase. However, contrarily to what happened in SBR1, where cycle 2 presented values in accordance to those measured in the remaining cycles, in SBR2 the homologue cycle had significantly higher protein content than the remaining ones, across most of cycle duration. This might be justified by the fact that the initial PN content in SBR1 cycle 2 was very low after the storage period, while the cycle 2 in SBR2 had a starting point value similar to the presented in the remaining monitored cycles. One can assume that although both reactors presented a PN content recovery along the cycle 2, more PN was consumed by the biomass of SBR1 during the storage period, as the starting point of this latter one was in line with the values measured in the remaining cycles.

The increase of PN content verified immediately after storage might be related to the higher COD removal in the same period (Figure 8A). Some patterns of aerobic granules-associated EPS during an SBR cycle have already been described, these were credited to the applied feed regime. The existence a short substrate feast phase and a relatively long famine phase would greatly influence both the PN and PS content (Deng, Wang, and Su 2016; Wang et al. 2006; Zhu et al. 2012). The EPS content would increase in the periods where COD removal was more significant. This way, an increase of PN and PS content was expected right after the fill phase, in the anaerobic portion of the reaction phase where most COD is removed. The use of EPS as source of carbon and energy by some microorganisms during the famine phase was also reported (Ortega et al. 2009; Sheng et al. 2010; Wang, Liu, and Tay 2007). Thus, the reduction of EPS content was expected in the aerobic phase. Synthetizing, the EPS production and consumption processes was expected to be closely dependent on the external substrate availability during the SBR cycle. However, analysing the results regarding the PN evolution across the SBR cycle, it appears that this EPS component did not follow this tendency, neither in SBR1 nor in SBR2. The only cycle that displayed a profile according to this theory was the one obtained immediately after the storage interruption (cycle 2), this was verified for both bioreactors. There was an evident production of PN in the second cycle of SBR1 and SBR2, possibly restoring the PN consumed during the 18-day starvation period. The set of the remaining monitored cycles presented an erratic behaviour, with no evident pattern. Despite oscillating, it appears that the PN content was not directly affected by the substrate availability, at least in the monitored period that corresponds to a period of stable SBR operation. That is why the cycle 2 was the one where the results were clear. Monitoring the PN content during aerobic granule formation would also probably result in different PN profiles.

The results regarding PN content were not clear since no general pattern was identified. The two bioreactors did not present very evident differences. The PN content in each monitored cycle profile of the two SBRs did not present a consistent variation pattern. The most likely is that both reactors were already in a steady state in what protein concerns. So, excluding the cycle immediately after the storage period, no major alterations were detected. The 18-day storage period allowed the visualization of the behaviour not visible in any other cycle because the reactors were already stabilized.

Similarly to the PN quantification, and due to the joint extraction process, the PS quantification analysis was only carried out after proper protocol optimization. The same seven cycles were monitored and are results are displayed in figure 14.

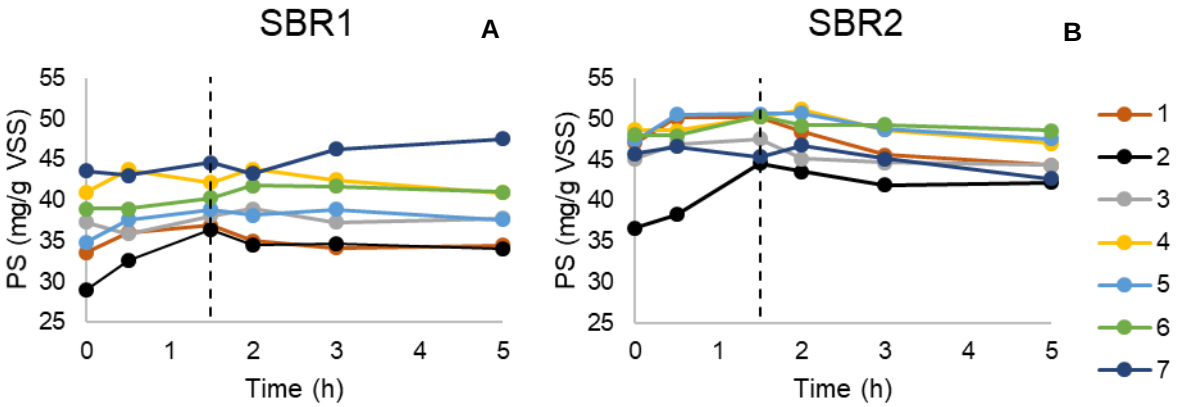

Figure 14. Evolution of the polysaccharide content in SBR1 (A) and SBR2 (B) across the reaction period of different cycles (1-7, numbered chronologically). Major STD = 1.49 mg/g VSS. The vertical line indicates the onset of aeration.

Overall the results for PS content appear to be less variable than those for PN. The obtained values ranged from 29.1 to 47.5 and 36.6 to 51.2 (mg/g VSS) for SBR1 and SBR2 respectively. Overall, SBR2 presented a slight higher PS content than SBR1.

Recurring to Figure 14 it is possible to perceive that the evolution of the PS content in the majority of the monitored cycles, unlike what was verified in the PN quantification, appeared to present a stable pattern. The PS content increased slightly in the anaerobic phase and slightly decreased with aeration. Once again, this is in agreement with previously reported results (Deng et al. 2016; Wang et al. 2006; Zhu et al. 2012) that showed an EPS increase in the periods where COD removal was more significant, in our case during the anaerobic portion of the reaction phase (Figure 8B). The subsequent consumption of EPS was also described, as these substances were used as carbon and energy source by some microorganisms during the famine phase (Ortega et al. 2009; Sheng et al. 2010; Wang et al. 2007).Thus, a reduction in the EPS content was expected during the aerobic phase. This behaviour was observed regarding the PS content but not the PN content. The PS content production and consumption processes across the SBR cycle appear to be closely related to the external substrate availability.

Despite the differences encountered between the bioreactors, the presence of AgNPs apparently did not affect the dynamic change of PS along the reaction phase, namely an increase of PS content during the anaerobic phase and a decrease during the aerobic phase. This was probably associated to the removal of easily biodegradable COD present in the mixed liquor at the beginning of the reaction phase. The biodegradable EPS produced in the feast phase was consumed during the subsequent famine phase (Liu 2007). This idea is clearer for the cycle tested after the storage period. The long-term starvation period induced by the 18-day storage clearly revealed this tendency that was not distinguishable during the normal (and more stable) functioning of the SBRs, suggesting that probably the feed was rich enough to be consumed throughout all cycle thus avoiding fluctuations in the PS content as its consumption was not required. Analysing Figure 8B, the residual COD profile for a typical SBR1 cycle presented approximately 14.6% residual COD after the five-hour reaction time, translating

in 85.4% COD removal, being 46.2% during the anaerobic phase and an additional 38.6% in the first hour and a half of the aerobic phase. This indicates that significant COD removal occurred until t=3h, with only the two remaining hours of actual famine phase (only 0.6% COD removal). SBR2 presented a similar COD removal profile.

In order to evaluate the evolution of PN and PS content across a larger time frame, and since a cycle was monitored per week, the average values were calculated for each monitored cycle. Figure 15 presents the average PN and PS content for each week-representing cycle.

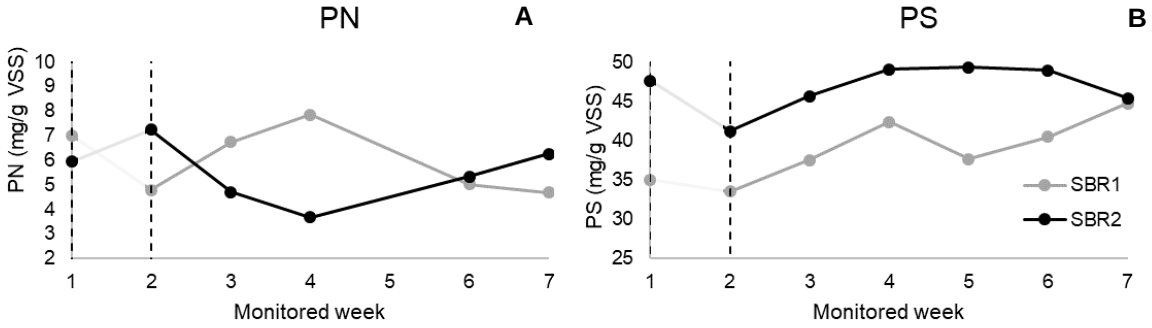

Figure 15. Average PN (A) and PS (B) content for each week-representing cycle. Note that between monitored week 1 and monitored week 2 lies the 18-day storage period, graphically delimited by the vertical lines. Major STD = 3.09 mg/g VSS (A) and 1.62 mg/g VSS (B).

Analysing the profiles obtained along the cycle duration (Figure 13), it is clear that some variations are detected in a matter of hours. With that in mind, weekly variations were somewhat expected. Analysing Figure 15A, it is evident that the largest divergence between the two SBRs occurred in the fourth week of the monitored period. It is possible to see that SBR1 has a significantly different profile from SBR2. SBR1 appeared to have consumed PN during the storage period and recovered in the following weeks. SBR2 presented the exact opposite profile.

Despite the different relative biomass size fractions of the mixed liquor in the two SBR (section 3.1.6), the results regarding the average PN content (mg/g VSS) in each SBR cycle were in the same range (varying from 4.7 to 7.8 and 4.7 to 7.2 for SBR1 and SBR2 respectively). Neither the AgNPs presence nor the different percentages in biomass size fractions, namely flocculent and granular, appeared to have contributed to a difference in the quantification of PN. Both SBR1 and SBR2 presented the highest values in different periods of the monitored operation (Figure 15), leading to the idea that the displayed variations are caused by the specific reactor dynamics, rather than a particular tendency caused by an external factor.

Considering Figure 15B, the two SBRs studied showed, at some degree, depletion in polysaccharide content from the first to the second cycle and then, although with differing patterns, they both increased, clearly indicating a recuperation period after which the initial values were attained or surpassed. According to these average cycle values, PS appeared to be consumed during the storage period (between monitored week 1 and 2), thus corroborating the published studies from Sheng, Yu, and Li 2010 and Wang, Liu, and Tay 2007. Given that the results are normalized to mixed liquor VSS content, one can hypothesize that the numerical differences between the calculated PS content are most likely caused by the different morphological states of the biomass in the mixed liquor. The results

already contemplate the difference in the amount of biomass present in the reactors, however, different granulation stages can cause alteration in the results. The PS content (mg/g VSS) in the totality of monitored cycles varied from 33.5 to 44.7 and 41.2 to 49.3 for SBR1 and SBR2, respectively, averaging 38.8 and 46.7 mg/g VSS, corroborating previously reported results where flocculent biomass presented a higher relative PS content (Zhang et al. 2007) (Figure 15b). It could be expected that the biomass from the Ag-fed SBR1 presented higher EPS content in order to capture AgNPs, but it did not occur. The PS content appeared to vary more significantly due to the granuled fraction in the biomass present in each bioreactor.

As previously seen, the independent study of both protein and polysaccharide content reveals itself very useful, particularly in the pattern analysis across one SBR cycle, allowing to infer some biomass dynamics across different culture conditions. However, even more significant than the quantification of both individual PN and PS fractions is the relative proportion between them. The PN/PS ratio is widely used in several studies to describe EPS content and to characterize AGS, thus the combined data of both EPS components is presented below in the form of PN/PS ratio (Figure 16).

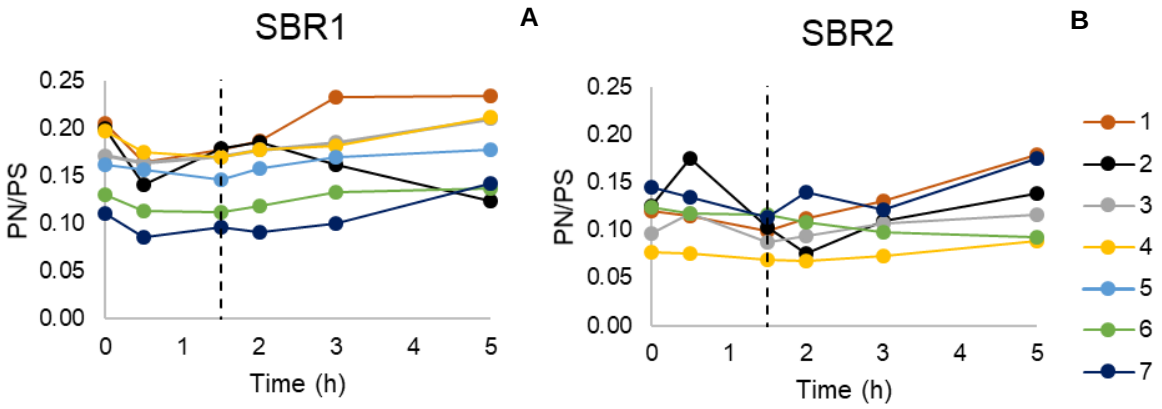

Figure 16. Evolution of PN/PS ratios in SBR1 (A) and SBR2 (B) across the reaction period of different cycles (1-7, monitored chronologically). Due to an experimental error cycle 5-SBR2 is not presented. The vertical line indicates the onset of aeration.

The combined analysis of the EPS components content showed PN/PS ratios around 0.15 and 0.12 for SBR1 and SBR2, respectively. According to these values, the content of PS was much higher than that of PN and the presence of AgNPs seemed to have no evident effect.

For a variety of biofilm types and EPS extraction methods, in the majority of the published studies, proteins have been reported as more abundant than polysaccharides in EPS (Batstone and Keller 2001; Frølund et al. 1996; Mcswain et al. 2005; Schmidt and Ahring 1994). There is, nonetheless, contradictive bibliography where the PS content appeared dominant over the PN content (Tay, Liu, and Liu 2001), raising the hypothesis that PS contributed more to granule structure and stability than the PN. Thus, there are no typical values for granular biomass PN/PS ratio, but overall, bibliography indicates that PN is the most abundant EPS component in granular biomass. Moreover, the PN/PS ratio seems to increase during the granulation process.

Given these considerations, the herein obtained results regarding PN/PS ratios are very low. The small percentage of actual granular biomass present in the bioreactors definitely contributes to low

PN/PS values, as these have been associated with non-granular biomass. The data concerning the mass fractioning indicated maximum values of only 25% and 4% of granular biomass in SBR1 and SBR2, respectively. Additionally, the low results obtained could also mean that the independent quantification of the EPS components was consistently miscalculated, most likely due to a low and selective extraction efficiency. This way, the underestimation of protein content is also a real possibility. Despite the efforts to optimize the extraction and quantification of EPS components, further studies are needed to attain more reliable procedures, especially concerning PN content.

3.5. Elemental spatial distribution using nuclear microscopy

In the context of this project, the Ag distribution was clearly one of the focal points, nonetheless concentration of other main elements was also monitored due to its importance from a structural and physiological point of view. The elemental distributions in granules from the two reactors AgNPs-fed SBR1 and AgNPs-free SBR2 showed important differences. The SBR2 granules displayed a decreased concentration gradient of structural elements towards the core of the granule, while micronutrients showed a tendency to be more concentrated at the periphery of the granules. The elemental distributions in SBR1 granules showed a different pattern, which for most of the structural elements is opposite to SBR2. In SBR1 granules exposed to AgNPs, the Ag distribution showed a preferential deposition at the periphery with a sharp decrease to inner regions of the granule.

The particularities of the elemental distributions and especially Ag will be described in detail below.

3.5.1. Quantification of Ag in AGS granular fraction

3.5.1.1. Ag spatial distribution

This assay provided a sectional view of the AGS morphology. The sections of AGS derived granules were analysed under nuclear microscopy. The elemental distribution maps were generated being the results of a representative sample depicted below (Figure 17C-17F). The correspondent optical microscopy image is also displayed (Figure 17B). It can be clearly depicted the sectioned granular structure surrounded by the OCT™ embedding matrix. A box plot graph illustrating the Ag distribution in three selected regions of the section, periphery, intermediate region and core is also present (Figure 17A).

The preferential peripheral distribution of Ag in AGS granules is evident. Other elements were also detected in considerable quantities such as P, S, K, Ca, Mn and Fe, which distributed non-uniformly, as can be depicted in figure 17D-F. The deposition of AgNPs appears to be made in agglomerates, which can be easily visualised in the granule peripheral region. The fact that Ag is not evenly distributed throughout the granule goes in accordance with the reported affinity of EPS for metals (Geyik and Çeçen 2015; Sheng, Yu, and Li 2010; Wang et al. 2016). It has been reported that the LB-EPS structure can facilitate the physical retention of AgNPs and promote its capture (Geyik and Çeçen 2015). Although presenting a clear peripheral distribution, Ag was also sporadically found in inner regions of the sectioned granule. The distribution of the structural elements (K, P and S) emphasise a porous-like

organization and the scarcer Ag detection in inner regions of the granules seem to be in their vicinity (Figure 17C).

The manipulation involved in the preparation of granules preceding microprobe analysis, particularly the sectioning procedure, might affect the results concerning the spatial distribution of elements, namely the ones that predominantly occur in the granular periphery, such as silver. These elements can be dragged to inner regions of the section. These artefacts can be easily detected, by correlating images of the distribution of structural elements and Ag, as exemplified above in Figure 17C-F. Whenever detected, the artefact data was excluded from the analysis accordingly.

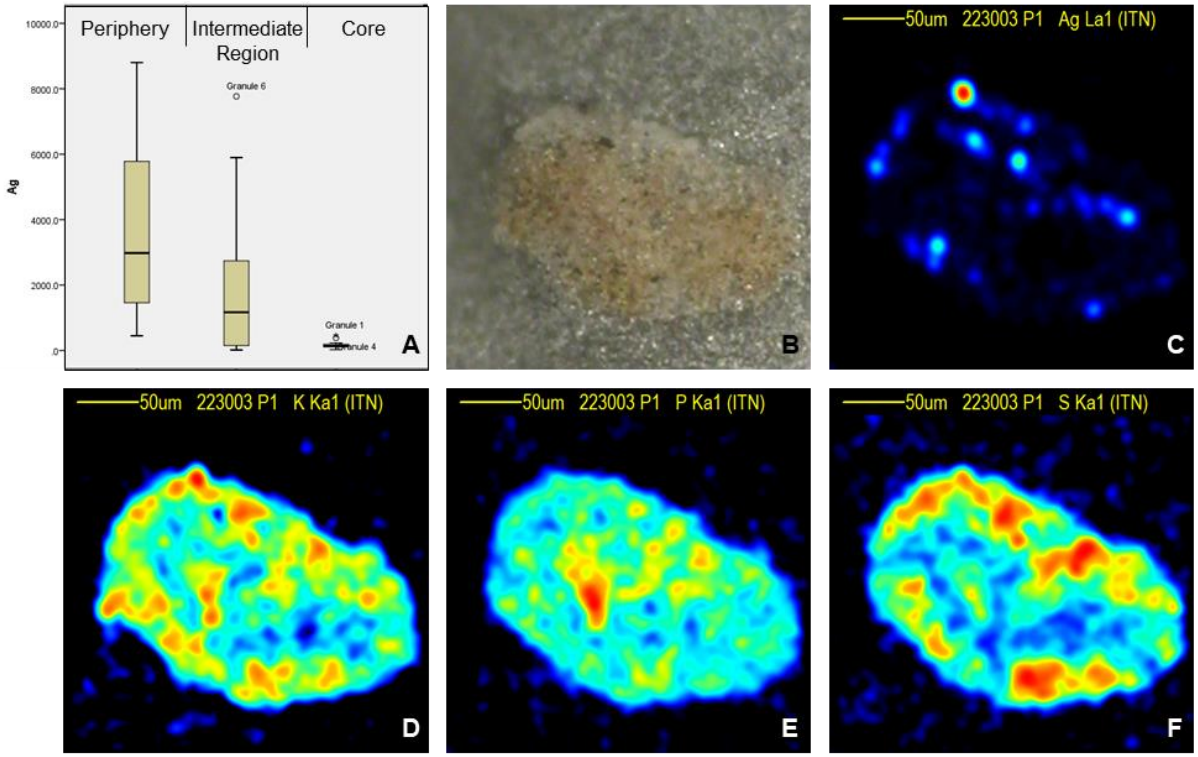

Figure 17. Box plot of Ag concentration in the three defined AGS regions (pheriphery, intermediate region and core) (A). Optical microscopy image of a AGS section (B) and corresponding Ag, K, P and S maps (C-F): The content gradient is represented by a dynamic colour scale: low–blue to high–red. In (A) the box represents the 25% and 75% interquartiles (IQ) and the dividing horizontal line indicates the median; whiskers indicate the maximum and minimum values.

3.5.1.2. Proto 3D-reconstruction

The analysis of several sequential sections from the same granule was carried out aiming at the reconstruction of the volume of the granule. This way it would be possible to reconstruct a rough 3D scenario that could potentially provide new information or confirm the already obtained data. These sections were treated exactly like the previously presented one, only adding in consideration the sectioning order of each granule.

In the following set of images, it is possible to observe three different sections all obtained from the same granule and treated independently, each section depicts the granule in different but parallel regions. Different elemental maps presented in this type of study allow to use 2D depictions to try to reconstruct a very raw conception of the real three-dimensional structure.

Similarly, to the three defined regions in a 2D approach (periphery, intermediate region and core) we can associate sectioning plans, starting in the polar region and progressively go to a more equatorial plane, to depict how elemental concentrations, especially Ag concentrations change in depth. By no means can this be considered a 3-D reconstruction, but some information can be retrieved from here that is not quite clear in the independent analysis of this very same images. Results are displayed in Figure 18.

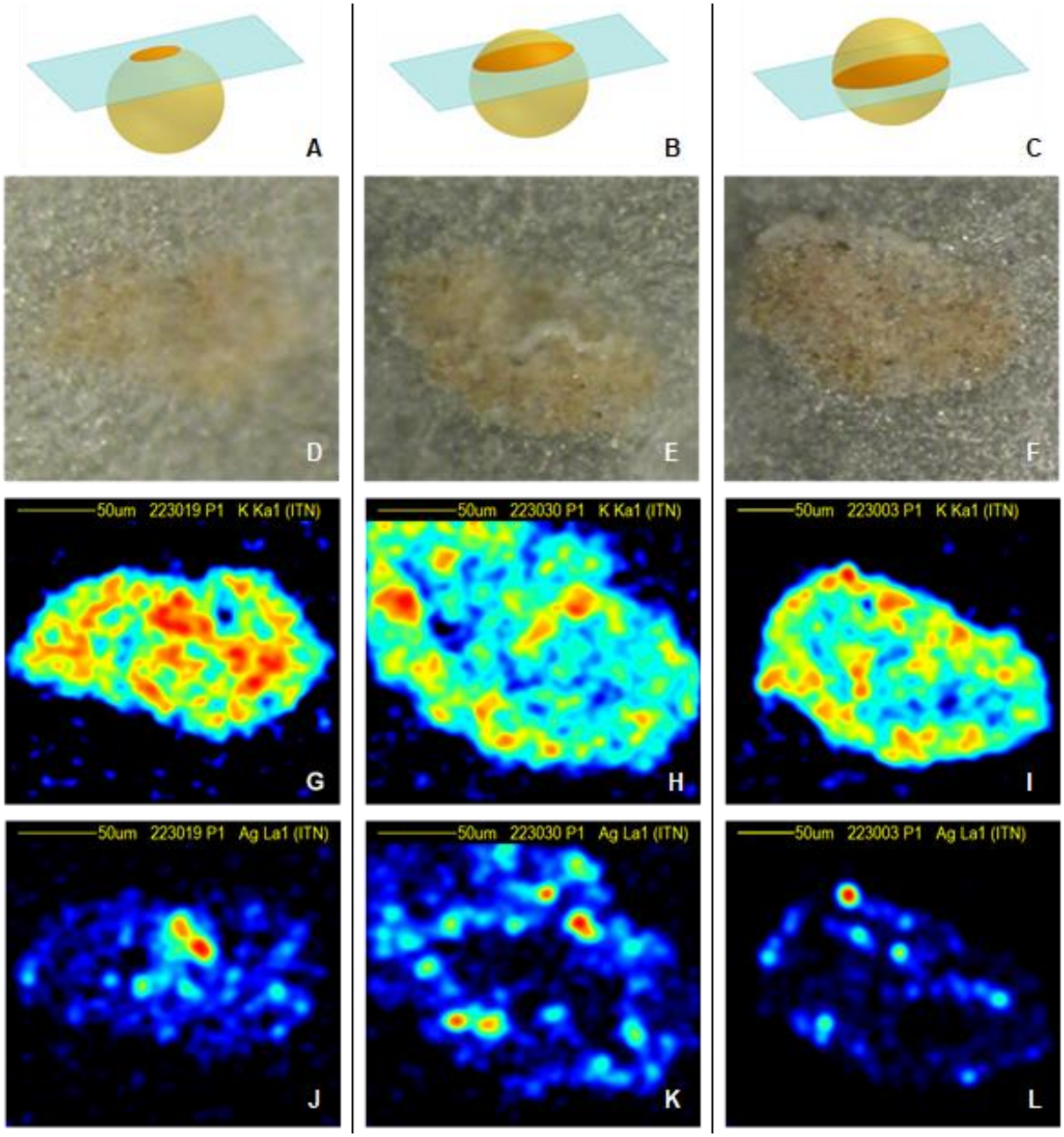

Figure 18. Graphical representation of the three AGS parallel sections obtained from the same granule (A-C). Optical microscopy image of the correspondent sections (D-F) and corresponding K (G-I) and Ag (J-F) elemental maps: The content gradient is represented by a dynamic colour scale: low–blue to high–red.

The first column of images is relative to one of the first distinct section of the granules. This area is the top region of the AGS structure and present a very homogenous PIXE map for the structural element of reference (K) while Ag deposition appears to be preferential in central region. The second column depicts a sectional plan somewhere in-between the first and the third sections. The Ag PIXE

map starts to emerge a sense of peripheral organization as the core of the granule contains significantly less Ag than the rest of the granule. The final column, depicts the more equatorial region of the granule in question, this section clearly shows a preferential peripheral distribution of silver in the granular section.

3.5.1.3. Overall elemental composition

A wide-ranging data-set comprising the estimated elemental composition of each point of interest in all analysed granules of each reactor was created. Several sections of both Ag-fed (SBR1) and Ag-free (SBR2) granules were inspected, being the median concentration values of the studied elements examined according to three regions of the granules, i.e., periphery, intermediate region and core. The elemental concentration differences, between the control SBR2 and the AgNPs-fed SBR1 were then studied and their significance calculated, using the Mann-Whitney non-parametric test (Table 9).

Table 9. Absolute median concentration values (mg/kg dry mass) of the studied elements in the three regions of the granule. The significant concentration variations of SBR1 relative to SBR2 (%) are also indicated.

		Elemental concentration							
		Structural elements				Micro nutrients			Ag
		P	S	K	Ca	Mn	Fe	Zn	
AgNPs (SBR1)	Periphery	14202	6546	3207	2444	18	124	58	2978
	Intermediate	16664	9748	5136	3073	21	138	82	1168
	Core	17793	10943	5428	3736	22	130	87	141
CTR (SBR2)	Periphery	12217	6820	2176	3189	28	265	162	-
	Intermediate	7232	4953	1622	1829	12	141	110	-
	Core	6147	8732	2066	2178	16	170	150	-
Variation (%)*	Periphery	-	-	-	-	-36%	-53%	-64%	-
	Intermediate	+130%	-	+217%	+68%	-	-	-	-
	Core	+189%	-	+163%	-	-	-	-	-

*Only significant values are presented ($p<0.05$)

Overall micro-PIXE analysis showed that absolute concentration values for structural elements were higher in SBR1, and that micronutrients concentrations were higher in the granules retrieved from the control bioreactor, especially at the periphery. Analysing the concentration variations (%) of the AgNPs-fed SBR1 relative to the control SBR2, the P, K and Ca elemental concentrations significantly increased ($p<0.05$) in the intermediate and core regions. Opposite, the concentrations of the micronutrients Mn, Fe and Zn showed a significant decrease ($p<0.05$) in the periphery region of AgNPs-feed SBR. A more explanatory statistical representation of this data recurring to box plots can be found in Annex 5.

The Ag distribution in granules of SBR1 showed a massive deposition at the periphery with a sharp decrease to intermediate regions of the granule. The core of the granules was practically void of Ag. The median concentration value of 114 mg/kg (interquartile 25% and 75% of 109 and 202 mg/kg, respectively) indicated in Table 9 referred to a limited number of the total number of core points analysed

and approximates the minimum quantifiable concentration in the analysis, which was of approximately 100 mg/kg. Therefore, the presence of Ag at inner regions of the granule should be taken with caution. It is possible that the AgNPs preferentially accumulated in the peripheral region, possibly leading to the concentration reduction of other elements in this area, namely micronutrients. The chelating properties of EPS are well described (Mu et al. 2012), being these substances essential for biomass to capture free nutrients in the surrounding media. Perhaps the high load of AgNPs that the tested biomass underwent may have hampered the association of EPS with other nutrients existing in a much smaller quantity. The disparity in the proportion of AgNPs and other metals in the media may have caused some sort of competition between the AgNPs and free micronutrients, such as Mn, Fe and Zn.

The AgNPs-fed granules showed higher contents of structural elements, such as, P, K and Ca, in the inner regions than the control. The presence of these elements in biological systems is strongly linked to an active metabolic activity. In some way the granular communities may be trying to compensate the micronutrient depletion in the more peripheral areas of the AGS, by producing more biomass that would ultimately produce more EPS maximizing the capture abilities. Moreover, this hypothesis explains the not so clear fact that the AgNPs exposed granules present higher development stage and biomass content.

3.5.1.4. Discriminant analysis

To study the association between elements quantified in the three selected regions of the granular biomass, i.e., periphery, intermediate and core regions, and how these associations may be linked to structure or reflect physiological aspects, a discriminant analysis was carried out. This discriminant analysis comprises the data values referent to the AgNPs-feed bioreactor. Linear discriminant function analysis performs a multivariate test of differences between groups being used to determine the minimum number of dimensions needed to describe these differences (Annex 6.). This analysis was performed by comparing the different concentration of some key elements in the different zones within the granule, namely periphery, intermediate region and core. In order to avoid the over estimation of silver concentration in the peripheral and intermediate regions, an independent group comprised large agglomerates of Ag. In Figure 19 the distance between group centroids (blue squares) is a measure of similarity between groups. Therefore, the centroids of core and intermediate regions are in close proximity to each other and more distant of the periphery region centroid, suggesting that peripheric regions are distinct from inner regions of the granule.

The variable (elements in the model) correlations with the discriminant functions provide information about the elements that can discriminate these regions. The model generated three functions that correlate the elements introduced in the analysis. The functions 1 and 2 explained most of the variance in the analysis. The first function expresses mostly the variance associated with Ag while the second function express the variance of K, Zn, Ca, Mn, Fe and the third function the variance associated with S and P. The importance of the functions in explaining the overall variance is analysed in terms of correlation coefficients and function eigenvalues, which can be translated also in terms of percentage of variance explained by each function. In the present analysis the first two functions could explain 98% of total variance, being the first function, which is correlated with Ag variance the most

relevant (eigenvalue=2.007; 84.9% of variance) (Table A1.1 and A1.2, Appendix section). Therefore, in this analysis only function one and two were considered. Basically, the three centroids, each correspondent to a granule region and the Ag agglomerates, were differentiated among themselves firstly trough the Ag concentration values (Function 1), and secondly for the concentration values of K, Zn, Ca, Mn, Fe (Function 2). The discriminant analysis showed that the peripheral region could be clearly distinguished from the remaining intermediate and core regions that sit close together, indicating a large degree of similarity. With that said, the AgNPs group was naturally the most distant of the remaining groups since it was constituted only by the analysed points where high Ag concentrations were measured. These data, probably corresponding to AgNPs agglomerates, was traded as one independent group regardless of their localization, although most of the data was localized at the granule periphery.

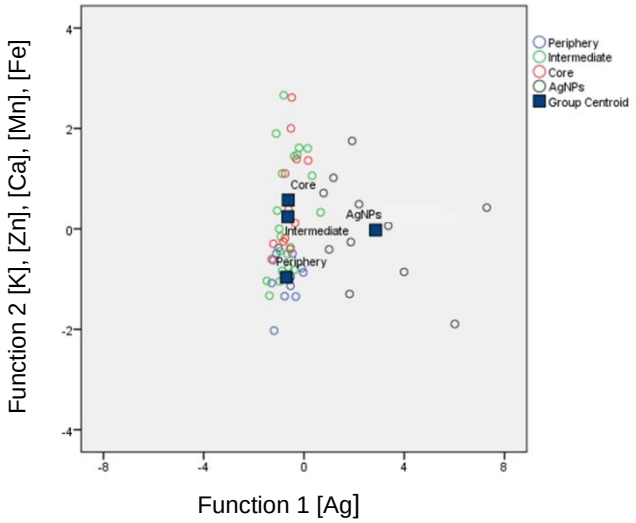

Figure 19. Canonical discriminant function, illustrating the elemental similarity degree between the three studied regions i.e., periphery, intermediate and core. An extra group (AgNPs) is also presented comprising large agglomerates of Ag. The first function expresses mostly the variance associated with Ag while the second function express the variance of K, Zn, Ca, Mn, Fe.

These results corroborate the findings described above, especially that the periphery region has distinct characteristics from inner regions, independently of the presence of Ag. The discriminant function 2, which correlated structural elements and micronutrients, such as K, Ca, Mn, Fe and Zn, enabled discriminating the outer layers of the granule from inner regions. Therefore, these findings support the differences in the elemental concentrations observed between SBR1 and SBR2 (control), as K and Ca concentration changes were associated to inner regions of the granule, whereas the Mn, Fe and Zn changes were only observed at the periphery (Annex 7).

3.5.2. Quantification of Ag in reactor (bulk) mixed liquor and effluent fractions

Whilst the previous chapter focused in the microanalysis of the granular fraction, in this section the distribution of AgNPs in major fractions of the SBR will be considered. It is of capital importance to understand how is the distribution of AgNPs in a broader scenario. Therefore, a new experimental design was adopted to quantify the Ag in the mixed-liquor and effluent fractions recurring to different techniques in an attempt to portray a rough mass balance of the AgNPs-fed reactor.

The physical characteristics of the mixed-liquor and effluent fractions require different approaches, which include different analytical techniques to determine Ag concentration in different media. The concentration of Ag in effluents or in the liquid portion of mixed liquor may be considerably low than in biomass fractions. Also, sample preparation requirements are totally different in what concerns homogenization of the materials for representative analysis (see Methods section).

Therefore, the Ag concentration in solid fractions obtained either by centrifugation (pellets) or filtration were analysed by PIXE, which is an expedite technique to analyse solid samples, whereas mixed-liquor supernatants and effluents were analysed by ICP-MS, which has a higher sensitivity than PIXE and is the gold standard technique for the analysis of liquid samples. The concentration of Ag in the input suspension was also analysed by ICP-MS.

A suspension of 100 mg/L AgNPs was continually used as input in the reactor to grant a starting concentration of 10mg/L in the Ag-fed bioreactor in each cycle. A sample of this feed input was collected directly at the end of the feeding tube revealing an Ag concentration of 76 mg/L, which is an acceptable value given the details in the feeding. From the feeding tank, passing through a peristatic pump in a plastic tube until reaching the bioreactor as a final destination, some losses might be expected.
In Table 10 the results of the total reactor content and total effluent fractions obtained by filtration, consisting of solid and liquid fractions are listed.

Table 10. Ag concentration estimated for both mixed liquor and effluent concerning Ag-fed SBR1 and Ag-free control SBR2. Solid fractions were analysed by PIXE and liquid fractions by ICP-MS. NA represents the fractions that were not analysed and MDL represents the method detection limit. Results are in mg/L. *This fraction was subjected to an additional washing and filtration step.

		Ag concentration (mg/L)	
		SBR1	**SBR2**
Mixed liquor	Solid fraction	$1.76x10^{+2}$*	$1.69x10^{0}$
		$2.89x10^{+2}$	NA
	Liquid fraction	$7.00x10^{-2}$	<MDL
		$8.00x10^{-2}$	<MDL
Effluent	Solid fraction	$2.05x10^{+1}$	<MDL
	Liquid fraction	$8.00x10^{-2}$	NA
		$8.00x10^{-2}$	NA

The solid fractions corresponding to the solid residue mainly composed by biomass that is retained in the filter, were analysed by PIXE. The liquid fractions corresponding to the filtrates were analysed by ICP-MS. In the solid fraction of mixed liquor, the Ag concentration was of 288.55 mg/L. To verify the methodology (filtration) and analytical results for Ag concentrations in the solid fraction of the SBR1 mixed liquor, a pool of samples taken in the same week as those reported above in Table 10 were subjected to different sample preparation methods and analysed by PIXE. The solid fraction was separated by centrifugation (4000 rpm, 10 min), lyophilized and the dry material obtained, pelletized and acid digested as described in section 2.3.2.1. The results obtained for the Ag concentration in the solid fraction were consistent with the filtered sample. The Ag concentration in the pelletized aliquot of the pool was of 147 mg/L, whereas in the digested aliquot was of 187 mg/L, legitimating the filtration procedure as the obtained concentration values are of the same magnitude. In the mixed liquor liquid

fraction (corresponding to the filtrate), Ag concentrations displayed much lower values (0.07 and 0.08 mg/L). This indicates that most Ag is retained in the biomass and not in suspension or dissolved in the liquid fraction.

Concerning the effluent samples, an Ag concentration 20.49 mg/L was found in the SBR1 effluent solid fraction, representing an 8-fold reduction when compared to the homolog mixed liquor solid fraction. The detected Ag concentration in the effluent liquid fraction was 0.08 mg/L, once again indicating that the majority of AgNPs are associated with the biomass. In this single assay, and considering all the silver quantified in the effluent, meaning the Ag concentration in solid and liquid fractions, the liquid fraction only represented 0.38%.

Moreover, when comparing the liquid fractions obtained from the mixed liquor and from the effluent, the Ag contents found were very similar. This suggests an even distribution of Ag content across both liquid fractions of the operational system (mixed liquor and effluent), which is much lower than the correspondent solid portions. Once again, the fact that Ag concentrations in the liquid fraction of both mixed liquor and effluent are similar can indicate that the majority of Ag in the reactor is associated to the mixed liquor solid content, that is to say biomass.

To explore the mobility of Ag in the solid fraction, replicates of the mixed liquor and effluent filtered samples of the Ag-fed system (SBR1) were additionally washed with 10mL of distilled water by filtration and Ag concentration measured in both solid and liquid fractions obtained. The procedure was run in parallel to the samples reported on Table 10. The results obtained were of the same order of magnitude, i.e., 176 mg/L in the mixed liquor solid fraction and 0.09 mg/L and 0.01 mg/L for the mixed liquor and effluent liquid fractions respectively. Therefore, the additional washing caused a loss of Ag in the mixed liquor solid fraction retained in the filter. This finding suggests that AgNPs in suspension were retained in the solid fraction during the filtration step or a small fraction of AgNPs may be loosely bound to biomass and can be therefore washed out. The test also showed that Ag concentration changes in the liquid fractions were minimal. In addition, the increase in Ag concentration in the filtrate does not reflect the amount of Ag lost in the solid fraction due to the washing procedure. The quantitative results may be affected by a number of uncertainties in the methodological procedure, which can be related to dry deposit weighting, mass loss during washing, among others. Finally, it is worth mentioning that it was not possible to analyse the effluent solid fraction obtained after the additional washing procedure as the deposit on the filter became very fragile hindering the subsequent analysis by PIXE. Despite the methodological issues that certainly need to be further examined, the test can give relevant information about the stability of Ag concentration in the liquid fraction and the massive retention of Ag in the biomass. Also, the significant differences found between the solid and liquid Ag-fed SBR1 effluent fractions, confirm the idea that the majority of Ag is biomass-associated. This way the Ag discharged from the reactor must be directly correlated with the amount of discharged biomass. Evidently the results herein obtained are insufficient to confirm or dismiss this type of supposition, but if proven to be true, by maximizing efforts to reduce biomass loss, the amount of AgNPs leaving the operational system could be drastically reduced.

In section 3.1.7 the AgNPs concentration in the reactor had already been estimated recurring to a VSS/TSS-based method. For the same operational day, values of 144mg/L were obtained. Therefore,

the four independently obtained results of AgNPs concentration in SBR1 mixed liquor recurring to different analytical and biomass separation methods (147-288 mg/L) were comparable to the AgNPs concentration estimated by VSS/TSS method.

The differences obtained in Ag concentration between the washed and unwashed biomass samples proved that a fraction of Ag that is trapped in the filtration but is not associated to biomass. In fact, without washing we are concentrating the sample, part of the Ag that is being detected in the biomass should be quantified in the supernatant. Therefore, when using filtration to separate the mixed liquor components, an additional washing step may be appropriate. Nevertheless, the methodology should be thoroughly checked in order to confirm its suitability.

Regarding SBR2, the mixed liquor was also tested to detect a possible presence of Ag in the reactor. In ideal conditions no Ag should be detected, however, a residual value was detected indicating minor contamination 1.7 mg/L in the biomass (solid) fraction. This Ag marginal presence was most likely caused by contamination of laboratory containers used in daily manipulation of the reactors. No Ag could be detected in the SBR2 effluent or in the liquid fraction of mixed liquor (Ag detection limit: 1 μg/L).

Some equipment difficulties compromised the number of performed experiments, reducing the desired statistical strength of this study. Thus, the analyses carried out were only exploratory. Replicates of the tests performed would be useful providing statistical power to the results obtained. Nevertheless, the exploratory analysis helped establishing the adequacy of methods and techniques to quantify Ag in the different fractions. Also, the level of Ag concentrations in both solid and liquid fractions provided strong indications about the capacity of biomass to retain AgNPs in a large scale and of the low solubilization of Ag. Clearly the results obtained in this study cannot be seen as a mass balance. Still, further efforts are needed to test different sampling methodologies in order to attain a more definitive protocol. The use of other techniques, such as ultracentrifugation can be advantageous to study the soluble AgNPs fraction.

As AgNPs are being fed into the reactor the biomass showed to become Ag enriched. An AgNPs input of 10mg/L is provided for each six-hour cycle and the estimated Ag concentration values for biomass showed values in a superior order of magnitude. The values correspond to a cycle from operational day number 79, but as biomass content appears to stabilize in the tested reactors, the Ag content should also reach a steady concentration value. Further studies are required to confirm this assumption. Nonetheless the large majority of the detected Ag was undoubtedly associated to the biomass.

4. Conclusions

The present study achieved the previously set objectives and unveiled some new insights on the interaction of AgNPs with a AGS system. An optimized procedure to extract and quantify protein and polysaccharides in AGS-EPS was attained with the effects of the AgNPs exposure on the total EPS content of the biomass being also subject of investigation.

The proportions of granular biomass in the two SBRs under study were found to be lower than what would be ideal in a AGS system. For both cases we are effectively in the presence of a mixed system were the majority of the biomass is in a flocculent state. Nonetheless, the Ag-fed SBR1 consistently presented the higher proportion of granular biomass. This reactor also exhibited a better overall performance. Thus, the impact of the relative granular biomass content, although lower than desired, appears to be significative. Most importantly, it seems that the continuous exposure of SBR1 biomass to AgNPs has enhanced the granulation process.

The performance of both tested reactors was very similar, the presence of AgNPs appeared to have a bigger influence in the physical parameters such as SVI a relative granular percentage, than in the treatment performance, namely colour and COD removal. The 18-day storage period clearly affected the VSS, TSS, SVI and colour removal values at startup, but they all quickly recovered. The COD profile was similar in both bioreactors and appeared to be enhanced by the occurrence of the storage period. In fact, in the first monitored cycle after storage showed that both reactors presented higher COD removal than in the cycles before storage, particularly SBR2. This effect is probably an attempt to compensate the starving conditions the biomass was subjected during storage.

The AgNPs-fed SBR1 presented a higher VSS and TSS content as well as a higher granular percentage than SBR2, so AgNPs appeared to have no toxic effect, on the contrary they appeared to have led to an overall better granulation stage. Also, AgNPs presence had a positive effect in the biomass settleability properties, which may have contributed to the granulation process.

EPS assume an important role both in granule formations (Liu and Tay 2002) and NPs capture (Geyik and Çeçen 2015) and defined methodologies to extract and quantify it in AGS are still scarce. This way different methods to extract the major components of EPS from AGS were tested in order to achieve an adequate method to our particular case. The use of more forceful pre-extraction methods appeared to be unnecessary to re-suspend and homogenize the sludge before the extraction method. This could be expected given the calculated mass fractions of each reactor, as mild methods are usually sufficient to extract EPS components in protocols developed for flocculent biomass. Regarding the tested extraction methods, considering the tests results, it was decided to adopt the heat extraction method, as the use of CER appeared to facilitate PN extraction compared to PS.

The use of trichloroacetic acid (TCA) to perform protein precipitation seemed to eliminate substances that possibly were interfering with EPS and compromising the PN quantification in the previous assays. The method was also tested adding Ag^{+} in relevant concentrations, what did not significantly influence any stage of the PN and PS quantification methods.

Regarding the PN and PS quantification, the overall profile across the totality of the monitored period showed that the concentration values of PN and PS varied unpredictably through time and were

within a limited range. This suggests that the registered alterations were most likely due to the specific reactor dynamic rather than to the presence or absence of AgNPs. No evident trend was observed in a cycle period concerning PN content, but the results on PS content appeared to reveal an incipient pattern where the total PS content increased in the anaerobic phase (feast phase) and later decrease with aeration (famine phase). This way, the total PS content production and consumption processes across the SBR cycle appear to be, to some extent, related to the external substrate availability. The starvation induced by an 18-day biomass storage appeared to have accentuated this tendency, evident in the first monitored cycle after the hiatus. The PS fraction was consumed during the storage period. The variations of both PN and PS were identical for SBR1 and SBR2, indicating that the AgNPs presence did not affect the overall EPS profile across a reaction cycle.

Despite the different relative biomass size fractionation of the mixed liquor in the bioreactors, the results regarding the PN overall content were found to be in the same range (Figures 13A and 13B). Neither the AgNPs presence nor the different percentages in flocculent and granular biomass appeared to have contributed to a difference in the quantification of PN. Both SBR1 and SBR2 presented the higher values in different periods of the monitored operation (Figure 14), leading to the idea that the displayed variations are caused by the specific reactor dynamic, rather than a particular tendency caused by an external factor.

As largely reported in the literature, protein is the most abundant EPS component in granular biomass. The results obtained in this thesis showed that PN/PS ratios were very low. The small percentage of granular biomass present in the bioreactors contributed to low PN/PS values that have also been associated with non-granular biomass. The low PN/PS ratios obtained could also reflect that the independent quantification of the EPS components was consistently underestimated most likely due to low and selective extraction efficiency. Consequently, the underestimation of protein content is also a real possibility. Despite the efforts put in optimizing EPS extraction and PS and PN quantification, further studies are still needed to improve extraction and quantification procedures, especially concerning the determination of PN content.

Further characterization of the granular fraction in both reactors involved elemental composition. Some elements, such as P, S, K, Ca, and Fe among others are essential to maintain cellular functions therefore their changes may give clues about the status of granular microbial communities. The elemental distributions in granules from the two reactors SBR1 and SBR2 showed important differences. The elemental distributions in SBR1 granules showed a different pattern, which for most of the structural elements is opposite to SBR2. The AgNPs-fed granules showed higher contents of structural elements such as, P, K and Ca, in the inner regions of the granule than the granules of the control reactor SBR2. On the other hand, the micronutrients, such as Mn, Fe and Zn showed a tendency to be more concentrated at the periphery of the SBR2 granules, contrasting with SBR1 granules where the contents of these elements decreased in the outer layers and important deposition of AgNPs, often in large agglomerates, were observed. Nevertheless, the preferential Ag deposition observed at the periphery of the granule sharply decreased towards the core of the granule. Ag was sporadically found in inner regions of the sectioned granule, although in significantly lower concentrations. Also, Ag was found to be retained in the biomass in large scale, and only a very small fraction of Ag seemed to be solubilized

or in suspension in the liquid fraction of the reactor. Altogether, the differences in elemental profiles enabled to differentiate granules exposed to AgNPs and importantly defined a signature for different regions of the granular structures. The elemental profiles and their associations with outer or inner regions of the granule seem to indicate that the external layers of the granule act as a barrier to AgNPs, protecting the microbiological communities of inner regions from potential Ag toxic effects. This is also consistent with the increase of structural elements concentration in inner regions of the SBR1 granules, which may reflect a more active metabolism in these regions. These findings may possibly indicate that the increased cellular activity counteract a loss in the capacity of capturing nutrients from media, required to the sustainability of the microbiological communities, due to presence of AgNPs and their binding to EPS. On the other hand, the presence of AgNPs did not significantly influence EPS profile or PS and PN contents in both Ag-fed and Ag-free bioreactors. However, it should be taken into account that the low granular biomass content in both SBR1 and SBR2 may impede the detection of significant changes in EPS contents that can be linked to the metabolic activity of granular biomass. Other aspect that may support the increased metabolic activity of granular biomass in the presence of AgNPs, is the positive effect that AgNPs, at least in the concentration levels used, had in granulation and therefore in the performance of the AGS system.

5. Future prospects

Future work should focus aspects that will enable setting parameters to estimate the reactor mass balance and process evaluation. This will consist of regular Ag concentration determination in biomass and liquid fractions through the reactor cycles and Ag concentration in the effluent.

Improve efficiency in EPS extraction and consequently a more adequate quantification of PN and PS. In this context the methodologies developed need to be standardized to assure rigorous measurements.

Despite being very laborious, the evolution of AgNPs concentration in the reactors, as well as the total EPS content should be studied simultaneously from the granulation phase to a more stable period, possibly enabling the establishment of a relation between the PN/PS content evolution during the granulation and the AgNPs retained in the system.

The AgNPs-AGS interaction can also potentially cause changes in the diversity of the microbial community. Thus, the analysis of the microbial consortium present in AGS would also be very pertinent since the diversity of the microbial communities can have implications in EPS production.

6. References

Adav, Sunil S. and Duu Jong Lee. 2008. “Extraction of Extracellular Polymeric Substances from Aerobic Granule with Compact Interior Structure.” *Journal of Hazardous Materials* 154(1–3):1120–26.

Adav, Sunil S., Duu Jong Lee, Kuan Yeow Show, and Joo Hwa Tay. 2008. “Aerobic Granular Sludge: Recent Advances.” *Biotechnology Advances* 26(5):411–23.

American Public Health Association. 1995. *Standard Methods for the Examination of Water and Wastewater*. edited by A. D. Eaton, L. S. Clesceri, and A. E. Greenberg. Washington DC: American Public Health Association.

Aoi, Y., S. Tsuneda, and A. Hirata. 2004. “Transition of Bacterial Spatial Organization in a Biofilm Monitored by FISH and Subsequent Image Analysis.” *Water Science and Technology* 49(11–12):365–70.

Arvidsson, Rickard, Sverker Molander, and Björn A. Sandén. 2011. “Impacts of a Silver-Coated Future Particle Flow Analysis of Silver Nanoparticles.” *Journal of Industrial Ecology* 15(6):844–54.

Banat, Ibrahim M., Poonam Nigam, Datel Singh, and Roger Marchant. 1996. “Microbial Decolorization of Textile-Dye-Containing Effluents: A Review.” *Bioresource Technology* 58(3):217–27.

Batstone, D. J. and J. Keller. 2001. “Variation of Bulk Properties of Anaerobic Granules with Wastewater Type.” *Water Research* 35(7):1723–29.

Benn, Troy M. and Paul Westerhoff. 2008. “Nanoparticle Silver Released into Water from Commercially Available Sock Fabrics.” *Environmental Science and Technology* 42(11):4133–39.

Bento, J. B. 2016. “Interaction of Silver Nanoparticles with Aerobic Granular Sludge in Textile Wastewater Treatment Bioreactors.” IST.

Beun, J. J. et al. 1999. “Aerobic Granulation in a Sequencing Batch Reactor.” *Water Research* 33(10):2283–90.

Beun, J. J., J. J. Heijnen, and M. C. M. Van Loosdrecht. 2001. “N-Removal in a Granular Sludge Sequencing Batch Airlift Reactor.” *Biotechnology and Bioengineering* 75(1):82–92.

Bilińska, Lucyna, Marta Gmurek, and Stanisław Ledakowicz. 2016. “Comparison between Industrial and Simulated Textile Wastewater Treatment by AOPs – Biodegradability, Toxicity and Cost Assessment.” *Chemical Engineering Journal* 306:550–59.

Breese, M. B., D. N. Jamieson, and P. J. King. 1996. *Materials Analysis Using a Nuclear Microprobe*. Chichester, Sussex PO 19 1 UD, UK: John! Wiley & Sons Ltd.

De Bruin, L. M. M., M. K. De Kreuk, H. F. R. van der Roest, C. Uijterlinde, and M. C. Van Loosdrecht. 2004. “Aerobic Granular Sludge Technology: An Alternative to Activated Sludge?” *Water Science and Technology* 49(11–12):1–7.

Bshena, Osama, Tiaan DJ Heunis, Leon MT Dicks, and Bert Klumperman. 2011. “Antimicrobial Fibers: Therapeutic Posibilities and Recent Advances.” *Future Med. Chem.* 3(14):1823–49.

Chen, Huan, Shungui Zhou, and Tianhong Li. 2010. “Impact of Extracellular Polymeric Substances on the Settlement Ability of Aerobic Granular Sludge.” *Enviromental Technology* 31(14):1601–12.

Chou, H. H. and J. S. Huang. 2005. “Comparative Granule Characteristics and Biokinetics of Sucrose-

Fed and Phenol-Fed UASB Reactors." *Chemosphere* 59(1):107–16.

Comte, S., G. Guibaud, and M. Baudu. 2006. "Relations between Extraction Protocols for Activated Sludge Extracellular Polymeric Substances (EPS) and EPS Complexation Properties Part I . Comparison of the Efficiency of Eight EPS Extraction Methods." *Enzyme and Microbial Technology* 38(1–2):237–45.

Dasgupta, Jhilly, Jaya Sikder, Sudip Chakraborty, Stefano Curcio, and Enrico Drioli. 2015. "Remediation of Textile Effluents by Membrane Based Treatment Techniques : A State of the Art Review." *Journal of Environmental Management* 147:55–72.

Dastjerdi, Roya and Majid Montazer. 2010. "A Review on the Application of Inorganic Nano-Structured Materials in the Modification of Textiles: Focus on Anti-Microbial Properties." *Colloids and Surfaces B: Biointerfaces* 79(1):5–18.

Deng, S., L. Wang, and H. Su. 2016. "Role and Influence of Extracellular Polymeric Substances on the Preparation of Aerobic Granular Sludge." *Journal of Environmental Management* 173:49–54.

Duarte, Filipa, V. Morais, F. J. Maldonado-hódar, and Luis M. Madeira. 2013. "Treatment of Textile Effluents by the Heterogeneous Fenton Process in a Continuous Packed-Bed Reactor Using Fe/activated Carbon as Catalyst." *Chemical Engineering Journal* 232:34–41.

Dubois, Michel, K. A. Gilles, J. K. Hamilton, P. A. Rebers, and Fred Smith. 1956. "Colorimetric Method for Determination of Sugars and Related Substances." *Analytical Chemistry* 28(3):350–56.

Dudkiewicz, Agnieszka et al. 2011. "Characterization of Nanomaterials in Food by Electron Microscopy." *Trends in Analytical Chemistry* 30(1):28–43.

Dulekgurgen, E., N. Artan, D. Orhon, and P. A. Wilderer. 2008. "How Does Shear Affect Aggregation in Granular Sludge Sequencing Batch Reactors? Relations between Shear, Hydrophobicity, and Extracellular Polymeric Substances." *Water Science and Technology* 58(2):267–77.

Van Espen, P., K. Janssens, and I. Swenters. 1986. "AXIL X-Ray Analysis Software." *Canberra Packard, Benelux*.

Fabrega, Julia, Samuel N. Luoma, Charles R. Tyler, Tamara S. Galloway, and Jamie R. Lead. 2011. "Silver Nanoparticles : Behaviour and Effects in the Aquatic Environment." *Environment International* 37(2):517–31. Retrieved (http://dx.doi.org/10.1016/j.envint.2010.10.012).

Fabricius, Anne-lena, Lars Duester, Björn Meermann, and Thomas A. Ternes. 2014. "ICP-MS-Based Characterization of Inorganic Nanoparticles - Sample Preparation and off-Line Fractionation Strategies." *Anal Bioanal Chem.* 406(2):467–79.

Fang, Herbert H. P. and X. S. Jia. 1996. "Extraction of Extracellular Polymer from Anaerobic Sludges." *Biotechnology Techniques* 10(11):803–8.

Farabegoli, G., A. Chiavola, E. Rolle, and M. Naso. 2010. "Decolorization of Reactive Red 195 by a Mixed Culture in an Alternating Anaerobic-Aerobic Sequencing Batch Reactor." *Biochemical Engineering Journal* 52(2–3):220–26.

Felz, Simon, Salah Al-zuhairy, Olav Andreas Aarstad, Mark C. M. Van Loosdrecht, and Yue Mei Lin. 2016. "Extraction of Structural Extracellular Polymeric Substances from Aerobic Granular Sludge." *Journal of Visualized Experiments* 115:1–8.

Fleischer, Candace C. and Christine K. Payne. 2014. "Nanoparticle − Cell Interactions: Molecular

Structure of the Protein Corona and Cellular Outcomes." *Accounts of Chemical Research* 47:2651–59.

Flemming, Hans-curt and Jost Wingender. 2010. "The Biofilm Matrix." *Nature Reviews Microbiology* 8(9):623–33.

Franca, Rita D. G. et al. 2015. "Effect of an Azo Dye on the Performance of an Aerobic Granular Sludge Sequencing Batch Reactor Treating a Simulated Textile Wastewater." *Water Research* 85:327–36.

Franze, Bastian and Carsten Engelhard. 2014. "Fast Separation, Characterization, and Speciation of Gold and Silver Nanoparticles and Their Ionic Counterparts with Micellar Electrokinetic Chromatography Coupled to ICP-MS." *Analytical Chemistry* (84):5713−5720.

Frølund, Bo, Rikke Palmagren, Kristian Keiging, and Per Halka Nielsen. 1996. "Extraction of Extracellular Polymers from Activated Sludge Using a Cation Exchange Resin." *Water Research* 30(8):1749–58.

Gao, Dawen, Xiangjuan Yuan, and Hong Liang. 2011. "Comparison of Biological Removal via Nitrite with Real-Time Control Using Aerobic Granular Sludge and Flocculent Activated Sludge." *Applied Microbiology and Biotechnology* 89(5):1645–52.

Gao, Yuan and R. Cranston. 2008. "Recent Advances in Antimicrobial Treatments of Textiles." *Textile Research Journal* 78(1):60–72.

Geyik, Ayse Gul and Ferhan Çeçen. 2015. "International Biodeterioration & Biodegradation Variations in Extracellular Polymeric Substances (EPS) during Adaptation of Activated Sludges to New Feeding Conditions." *International Biodeterioration & Biodegradation* 105:137–45.

Ghaly, AE, R. Ananthashankar, M. Alhattab, and VV Ramakrishnan. 2014. "Production, Characterization and Treatment of Textile Effluents: A Critical Review." *Chemical Engineering and Process Technology* 5(1):1–18.

Godinho, R. M., M. T. Cabrita, L. Alves, and T. Pinheiro. 2014. "Imaging of Intracellular Metal Partitioning in Marine Diatoms Exposed to Metal Pollution: Consequences to Cellular Toxicity and Metal Fate in the Environment." *Metallomics* 6(9):1626–31.

González-Gutiérrez, Linda V., Guillermo González-Alatorre, and Eleazar M. Escamilla-Silva. 2009. "Proposed Pathways for the Reduction of a Reactive Azo Dye in an Anaerobic Fixed Bed Reactor." *World Journal of Microbiology and Biotechnology* 25(3):415–26.

Grime, G. W. 1996. "The 'Q Factor' Method: Quantitative microPIXE Analysis Using RBS Normalisation." *Nuclear Instruments and Methods in Physics Research Section B: Beam Interactions with Materials and Atoms* 109:170–74.

Grime, G. W. and M. Dawson. 1995. "Recent Developments in Data Acquisition and Processing on the Oxford Scanning Proton Microprobe." *Nuclear Instruments and Methods in Physics Research Section B: Beam Interactions with Materials and Atoms* 104:107–13.

Gu, Lingyun, Qilin Li, Xiangchun Quan, Yan Cen, and Xiaoman Jiang. 2014. "Comparison of Nanosilver Removal by Flocculent and Granular Sludge and Short- and Long-Term Inhibition Impacts." *Water Research* 58:62–70.

Heine, E., HG Knops, K. Schaefer, P. Vangeyte, and M. Moeller. 2007. "Antimicrobial

Functionalisation of Textile Materials: Multifunctional Barriers for Flexible Structure." P. 292 in *Multifunctional Barriers for Flexible Structure*, edited by S. Duquesne, C. Magniez, and G. Camino. Berlin Heidelberg: Springer.

Jeynes, Chris and Julien L. Colaux. 2016. "Thin Film Depth Profiling by Ion Beam Analysis." *Analyst* 141(21):5944–85.

Jin, Xian Chun, Gao Qiang Liu, Zheng Hong Xu, and Wen Y. Tao. 2007. "Decolorization of a Dye Industry Effluent by Aspergillus Fumigatus XC6." *Applied Microbiology and Biotechnology* 74(1):239–43.

Johansson, S. A., J. L. Campbell, and K. G. Malmqvist. 1995. *Particle-Induced X-Ray Emission Spectrometry (PIXE)*. New York: John Wiley & Sons.

Kaegi, Ralf, Andreas Voegelin, Brian Sinnet, Harald Hagendorfer, and Michael Burkhardt. 2011. "Behavior of Metallic Silver Nanoparticles in a Pilot Wastewater Treatment Plant." *Environmental Science & Technology* 45(9):3902–8.

Kang, Fuxing, Pedro J. Alvarez, and Dongqiang Zhu. 2013. "Microbial Extracellular Polymeric Substances Reduce Ag+ to Silver Nanoparticles and Antagonize Bactericidal Activity." *Environmental Science and Technology* 48(1):316–22.

Khan, S. and A. Malik. 2014. "Environmental and Health Effects of Textile Industry Wastewater." Pp. 55–71 in *Environmental Deterioration and Human Health.* Springer Netherlands.

Kiser, Mehlika A., Hodon Ryu, Hyunyoung Jang, Kiril Hristovski, and Paul Westerhoff. 2010. "Biosorption of Nanoparticles to Heterotrophic Wastewater Biomass." *Water Research* 44(14):4105–14.

De Kreuk, M. K., J. J. Heijnen, and M. C. Van Loosdrecht. 2005. "Simultaneous COD, Nitrogen and Phosphate Removal by Aerobic Granular Sludge." *Biotechnology Advances* 90(6):761–69.

De Kreuk, M. K., N. Kishida, and M. C. Van Loosdrecht. 2007. "Aerobic Granular Sludge - State of the Art." *Water Science and Technology* 55(8–9):75–81.

De Kreuk, M. K. and M. C. Van Loosdrecht. 2004. "Selection of Slow Growing Organisms as a Means for Improving Aerobic Granular Sludge Stability." *Water Science and Technology* 49(11–12):9–17.

Li, X. Y. and S. F. Yang. 2007. "Influence of Loosely Bound Extracellular Polymeric Substances (EPS) on the Flocculation, Sedimentation and Dewaterability of Activated Sludge." *Water Research* 41:1022–30.

Li, Ya-chieh, Chen-yeon Chu, Shu-yii Wu, Chia-ying Tsai, and Chia-chi Wang. 2012. "Feasible Pretreatment of Textile Wastewater for Dark Fermentative Hydrogen Production." *International Journal of Hydrogen Energy* 37(20):15511–17.

Liang, Zhihua, Atreyee Das, and Zhiqiang Hu. 2010. "Bacterial Response to a Shock Load of Nanosilver in an Activated Sludge Treatment System." *Water Research* 44(18):5432–38.

Liao, B. Q., D. G. Allen, I. G. Droppo, G. G. Leppard, and S. N. Liss. 2001. "Surface Properties of Sludge and Their Role in Bioflocculation and Settleability." *Water Research* 35(2):339–50.

Liu, Hong and Herbert H. P. Fang. 2002. "Extraction of Extracellular Polymeric Substances (EPS) of Sludges." *Journal of Biotechnology* 95:249–56.

Liu, Xiao-Meng et al. 2010. “Contribution of Extracellular Polymeric Substances (EPS) to the Sludge Aggregation.” *Environmental Science & Technology* 44(11):4355–60.

Liu, Yu. 2007. *Wastewater Purification: Aerobic Granulation in Sequencing Batch Reactors*. CRC Press.

Liu, Yu and Joo Hwa Tay. 2002. “The Essential Role of Hydrodynamic Shear Force in the Formation of Biofilm and Granular Sludge.” *Water Research* 36(7):1653–65.

Van Loosdrecht, M. C., A. M. Martins, and G. A. Ekama. 2008. “Bulking Sludge.” Pp. 291–308 in *Biological Wastewater Treatment: Principles, Modelling and Design*, edited by M. Henze, M. C. M. van Loosdrecht, G. A. Ekama, and D. Brdjanovic. London: IWA Publishing.

Lorenz, C. et al. 2012. “Characterization of Silver Release from Commercially Available Functional (Nano)textiles.” *Chemosphere* 89(7):817–24.

Lourenço, N. D. et al. 2015. “Comparing Aerobic Granular Sludge and Flocculent Sequencing Batch Reactor Technologies for Textile Wastewater Treatment.” *Biochemical Engineering Journal* 104:57–63.

Lourenço, N. D., J. M. Novais, and H. M. Pinheiro. 2001. “Effect of Some Operational Parameters on Textile Dye Biodegradation in a Sequential Batch Reactor.” *Journal of Biotechnology* 89(2–3):163–74.

Mcswain, B. S., R. L. Irvine, M. Hausner, and P. a Wilderer. 2005. “Composition and Distribution of Extracellular Polymeric Substances in Aerobic Flocs and Granular Sludge.” *Applied and Environmental Microbiology* 71(2):1051–57.

Metcalf, L., H. P. Eddy, and Georg Tchobanoglous. 2004. *Wastewater Engineering: Treatment, Disposal, and Reuse*.

Mitrano, D. M. et al. 2014. “Tracking Dissolution of Silver Nanoparticles at Environmentally Relevant Concentrations in Laboratory, Natural, and Processed Waters Using Single Particle ICP-MS (spICP-MS).” *Environmental Science Nano* 1:248–59.

Morgenroth, E., T. Sherden, M. C. Van Loosdrecht, J. J. Heijnen, and P. A. Wllderer. 1997. “Aerobic Granular Sludge in a Sequencing Batch Reactor.” *Water Research* 31(12):3191–94.

Mosquera-Corral, A., M. K. De Kreuk, J. J. Heijnen, and M. C. Van Loosdrecht. 2005. “Effects of Oxygen Concentration on N-Removal in an Aerobic Granular Sludge Reactor.” *Water Research* 39(12):2676–86.

Moy, B. Y. P., J. H. Tay, S. K. Toh, Y. Liu, and S. T. L. Tay. 2002. “High Organic Loading Influences the Physical Characteristics of Aerobic Sludge Granules.” *Letters in Applied Microbiology* 34(6):407–12.

Mu, Hui, Xiong Zheng, Yinguang Chen, Hong Chen, and Kun Liu. 2012. “Response of Anaerobic Granular Sludge to a Shock Load of Zinc Oxide Nanoparticles during Biological Wastewater Treatment.” *Environmental Science & Technology* 5997–6003.

Mueller, N. C. and B. Nowack. 2008. “Exposure Modelling of Engineered Nanoparticles in the Environment.” *Environmental Science & Technology* 42(12):44447–53.

Mulware, Stephen Juma. 2014. “Analysis of Biological Materials Using a Nuclear Microprobe.”

Mulware, Stephen Juma. 2015. “The Review of Nuclear Microscopy Techniques: An Approach for

Nondestructive Trace Elemental Analysis and Mapping of Biological Materials." *Journal of Biophysics* 2015:7.

Nastasi, M., J. W. Mayer, and Y. Wang. 2014. *Ion Beam Analysis: Fundamentals and Applications*.

Nielsen, P. H. and A. Jahn. 1999. "Extraction of EPS." Pp. 49–72 in *Microbial extracellular polymeric substances*, edited by J. Wingender, T. Neu, and H. Flemming. Berlin: Springer-Verlag.

Ortega, Richard, Guillaume Devès, and Asunción Carmona. 2009. "Bio-Metals Imaging and Speciation in Cells Using Proton and Synchrotron Radiation X-Ray Microspectroscopy." *Journal of the Royal Society Interface* 6 Suppl 5:S649-58.

Ostrowski, Anja et al. 2015. "Overview about the Localization of Nanoparticles in Tissue and Cellular Context by Different Imaging Techniques." *Beilstein Journal of Nanotechnology* 6:263–80.

Oura, K., V. G. Lifshits, A. A. Saranin, A. V Zotov, and M. Katayama. 2013. *Surface Science: An Introduction*.

Pan, Xiangliang et al. 2010. "A Comparison of Five Extraction Methods for Extracellular Polymeric Substances (EPS) from Biofilm by Using Three- Dimensional Excitation-Emission Matrix (3DEEM) Fluorescence Spectroscopy." *Water SA* 36(1):111–16.

Pandey, Anjali, Poonam Singh, and Leela Iyengar. 2007. "Bacterial Decolorization and Degradation of Azo Dyes." *International Biodeterioration and Biodegradation* 59(2):73–84.

Pang, Yean L. and Ahmad Z. Abdullah. 2012. "Review Current Status of Textile Industry Wastewater Management and Research Progress in Malaysia: A Review." *CLEAN – Soil, Air, Water* 41(8):751–64.

Park, H. D., J. M. Regan, and D. R. Noguera. 2002. "Molecular Analysis of Ammonia-Oxidizing Bacterial Populations in Aerated-Anoxic Orbal Processes." *Water Science and Technology* 46(1–2):273–80.

Pinheiro, T. et al. 1997. "Elemental Distribution in the Human Respiratory System and Excretion Organs: Absorption and Accumulation." *X-Ray Spectrometry* 26(4):217–22.

Pinheiro, T., H. Duflou, and W. Maenhaut. 1990. "Applicability of Microwave Acid Digestion to Sample Preparation of Biological Materials for Analysis by Particle-Induced X-Ray Emission (PIXE)." *Biol Trace Elem Res* 26–27:589–97.

Pinheiro, Teresa et al. 2014. "Distribution and Quantitation of Skin Iron in Primary Haemochromatosis : Correlation with Total Body Iron Stores in Patients Undergoing Phlebotomy." *Acta Dermato-Venereologica* 94(1):14–19.

Pinheiro, Teresa, Maria Dolores Ynsa, and Luís C. Alves. 2007. "Imaging Biological Structures with a Proton Microprobe." *Modern Research and Educational Topics in Microscopy* 237–44.

Plascencia-Villa, Germán, Clarise R. Starr, Linda S. Armstrong, Arturo Ponce, and José-Yacamán Miguel. 2012. "Imaging Interactions of Metal Oxide Nanoparticles with Macrophage Cells by Ultra-High Resolution Scanning Electron Microscopy Techniques." *Integrative Biology* 4(11):1358–1366.

Quan, Xiangchun, Yan Cen, Fang Lu, Lingyun Gu, and Jingyun Ma. 2015. "Response of Aerobic Granular Sludge to the Long-Term Presence to Nanosilver in Sequencing Batch Reactors: Reactor Performance, Sludge Property, Microbial Activity and Community." *Science of the Total*

Environment 506–507:226–33.

Radetić, M. 2013. “Functionalization of Textile Materials with Silver Nanoparticles.” *Journal of Materials Science* 48(1):95–107.

Reis, M. A. and L. C. Alves. 1992. “DATTPIXE, a Computer Package for TTPIXE Data Analysis.” *Nuclear Instruments and Methods in Physics Research Section B: Beam Interactions with Materials and Atoms* 68(1–4):300–304.

Saratale, R. G., G. D. Saratale, J. S. Chang, and S. P. Govindwar. 2011. “Bacterial Decolorization and Degradation of Azo Dyes: A Review.” *Journal of the Taiwan Institute of Chemical Engineers* 42(1):138–57.

Sarayu, K. and S. Sandhya. 2012. “Current Technologies for Biological Treatment of Textile Wastewater - A Review.” *Applied Biochemistry and Biotechnology* 167(3):645–61.

Schierholz, J. 1998. “Efficacy of Silver-Coated Medical Devices.” *Journal of Hospital Infection* 40(4):257–62.

Schmidt, J. E. and B. K. Ahring. 1994. “Extracellular Polymers in Granular Sludge from Different Upflow Anaerobic Sludge Blanket (UASB) Reactors.” *Applied Microbiology and Biotechnology* 42:457–62.

Scientific, Thermo. 2010. *Eliminate Interfering Substances from Samples for BCA Protein Assays*.

Seviour, Thomas, Maite Pijuan, Timothy Nicholson, Jürg Keller, and Zhiguo Yuan. 2009. “Understanding the Properties of Aerobic Sludge Granules as Hydrogels.” *Biotechnology and Bioengineering* 102(5):1483–93.

Shafer, Martin, Joel Overdier, and David Armstong. 1998. “Removal, Partitioning, and Fate of Silver and Other Metals in Wastewater Treatment Plants and Effluent-Receiving Streams.” *Environmental Toxicology and Chemistry* 17(4):630–41.

Sheng, Guo-ping, Han-qing Yu, and Xiao-yan Li. 2010. “Extracellular Polymeric Substances (EPS) of Microbial Aggregates in Biological Wastewater Treatment Systems : A Review.” *Biotechnology Advances* 28(6):882–94.

Silvestry-Rodriguez, EE Sicairos-Ruelas, CP Gerba, and KR Bright. 2007. “Silver as a Disinfectant.” *Reviews of Environmental Contamination and Toxicology* 191:23–45.

Som, Claudia, Peter Wick, Harald Krug, and Bernd Nowack. 2011. “Environmental and Health Effects of Nanomaterials in Nanotextiles and Façade Coatings.” *Environment International* 37(6):1131–42.

Stephan, Chady and Ken Neubauer. 2014. “Single Particle Inductively Coupled Plasma Mass Spectrometry : Understanding How and Why.” *White Paper. PerkinElmer, Inc. Shelton, CT* 1–5.

Tarayre, Cédric et al. 2016. “Characterisation of Phosphate Accumulating Organisms and Techniques for Polyphosphate Detection: A Review.” *Sensors* 16(6):797.

Tay, J., Q. Liu, and Y. Liu. 2001. “The Role of Cellular Polysaccharides in the Formation and Stability of Aerobic Granules.” *Letters in Applied Microbiology* 33(3):222–26.

Tenzer, Stefan et al. 2013. “Rapid Formation of Plasma Protein Corona Critically Affects Nanoparticle Pathophysiology.” *Nature Nanotechnology* 8:772–781.

Tiede, Karen et al. 2008. “Detection and Characterization of Engineered Nanoparticles in Food and

the Environment." *Food Additives & Contaminants* 25(7):795–821.

Tiede, Karen et al. 2010. "Application of Hydrodynamic Chromatography-ICP-MS to Investigate the Fate of Silver Nanoparticles in Activated Sludge." *Journal of Analytical Atomic Spectrometry* 25:1149–54.

Tijhuis, L., M. C. M. Van Loosdrecht, and J. J. Heijnen. 1994. "Formation and Growth of Heterotrophic Aerobic Biofilms on Small Suspended Particles in Airlift Reactors." *Biotechnology and Bioengineering* 44:595–608.

Tulve, Nicolle S. et al. 2015. "Characterization of Silver Nanoparticles in Selected Consumer Products and Its Relevance for Predicting Children's Potential Exposures." *International Journal of Hygiene and Environmental Health* 1–13.

U.S. Environmental Protection Agency. 1997. *U.S. EPA. Exposure Factors Handbook*.

Vajnhandl, Simona and Julija Volmajer Valh. 2014. "The Status of Water Reuse in European Textile Sector." *Journal of Environmental Management* 141:29–35.

Vanhecke, Dimitri, Fabian Blank, and Alke Petri-fink. 2014. "Quantification of Nanoparticles at the Single-Cell Level: An Overview about State-of-the-Art Techniques and Their Limitations." *Nanomedicine* 9(12):1885–1900.

Vasco, M. S. et al. 2017. "3D Map Distribution of Metallic Nanoparticles in Whole Cells Using MeV Ion Microscopy." *Journal of Microscopy* 267(2):227–36.

Verma, Akshaya Kumar, Rajesh Roshan Dash, and Puspendu Bhunia. 2012. "A Review on Chemical Coagulation/flocculation Technologies for Removal of Colour from Textile Wastewaters." *Journal of Environmental Management* 93(1):154–68.

Wang, Qi, Zhaokun Luan, Ning Wei, Jin Li, and Chengxi Liu. 2009. "The Color Removal of Dye Wastewater by Magnesium Chloride/red Mud (MRM) from Aqueous Solution." *Journal of Hazardous Materials* 170(2–3):690–98.

Wang, Qian, Fuxing Kang, Yanzheng Gao, Xuewei Mao, and Xiaojie Hu. 2016. "Sequestration of Nanoparticles by an EPS Matrix Reduces the Particle-Specific Bactericidal Activity." *Scientific Reports* 6:1–10.

Wang, Zhi-wu, Yu Liu, and Joo-hwa Tay. 2007. "Biodegradability of Extracellular Polymeric Substances Produced by Aerobic Granules." *APPLIED MICROBIAL AND CELL PHYSIOLOGY* 74:462–66.

Wang, Zhiping, Lili Liu, Jie Yao, and Weimin Cai. 2006. "Effects of Extracellular Polymeric Substances on Aerobic Granulation in Sequencing Batch Reactors." *Chemosphere* 63:1728–35.

Watt, F. et al. 2013. "Whole Cell Structural Imaging at 20 Nanometre Resolutions Using MeV Ions." *Nuclear Inst. and Methods in Physics Research* 306:6–11.

Weber, S. D., W. Ludwig, K. Schleifer, J. Fried, and Weber E. T. Al. 2007. "Microbial Composition and Structure of Aerobic Granular Sewage Biofilms." *Applied and Environmental Microbiology* 73(19):6233–40.

Weissbrodt, David G. et al. 2012. "Bacterial Selection during the Formation of Early-Stage Aerobic Granules in Wastewater Treatment Systems Operated under Wash-out Dynamics." *Frontiers in Microbiology* 3:1–22.

Wijetunga, Somasiri, Xiu Fen Li, and Chen Jian. 2010. “Effect of Organic Load on Decolourization of Textile Wastewater Containing Acid Dyes in Upflow Anaerobic Sludge Blanket Reactor.” *Journal of Hazardous Materials* 177(1–3):792–98.

Windler, Lena, Murray Height, and Bernd Nowack. 2013. “Comparative Evaluation of Antimicrobials for Textile Applications.” *Environment International* 53:62–73.

Wingender, Jost, Thomas R. Neu, and Hans-Curt Flemming. 2012. *Microbial Extracellular Polymeric Substances: Characterization, Structure and Function*. Springer Science & Business Media.

Winkler, M-k H., R. Kleerebezem, and L. M. M. De Bruin. 2012. “Microbial Diversity Differences within Aerobic Granular Sludge and Activated Sludge Flocs.” *Enviromental Biotechnology* 97:7447–58.

World Trade Organization. 2016. *World Trade Statistical Review*.

Wu, J., H. M. Zhou, H. Z. Li, P. C. Zhang, and J. Jiang. 2009. “Impacts of Hydrodynamic Shear Force on Nucleation of Flocculent Sludge in Anaerobic Reactor.” *Water Research* 43(12):3029–36.

Yang, Yuan, Chen-Lu Long, Hai-Pu Li, Qiang Wang, and Zhao-guang Yang. 2016. “Analysis of Silver and Gold Nanoparticles in Environmental Water Using Single Particle-Inductively Coupled Plasma-Mass Spectrometry.” *Science of the Total Environment* 563–564(392):996–1007.

Van Der Zee, Frank P. and Santiago Villaverde. 2005. “Combined Anaerobic-Aerobic Treatment of Azo Dyes - A Short Review of Bioreactor Studies.” *Water Research* 39(8):1425–40.

Zhang, Lili, Xinxing Feng, Nanwen Zhu, and Jianmeng Chen. 2007. “Role of Extracellular Protein in the Formation and Stability of Aerobic Granules.” *Enzyme and Microbial Technology* 41:551–57.

Zhang, P. et al. 2015. “Extracellular Protein Analysis of Activated Sludge and Their Functions in Wastewater Treatment Plant by Shotgun Proteomics.” *Nature Publishing Group* (July):1–11.

Zhu, L., X. Dai, Y. W. Yu, H. Y. Qi, and X. Y. Xu. 2012. “Role and Significance of Extracellular Polymeric Substances on the Property of Aerobic Granule.” *Bioresource Technology* 107:46–54.

Zima, B. E., L. Díez, W. Kowalczyk, and A. Delgado. 2007. “Sequencing Batch Reactor (SBR) as Optimal Method for Production of Granular Activated Sludge (GAS) - Fluid Dynamic Investigations.” *Water Science and Technology* 55(8–9):151–58.

Zollinger, Heinrich. 2004. *Color Chemistry: Syntheses, Properties, and Applications of Organic Dyes and Pigments*. 3rd ed.

7. Appendix

Annex 1.

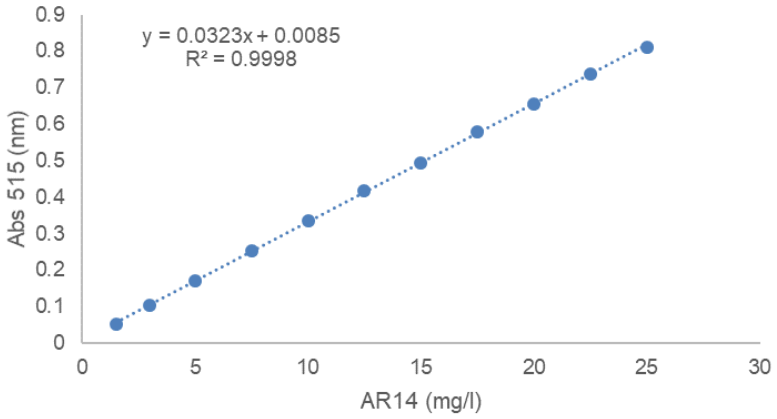

Figure A1. Linear regression to determine AR14 concentration recurring to spectrophotometer ranging from 1.5 to 25.0 AR14 mg/L

Annex 2.

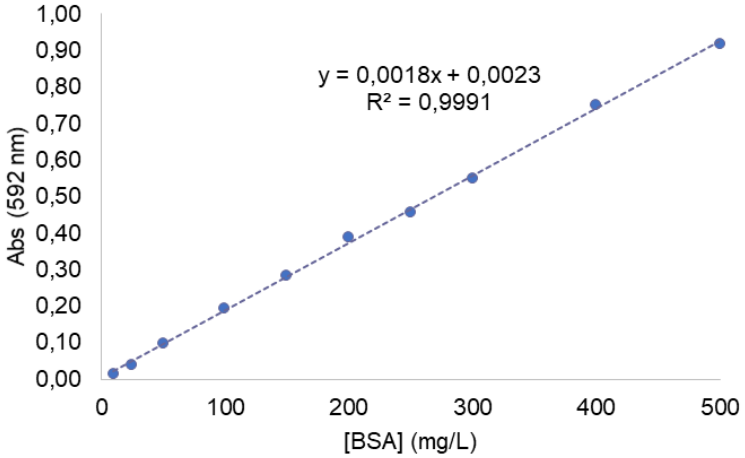

Figure A2. Linear regression to determine total PN concentration. BSA was used as standard for method calibration, in a concentration range between 10 to 500 mg/L

Annex 3.

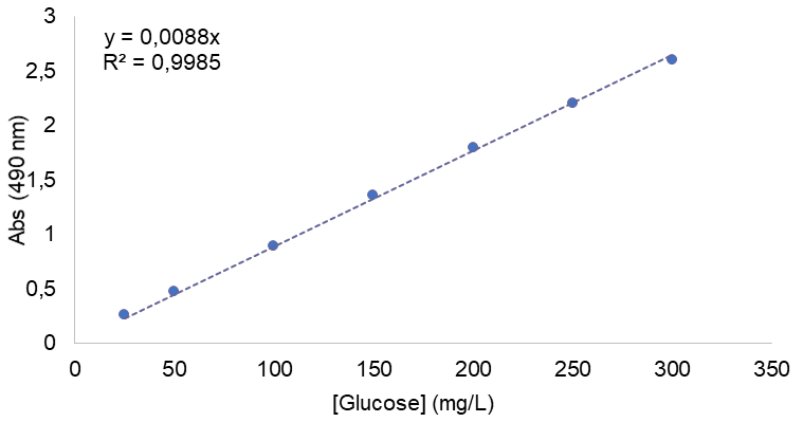

Figure A3. Linear regression to determine total PS concentration. Glucose was used as standard for method calibration, in a concentration range between 25 and 300 mg/L.

Annex 4.

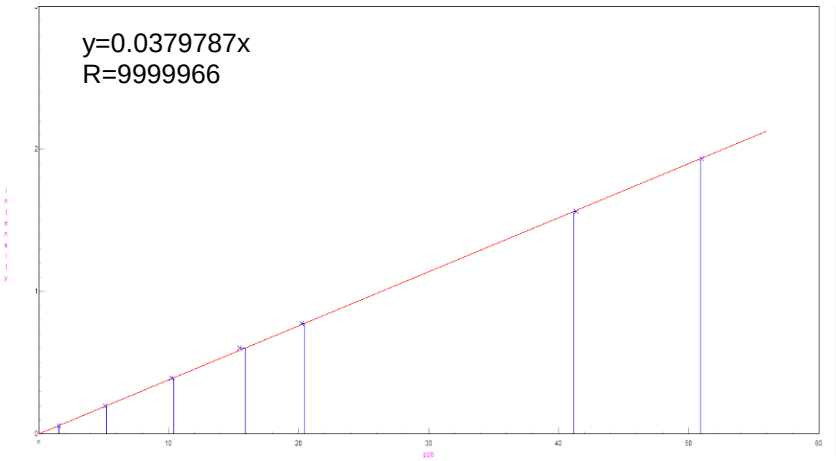

Figure A4. Linear regression to determine Ag concentration recurring Multielement standard ICP-MS STD3 solution (Perkin Elmer, USA) ranging from 1 to 20 ng/L [Ag].

Annex 5.

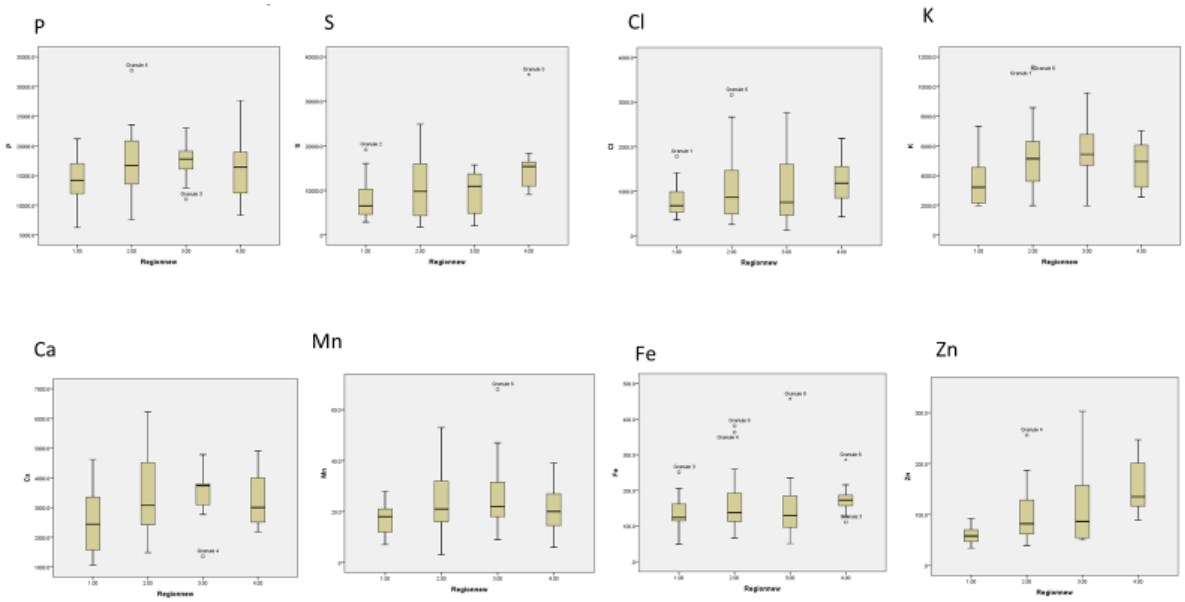

Figure A5.1. Exploratory statistical analysis for the concentration of the studied elements in the three characterized regions in granular section obtained from SBR1 AGS in box plot graphical representation (N=65), (from left to right: periphery, intermediate, core and an extra category comprising Ag deposits). The box comprises data between the 25% and 75% interquartiles (IQ) and the dividing horizontal line indicates the median; whiskers indicate the maximum and minimum values. Outliers are represented by the Isolated circles.

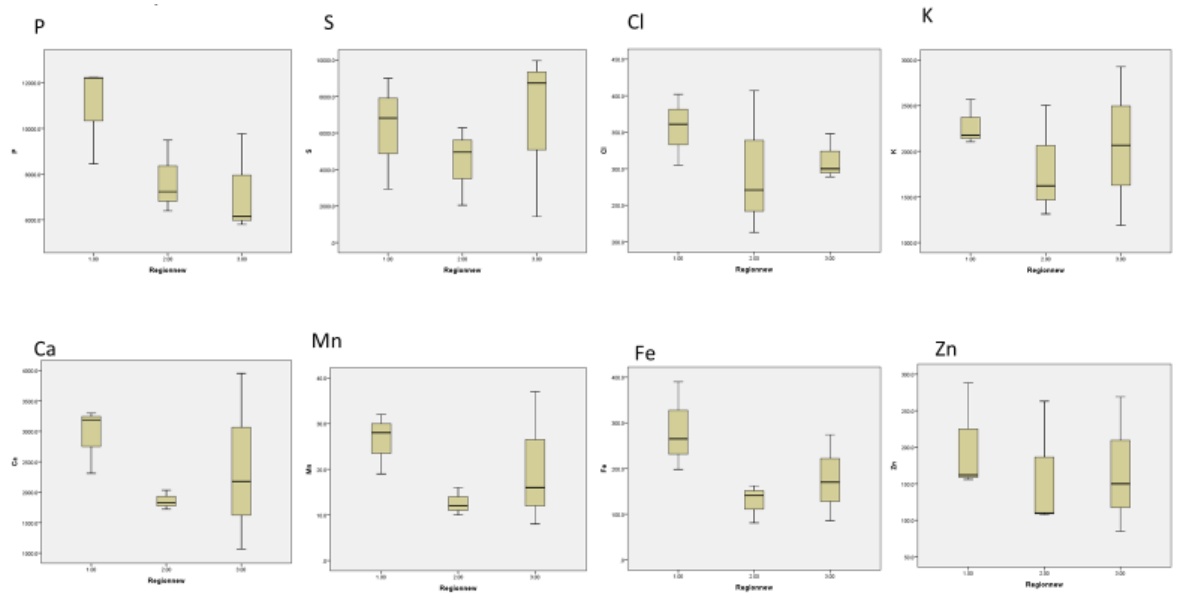

Figure A5.2. Exploratory statistical analysis for the concentration of the studied elements in the three characterized regions in granular section obtained from SBR2 AGS in box plot graphical representation (N=8), (from left to right: periphery, intermediate, core). The box represents comprises data between the 25% and 75% interquartiles (IQ) and the dividing horizontal line indicates the median; whiskers indicate the maximum and minimum values. Outliers are represented by the Isolated circles.

Annex 6.

The structure matrix (Table A1.1) indicates the correlation of each variable with the discriminant functions. The significant correlation values are indicated with an asterisk (*). Ag is mainly associated with Function 1, whereas the remaining structural and minor elements in the model were correlated with Function 2 and 3. Function 1 is the most powerful discriminant function, as it separates the regions containing large concentrations of Ag at the periphery of the granules from the outer and intermediate regions with low to nil Ag concentrations and core region. Function 2 is correlated with K, Zn, Ca, Mn and to a less extend with Cl and Fe. This function can discriminate between outer (periphery) and inner regions of the granule. The Function 3 expressed a very small fraction of the variance in the model as referred above, meaning that although the variance of S and P was correlated, their contribution to discriminate granule regions is negligible. (see Figure 19 in section 3.5.1.4). The relative contribution of each function to discriminate the data is indicated by the eigen values (Table A1.2.)

Table A6.1 Structure Matrix table displaying pooled within-groups correlations between discriminating variables and standardized canonical discriminant functions. Variables ordered by absolute size of correlation within function. *Largest absolute correlation between each variable and any discriminant function.

	Function		
	1	**2**	**3**
Ag	0.901*	-0.180	0.159
K	-0.039	.0653*	0.353
Zn	0.039	0.625*	-0.074
Ca	0.020	0.600*	0.524
Mn	-0.046	0.509*	0.068
Fe	0.075	0.207*	0.202
S	0.249	0.208	0.809*
P	-0.032	0.445	0.538*

Table A6.2. Eigenvalues and respective independent and cumulative variance of each function as well as canonical correlation, function 1 and 2 are responsible for a variance of 98.5% in elemental concentration of the tested section regions.

Function	**Eigenvalue**	**Variance (%)**	**Cumulative (%)**	**Canonical correlation**
1	2.007a	84.9	84.9	0.817
2	0.321a	13.06	98.5	0.493
3	0.035a	1.5	100.0	0.184
a. First 3 canonical discriminant functions were used in the analysis				

Annex 7.

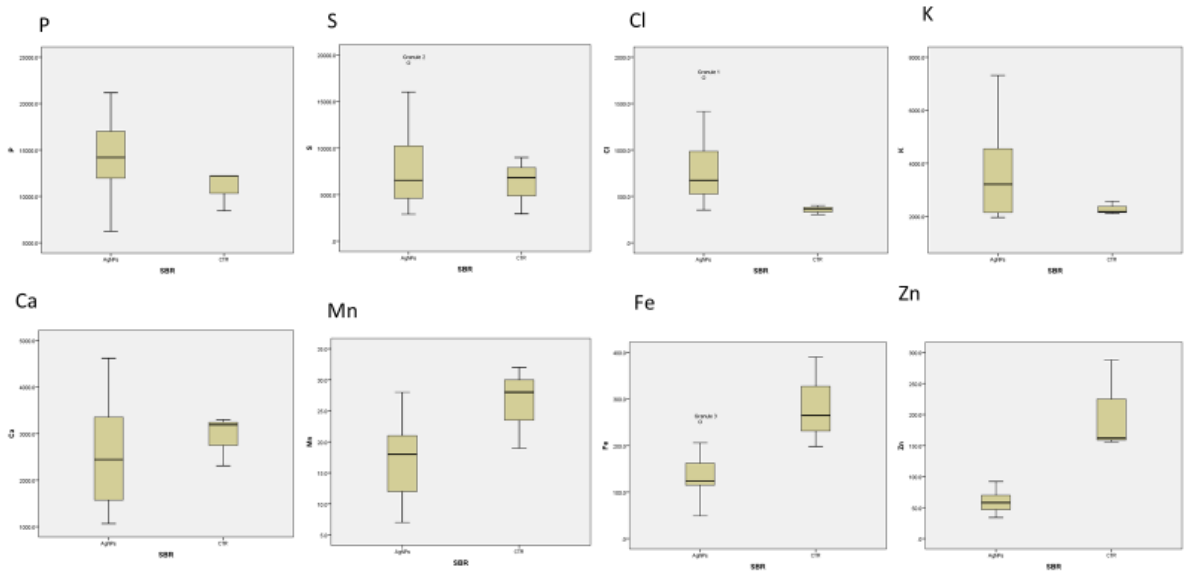

Figure A7.1. Exploratory statistical analysis for the concentration of the studied elements in the Peripheral granular region for SBR1 and SBR2 (in left and right, respectively). Box plot graphical representation. The box represents the 25% and 75% interquartiles (IQ) and the dividing horizontal line indicates the median; whiskers indicate the maximum and minimum values.

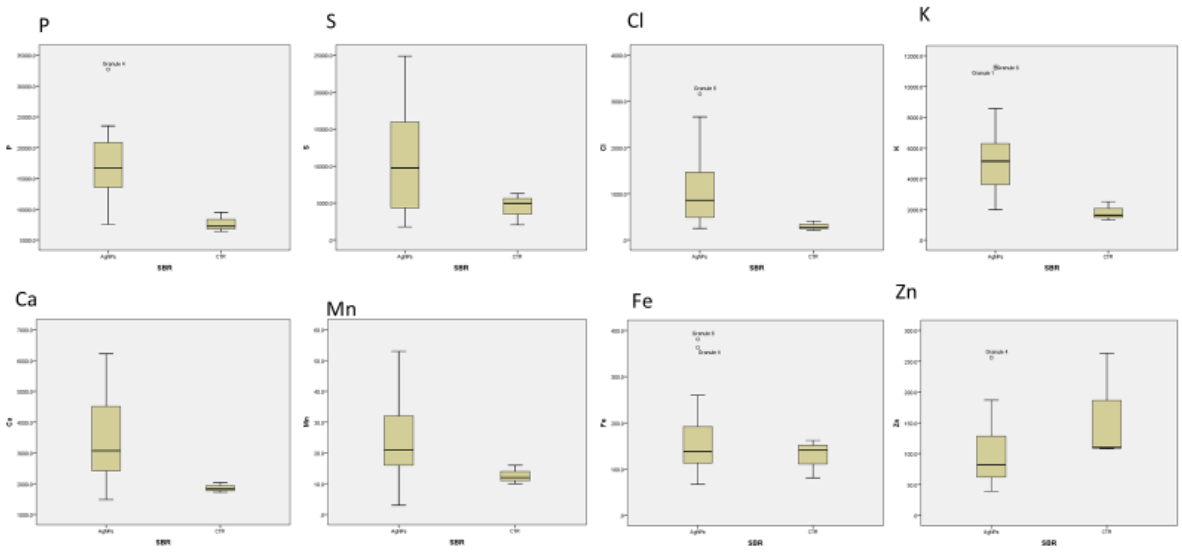

Figure A7.2. Exploratory statistical analysis for the concentration of the studied elements in the intermediary granular region for SBR1 and SBR2 (in left and right, respectively). Box plot graphical representation. The box represents the 25% and 75% interquartiles (IQ) and the dividing horizontal line indicates the median; whiskers indicate the maximum and minimum values.

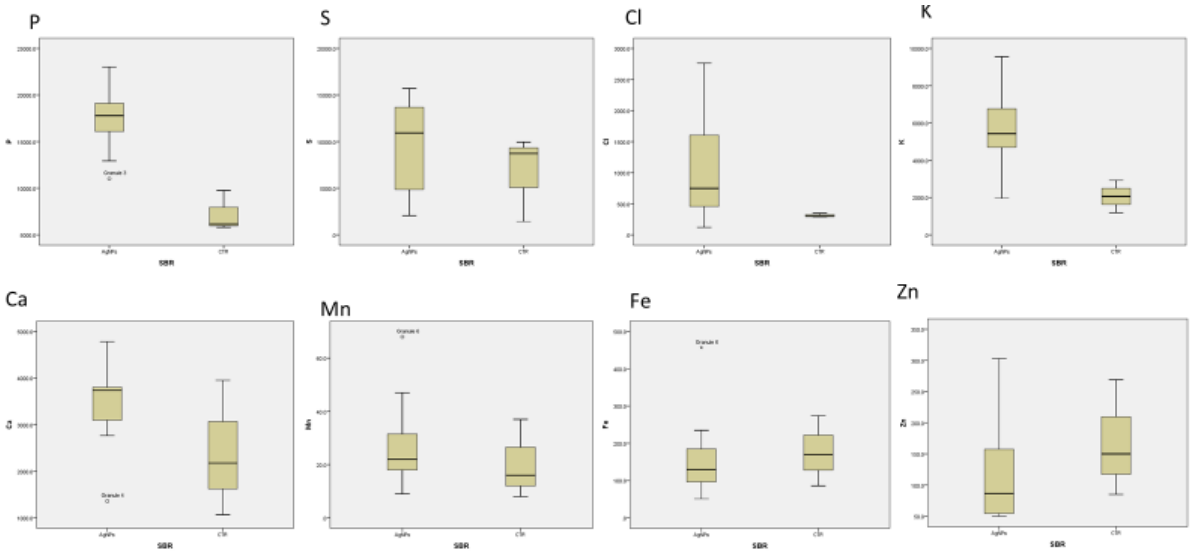

Figure A7.3. Exploratory statistical analysis for the concentration of the studied elements in the core granular region for SBR1 and SBR2 (in left and right, respectively). Box plot graphical representation. The box represents the 25% and 75% interquartiles (IQ) and the dividing horizontal line indicates the median; whiskers indicate the maximum and minimum values.